Stony Brook University

Gold Nanoparticles Cytotoxicity

A Dissertation Presented

by

Tatsiana Mironava

to

The Graduate School

in Partial Fulfillment of the

Requirements

for the Degree of

Doctor of Philsophy

in

Materials Science and Engineering

Stony Brook University

August 2011

Stony Brook University

The Graduate School

Tatsiana Mironava

We, the dissertation committee for the above candidate for the

Doctor of Philosophy degree, hereby recommend

acceptance of this dissertation.

Professor Miriam Rafailovich,
Materials Science and Engineering

Assistant Professor Yizhy Meng - Chairperson of Defense
Materials Science and Engineering

Professor Marcia Simon,
Oral Biology and Pathology, School of Dental Medicine

Associate Professor Michael Hadjiargyrou,
Biomedical Engineering

This dissertation is accepted by the Graduate School

Lawrence Martin
Dean of the Graduate School

Abstract of the Dissertation

Gold Nanoparticles Cytotoxicity

by

Tatsiana Mironava

Doctor of Philosophy

in

Materials Science and Engineering

Stony Brook University

2011

Over the last two decades gold nanoparticles (AuNPs) have been used for many scientific applications and have attracted attention due to the specific chemical, electronic and optical size dependent properties that make them very promising agents in many fields such as medicine, imagine techniques and electronics. More specifically, biocompatible gold nanoparticles have a huge potential for use as the contrast augmentation agent in X-ray Computed Tomography and Photo Acoustic Tomography for early tumor diagnostic as well these nanoparticles are extensively researched for enhancing the targeted cancer treatment effectiveness such as photo-thermal and radiotherapy.

In most biomedical applications biocompatible gold nanoparticles are labeled with specific tumor or other pathology targeting antibodies and used for site specific drug delivery. However, even though gold nanoparticles poses very

high level of anti cancer properties, the question of their cytotoxicity ones they are released in normal tissue has to be researched. Moreover, the huge amount of industrially produced gold nanoparticles raises the question of these particles being a health hazard, since the penetration is fairly easy for the "nano" size substances.

This study focuses on the effect of AuNPs on a human skin tissue, since it is fall in both categories – the side effects for biomedical applications and industrial workers and users' exposure during production and handling. Therefore, in the present project, gold nanoparticles stabilized with the biocompatible agent citric acid were generated and characterized by Transmission Electron Microscopy (TEM) and Scanning Electron Microscopy (SEM). The cytotoxic effect of AuNPs release to healthy skin tissue was modeled on 3 different cell types: human keratinocytes, human dermal fibroblasts, and human adipose derived stromal (ADS) cells. The AuNPs localization inside the cell was found to be cell type dependent. Overall cytotoxicity was found to be dependent on time, concentration and nanoparticle size. Additionally, the question of cell recovery once the source of AuNPs is removed was investigated in the present work. It was found that full cell functions recovery is possible after removing the source of nanoparticles.

TABLE OF CONTENTS

List of Figures

List of Tables

List of Abbreviations

AuNPs – Gold Nanoparticles

ADS cells – Adipose Derived Stromal cells

TEM – Transmission Electron Microscopy

UV-vis – Ultraviolet-visible Spectroscopy

SEM – Scanning Electron Microscopy

UV – Ultraviolet

NIR - Near-infra red

SPR - Surface Plasmon Resonance

CT - Computed Tomography

NAPT - Nanoshell-Assisted Photo-Thermal Therapy

PEG - Polyethylene Glycol

EPR effect - Enhanced Penetration and Retention effect

BSA - Bovine Serum Albumin

SLN - Solid Lipid Nanoparticles

PLA - Polylactic Acid

QD - Quantum Dots

MSDS - Material Safety Data Sheets

BMZ - Basement Membrane Zone

DEJ - Dermal-Epidermal Junction

DNA – Deoxyribonucleic Acid

ECM – Extracellular Matrix

DMEM - Dulbecco's Modified Eagle's Medium

FBS - Fetal Bovine Serum

PS - Penicillin-Streptomycin

KGM - Keratinocyte Growth Media

NIA - National Institute on Aging

SPF - Sun Protection Factor

PBS - Phosphate Buffered Saline

SDS-PAGE - Sodium Dodecyl Sulfate Polyacrylamide Gel Electrophoresis

IBMX - 3-isobutyl-1-methylxanthine

PDGF - Platelet-Derived Growth Factor

RIPA - Radioimmunopresipitation Assay

HRP –Horse Radish Peroxide

ECL – Enhanced Chemiluminescence

CHAPTER 1

INTRODUCTION

Nanotechnology is a relatively new and rapidly developing field in modern science. Prefix ‘nano’ refers to a structure or system with a size range starting at 100 nm and below. The properties of nanomaterials and nanosystems are extensively different from the properties of the bulk, since we are using material at submolecular level where one nanometer is roughly the size of ten aligned atoms. For example, when we reduce the material to the nanoscale level, we start to expose conductive properties, with some becoming transparent or soluble. AuNPs, depending on size can be blue, purple or green.

Over the last two decades, some of the more promising areas of nanotechnology and its applications, is in electronics, novel imaging systems and medicine. However, due to exciting fact that nanosized objects posses new properties, these particles also can be potential health hazards, especially since they can penetrate through the skin, be inhaled and enter the body through the intestinal tract. Oberdorster at el showed that carbon nanoparticles can cause brain damage [1, 2], Muhlfeld et al. and also Rothen-Rutishauser et al. reported nanoparticles damaging lung tissue [3, 4].

There are no government regulations for nanoparticles risk assessment if the bulk material is assessed. Specifically for gold nanoparticles, the FDA materials safety datasheets says: “*Routes of Entry: inhalation, ingestion and skin absorption. Effects of Overexposure: Exposure to Gold Compounds may be harmful. Can*

cause contact dermatitis. The toxicological properties have not been thoroughly investigated".

Therefore, this dissertation is divided into 4 chapters. The first chapter starts with description of nanoparticles and their properties and focuses on gold nanoparticles and their applications in different fields starting from gold nanoparticles conjugated anti-cancer drugs to biosensors and enhancement agents for the bioimaging. The chapter also discusses the potential health risks and penetration pathways of AuNPs. More detailed skin penetration is described toward the end of first chapter along with skin layers interactions. The second chapter is devoted to the synthesis and properties of the AuNPs and the toxicity of the particle supernatant. The next chapter describes the effect of AuNPs on human skin cells, it has experimental procedures, material and methods and discusses the results. The last chapter summaries the main findings and future work.

1.1. Nanoparticles properties

By definition nanoparticles are materials that have all three dimensions in the nanoscale size. The prefix 'nano' comes from the Greek and means dwarf and has been adopted for the measurement of an object that is in a range of one thousand millionth of a standard unit, For example, one nanometer (nm) is one thousand millionth of a meter. Even though, nanoparticles are small enough in size to exhibit properties that greatly vary from the bulk material, where they are big enough not to be treated as clusters of isolated atoms or molecules. In other words, nanoparticles are in the size range when material cannot be described by classical mechanics that explains behavior for large objects, and quantum mechanics

component start to dominate in their properties. Quantum mechanics describes the matter and radiation taking into account that all energy exists in a small separate packets, called “quantums”, which are passed around from one material to the next.

Nano-sized materials are known and used for many centuries, for example carbon black nanoparticles were used in ancient Egypt in makeup and ink, and metal oxide nanoparticles were used in middle ages for staining glass, etc. Nanomaterials are present in nature from forest fires, volcanoes and as minerals (titanium dioxide); they are also made as a byproduct in anthropogenic activities and intentionally as a primary product. They exist as spherical, cubical, rod-shapes, triangular, ellipsoidal, etc. Currently there are huge varieties of materials that nanoparticles can be made of; the most commonly used are different metal oxides, metals and silicates that have applications in medicine, cosmetics, electronics, optics and catalysis. For example, platinum and palladium are used as excellent catalysts [5-11], silver nanoparticles are used in glucose and cholesterol sensors [12-15], gold nanoparticles enhance quantum efficiency and electroluminescence in organic light emitting diodes [16-19], and many silicate nanoparticles can be mixed into polymers and used to improve coatings and thin films [20, 21].

One of the reasons that nanomaterials have unique properties is a large surface to volume ratio that allows to easily vary surface related properties by modification of size, shape or surroundings. Therefore, the desired nanoparticles properties for the optical, electronic or other applications can be tuned by varying the nanomaterial’s three parameters: size, shape and surrounding.

1.2. Gold nanoparticles and their properties

Gold is known as an inert material when it is in bulk, however nano-sized gold is known to be highly reactive [22, 23]. Gold nanoparticles are defined as a

stable colloidal solution of gold atoms clusters in a range 1-100 nm. The most noticeable change in properties at this nanoscale is a color change to purple-red from yellow in bulk. This change is due to the red shift of the Plasmon band to visible frequencies, in contrast, one of bulk gold where the Plasmon absorption is in the UV region. More specifically, the "Surface Plasmonic" theory explains that the six surface free electrons present in the conduction band of AuNPs oscillate back and forth, creating a Plasmon band with an absorption peak at 530-540 nm, when hit by the electromagnetic field of the incoming light. Physical properties of gold nanoparticles depend on size and shape of the particles itself, particle-particle distance, the nature of a colloidal stabilizer as well as dielectric constant of the surrounding matter. In example, with increasing size of spherical gold nanoparticles the Plasmon absorption red shift is increasing also, changing the color from red to purple. Gold nanorods show two different Plasmon resonances at 520 nm transverse wavelength and longitudinal at higher wavelength 550-600 nm, which increases with nanorod increasing aspect ratio [24], [25]. This unique property of gold nanorods, to change the absorption region from visible to Near-infra red (NIR), is due to the longitudinal band sensitivity to aspect ratio, used in Near-infra red ray therapy [26, 27] and enhanced scattering of absorbed biomolecules [28]. The effect of the surrounding media is derived from the different wavelength of the Plasmon absorption resonance of the gold nanoparticles dispersed in different solvents. Thus, by changing the shape, size and surroundings of AuNPs, the surface Plasmon resonance can be tuned for various applications such as drug delivery, cellular imaging and biosensors [29-32].

The six free electrons in the conduction band of AuNPs makes them excellent contrast enhancement agents in X-ray and CT-imaging [33-36], where the studies are based on contrast comparison due to the difference in electron

densities of different tissues [37]. In addition, rich surface chemistry of AuNPs allowed them to be modified with wide varieties of biological molecules [38-40]. These hybrid gold nanoparticles tagged with tumor recognizing molecules are efficient site specific vehicles delivering imaging (due to gold high electron density) and therapeutic probes to targeted tumor cells [41-46].

1.2.1. Gold nanoparticles in cancer diagnostic and therapy

In order to develop appropriate hybrid gold nanoparticle for drug delivery and imaging, it is important to specify the difference between normal and cancerous tissue. It is well known, that normal tissue has tightly structured and continuous vessel walls regularly intermingled with 9 nm pores and sometimes with 50 nm pores. As a result small molecules can easily penetrate into the different types of normal tissue in contrast to large molecules that have an insignificant penetration rate. Tumor tissues as well as inflammatory tissues and some reticulo-endothelial system rich organs, have discontinuous capillary walls with no basal lamina and a huge number of pores approximately 100 nm in size. Therefore, particles with a size range of 25-100 nm that are unable to penetrate normal tissue can easily enter tumors and accumulate inside [47, 48]. The accumulation is a result of the lack of a lymphatic system in tumors that typically helps to eliminate lipophilic and polymeric materials [49-51]. This makes these gold nanoparticles conjugated with suitable tumor seeking biomolecules with a mean size 40-100 nm excellent agents for cancer therapy and imaging purposes [52-55].

There are many different cancer treatments, including chemotherapy, radiotherapy (X-rays therapy) and photo-thermal therapy. Selective cell and receptor targeting of gold conjugates can provide new pathways for the targeted

delivery of agents for the therapeutic and diagnostic purposes. Gold nanoparticles have been used as target contrasts agents for different types of tumors [33, 35, 36, 56-58]. For example, in cervical cancer they are used for detection by labeling them with antibodies and oncoproteins associated with human papilomavirus [59]. Gold nanoshells conjugated with Her-2, breast tumor protein marker, were found localized in microscopic tumors [60]. AuNPs conjugated with mercaptoalkyl-oligonucleotide have been used in polynucleotide detection by interaction of the Plasmon absorption band with environment [61, 62].

Different conjugates of gold nanoparticles have been intensively researched for the potential application in photo-thermal and radiotherapy, due to their sensitizing properties to specific auto-amplified electronic cascades together with charge transfer processes; these AuNPs are able to augment irradiation damage.

In a recent study by O'Neal et al [63], the practicability of nanoshell-assisted photo-thermal therapy (NAPT) was proved. Polyethylene glycol (PEG) coated silica core-gold shell nanoparticles of diameter less than 130 nm with and Plasmon absorption peak at 805-810 nm were intravenously injected in mice with colon tumors. In a relatively short period of time (6 hours) nanoshells were able to accumulate in the tumors due to enhanced penetration and retention (EPR effect) after that tumors were exposed to NIR light resulting in absorption of light by particles and generation of heat that cased permanent tumor damage. Nanoshell enhanced photo-thermal treatment led to complete tumor degradation and allowed mice to remain healthy and tumor free up to 90 days after treatment. In contrast, the control group that was exposed to NIR without nanoshell injection,the tumors continued to grow [63]. These results showed the feasibility of using AuNPs as a tumor targeting agents due to the photo-thermal treatment effectiveness increase by tuning plasmon absorbance at NIR range. Tkachenko et al [64] found out by

differential contrast microscopy that AuNPs coated with bovine serum albumin (BSA) specifically targeted cell nuclei. Another research group [65] showed that irradiation with X-rays of AuNPs accumulated in mammary carcinoma tumor caused its significant shrinkage. On the other hand, treatment with only X-rays irradiation had no effect on tumor [66]. Recently, different groups investigated the combination of radioactive gold and target specific biomolecule "gum Arabic" for the radiopharmaceutical drug delivery, where the therapeutic effect is achieved by delivering radioactive gold particles directly to the tumor [67-69].

To summarize, gold nanoparticles are used in various applications for cancer diagnosis and treatment; however there is a huge necessity for further investigation and development of more specific and extremely tuned gold nanoparticles conjugates that can have an even bigger potential for cancer therapy.

1.3. Nanoparticles pathways into the human body

There are numerous reports indicating than nanoparticles are found in different organs in the human body [70-76]. Since nanoparticles are able to travel in the body after they entry, the most important thing is to identify the pathways by which they penetrate if we are to be able to take the necessary precautions.

1.3.1. Inhalation of nanoparticles

It is well known that due to the small size nanoparticles they can easily become airborne to form aerosols. These types of nanoparticles are usually perceived to be the most potentially hazardous ones. Once insoluble particles are inhaled they accumulate in the lungs and may lead to adverse effects.

The modern lung toxicity theory implies that ultrafine particles made of low-soluble and low-toxicity materials cause much stronger reaction in lung tissue than finer particles made of the same material [1, 77-82]. The inflammation caused by the inhaled nanoparticles is a sign of the tissue's attempt to recover from injury or irritation that follows redness, swelling, heat and pain in the affected area. The high level of inflammation may damage the cell layer at the surface of the tissue and also other cells such as macrophages that will lead to tissue damage and loss of functionality [2, 83-85]. Zhang et al showed that lung injury was much higher with nickel nanoparticles (20 nm) than with the same concentration of the standard nickel particles (5 μm) proving that the toxicity is increasing with the decreasing particles size [86].

1.3.2. Absorption through the skin

There are many consumer products that contain nanoparticles including sunscreens, skin care, cosmetics, etc. Nanoparticles are used for product property improvement such as color, odor or moisture or as sun protection factor (SPF) agents. There are studies that indicate the ability of the nanoparticles to penetrate into the top layers of skin and even reach the blood stream [87-89]. On the other hand, penetration as well as damage seems to be particles size and nature dependent and no direct generalization about nanoparticles hazards can be extrapolated from current findings. However, considering the total variety of skin care products on the market that contain nanoparticles, the potential for hazards has to be investigated in all possible aspects [90-92].

Micro and macromolecules can enter skin through three distinct pathways:
(1)The intercellular pathway, through the lipid matrix occupying the intercellular spaces between the corneocytes.

(2) The transcellular pathway, which is through the keratinocytes.
(3) Transappendageal pathway, which is across hair follicles, sebaceous glands and sweat glands. All these ways have shown considerable interaction with nanoparticulate formulations [93-96].

Nanoparticle interactions with skin depend on the physicochemical properties of nanoparticle size, surface charge, properties of material used, drug-loading efficiency, lamellarity and mode of application.

Nanoparticles can be made of various types of chemicals such as lipids, sugars, polymers (degradable and non-degradable), organic and inorganic compounds and also metals. For example, solid lipid nanoparticles (SLN), that are made from lipids and are solid at room temperature by the high pressure homogenization process, were found to be able to slide in between the superficial corneocytes by intense contact between skin lipids with a higher rate for the increased lipophilicity of the SLN [97-99].

According to Alvarez-Roman et al [94] 20 nm polymeric nanoparticles can accumulate in the hair follicles and create high local concentrations of NPs that can later diffuse to the viable layers of the skin. PLA nanoparticles we able to penetrate 50% of the vellums hair follicles and from there, they reached and entered into sebaceous glands [100]. The metallic nanoparticles are usually smaller in size that can lead to faster and easier skin penetration. Recently two different groups [101, 102] have shown that the rigid nanoparticles and quantum dots (QD) less than 10nm in size can passively penetrate skin through hair follicles and the stratum corneum lipid matrix reaching the viable dermis. Ryman-Rasmussen [103] addressed the question of QD coating and showed that QD with neutral or anionic coating penetrate only up to the epidermal layers while cationic ones localized in dermis within 8 hours. Zhang et al [104, 105] showed that PEG-coated QDs with diameter less than 40 nm penetrate into the stratum corneum lipids and hair

follicles. The mechanical stress applied to the skin seems to be one of the important conditions for nanoparticle penetration into the skin. Kohl and Alpar [106] found that latex nanoparticles up to the 500 nm in diameter are able to penetrate skin under the stress.

Hence, there is much evidence [95, 107, 108] that irrespective of material used, shows that most nanoparticles do not cross the stratum corneum and that the transappendageal pathway appears to be the dominant mode of nanoparticle entry into the skin. And the possibility of the adverse effects of the nanoparticles on the skin upon the penetration has to be considered, including how nanoparticles interact with proteins, as well as their genotoxic effects and oxidative stress induction [82].

1.3.3. Absorption through the intestinal tract

Oral drug delivery is the preferred route of administration of drugs. Because of their versatility, nanoparticles often have been investigated for the delivery of a wide number of drugs by this route.

There are also two “natural” or unintentional ways for nanoparticles to end up in the intestinal tract: by swallowing the airborne particles and with food containing nanoparticles. The intestinal tract has a natural mechanism of eliminating the “unwanted material”, however; there is no evidence that nanoparticles can be removed by that method. It was reported [109-117] that particles under 300 nm are able to reach the blood stream and smaller once, under 100 nm are also were found to be absorbed in various tissues and organs. The kinetics of particle uptake is clearly important, especially in relation to rates of biodegradation of the nanoparticles [118]. By all accounts uptake can occur quite

rapidly, being completed within 1 h. Once absorbed and passaged through the epithelial cell layer there can be deposition in the lymphatics, movement through or entrapment in the lymph nodes or transfer to the blood, provided that the particles remain intact and are below a certain threshold size. Clearly, particle diameter is a determinant of its ability to freely translocate [119]. There are numerous of the research groups working on the nanoparticles oral drug delivery for the Alhzeimer's disease, delivery of the insulin and vaccination [120-123] and in all cases nanoparticles absorption has to be investigated since it is cell specific and can not be predicted.

1.4. Gold nanoparticles as a potential health hazard

Gold nanoparticles have been manufactured for more than a decade now and have been intensively used for the cellular imaging. Nevertheless, the Material Safety Data Sheets (MSDS) only indicates that the roots of entry to the body for the AuNPs are: injection, inhalation and absorption through the skin. As for the toxic properties it only indicates that they were not thoroughly investigated.

There have been a number of attempts to study AuNPs toxicity; however, the data reported have been contradictory. This can be explained by the large disparity in the experimental design, using various particles shapes and sized, doses and functionalization methods. For example, Goodman et al [124] investigated the cytotoxic properties of the 2 nm AuNPs and found that cationic particles are seven fold more toxic than anionic. Pan [125] and Tsoli [126] found the peak of toxicity for the 1.4nm particles to be in the range of 0.8-15nm and explained this phenomenon by AuNPs size similarity to B-form of DNA. Also, as Pernodet et al [127] reported the AuNPs toxicity depends on the nanoparticle

concentration that in turn represents the number of particles inside the cell. Another study [128] revealed that 10nm and 50nm citrate-coated AuNPs are not toxic to the embryonal fibroblasts, however the same study indicated changes in cell morphology induced by the nanoparticles. Another research group found that AuNPs have no cytotoxic effects on HepG2 cells, though, they did inhibit the proliferation and intracellular calcium release [129]. Shukla et al [130] observed no cytotoxic effects of 3.5nm AuNPs on the macrophage cells up to the concentration of 100 μM despite of the fact that nanoparticles were found in the lysosomes and perinuclear space of the cells.

On the other hand, cytotoxicity depends on the cell type. Thus, Patra et al [131] established that 33nm AuNPs were not toxic to hamster kidney cells HepG2 but were toxic to the human carcinoma lung cell line A549. Another way to estimate toxicity of AuNPs was proposed by Ryan et al [132] where it was linked to the amount of proteins absorbed on the surface on AuNP. They have shown that for 5 nm particles, where absorption increases from 30 to 150 molecules per particle had resulted in a decline of cell viability from 98% to 66%.

A more recent study [133] showed that gold nanoparticles are able to penetrate skin depending on the particle size, 15 nm particles were located in the deeper skin layer, whereas the 100nm particles were only able to reach the viable epidermis and dermis.

In conclusion, there are many studies on AuNPs toxicity, though; the majority of reports dealing with the effects of AuNPs on normal cells have focused on the short term effects (2-12 hours) of particle exposure instead of more long term consequences that can affect overall cellular function. Collectively, results from these studies are thoroughly discussed in detail in recent reviews [134, 135]. The detrimental effects cannot be detected simply by general proliferation or

apoptosis assays, since the presence of the AuNPs inside the cells may be interfering with the proper execution of other specific functions. Furthermore, the short experimental times (less than 24 hours) frequently reported in the literature [124, 136-139] are not sufficient to observe many of these effects, which were shown to appear after 72 hours, and several rounds of cell division [127].

1.5. Skin layers their properties and interactions

Skin is the largest organ and least permeable barrier and therefore can be used to evaluate how nanoparticles found in its outermost layers generate signals that impact the lower proliferative layers of the tissue (fig. 1).

The skin has three layers - the epidermis, dermis, and fat layer (also called the subcutaneous adipose tissue). Each layer performs specific tasks.

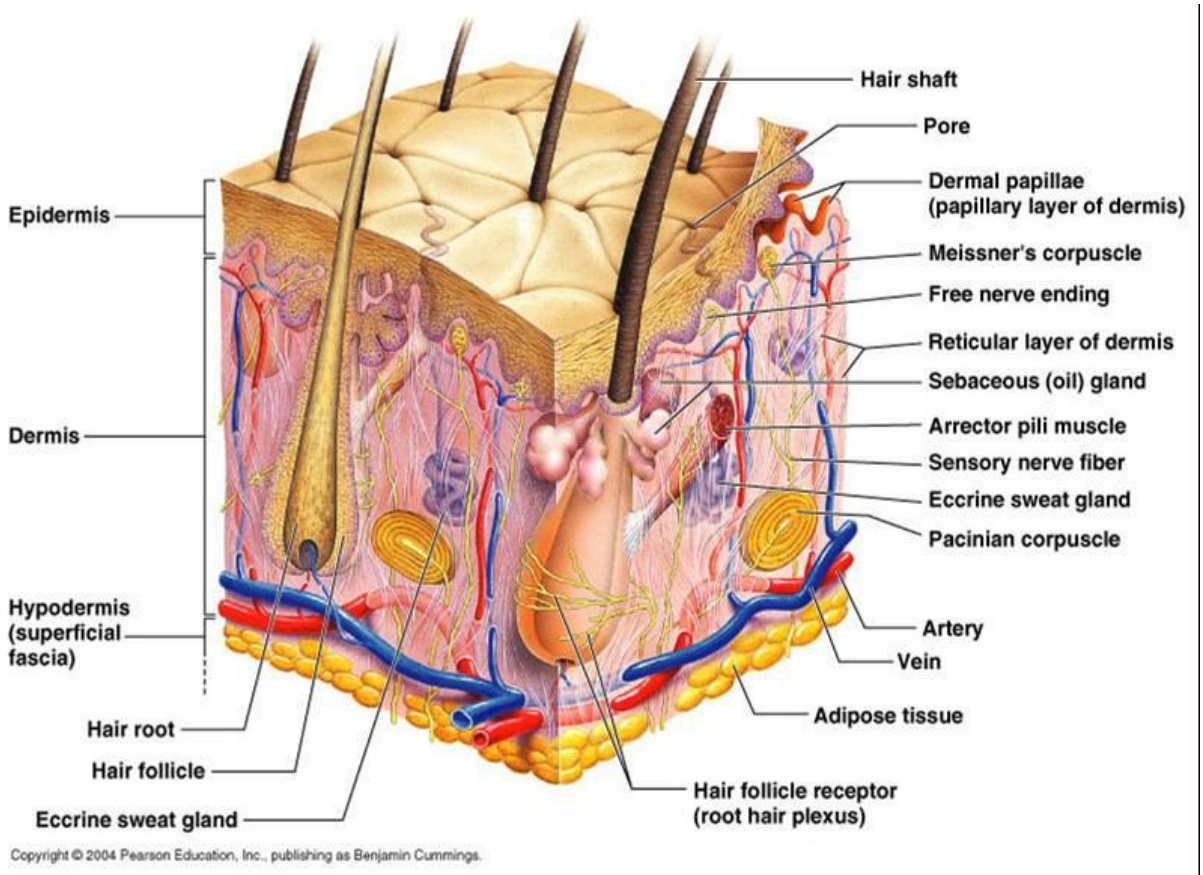

Copyright 2004, Pearson Corporation Inc.

Figure 1. Human Skin Layers.

The epidermis (From the Greek “epi”, on top and “derma”, the skin) is the skin's outer structure serving a protective function. The epidermis is the relatively thin, tough, outer layer of the skin. The thickness of the epidermis varies in different types of skin. It is the thinnest on the eyelids at .05 mm and the thickest on the palms and soles at 1.5 mm.

The epidermis contains 5 layers: stratum basale, stratum spinosum, stratum granulosum, stratum licidum and stratum corneum.

The different strata as well as the cells that make up the epidermis have their own function. These include protecting the body from foreign pathogens, waterproofing the body, skin pigmentation and fighting off foreign bodies as part of the immune system. They are also responsible for the sensation of touch. The importance of the functions of the epidermis is quite obvious. Infections cause a variety of diseases, so protection from foreign agents and pathogens is necessary. Similarly, waterproofing the body keeps liquids from penetrating the skin. Skin color or the pigment in the skin is important for protection from ultraviolet radiation.

The dermis, the skin's next layer, is a thick layer of fibrous and elastic tissue, dermis is divided into 2 layers: papillary (superficial) and reticular (deep) layer. The dermis is 10 to 40 times thicker than the epidermis. In contrast with the epidermis, it is vascularised, making it possible not only to provide energy and nutrition to the epidermis but also to maintain thermoregulation and in healing.

The fibroblasts are the main cells in the dermis. They are essentially located in the dermal papillae close to the epidermis, and found only in very low numbers in the deep layers of the dermis known as the reticular dermis. They are specialized in producing two types of protein fibers, collagen and elastin fibers constituent of the extra-cellular matrix. Collagen fibers are responsible for resistance to strain and traction, while elastin supplies elastic properties giving the skin its flexibility and strength. The reticular dermis accounts for the greater part of the dermis. On this level, the elastin and collagen fibers are multidirectional, whereas in the dermal papillae the elastin fibers are mainly oriented perpendicular to the skin surface.

Below the dermis lies a subcutaneous layer also called hypodermis, Hypoderm and subcutaneous are from Greek and Latin words, respectively,

meaning "beneath the skin". This tissue consists of a layer of fat and connective tissue that houses larger blood vessels and nerves. The subcutaneous layer helps insulate the body from heat and cold, because it conducts heat only one a third as readily as other tissues, and provides protective padding and defines the body contour.

The hypodermis is the innermost and thickest layer of the skin, however it is thickness varies greatly from person to person. It invaginates into the dermis and is attached to the latter, immediately above it, by collagen and elastin fibers. It is essentially composed of a type of cells specialized in accumulating and storing fats, known as adipocytes, other cell types that are found in the hypodermis are fibroblasts and macrophages.

The hypodermis behaves as an energy reserve. The fat contained in the adipocytes can be returned back into circulation, through the venous route, during intense effort or when there is a lack of energy providing substances, and are then transformed into the energy.

The interactions among skin layers have been extensively studied in the last decade for the skin constructs and wound healing improvement [140-144].

The basement membrane zone (BMZ) in the skin is a highly specialized critical interface between the epidermis and dermis that allows for communication between different cell types [145]. Basement membranes throughout the body provide tissue-specific functions; however, all share similar attributes. Regardless of site, the BMZ functions as a vehicle for cellular attachment of cells, a matrix for cellular migration, a gatekeeper for cellular and macromolecule transit, and as the moderator of cellular activities ranging from differentiation to apoptosis.

The cutaneous BMZ is located between the epidermis, a stratifying squamous epithelium, and the dermis of the skin and is known as the dermal-epidermal junction (DEJ). The DEJ separates these two distinct cellular compartments of the skin and provides adhesion and a dynamic interface between them providing the structural integrity of the skin. The DEJ controls the transit of molecules between the epidermis and the dermis on the basis of charge and size, but it allows the passage of migrating and invading cells under normal (i.e. melanocytes and Langerhans cells) or pathological (i.e. lymphocytes and tumor cells) conditions. It also influences the behavior of keratinocytes by adjusting the cell polarity, proliferation, migration, and differentiation. In addition to this, its role is important during morphogenesis and development, wound healing, and remodeling of the skin [145].

In the skin, both the ectodermally derived keratinocytes and the enodermally derived fibroblasts supply protein components to the BMZ during development. The hemidesmosomal plaque proteins, type IV collagen, type V collagen, laminins 5 and 6, heparan sulfate proteoglycan, and type VII collagen are all products of the basal keratinocytes [146]. Fibroblasts of the papillary dermis contribute to basement membrane formation partly by producing nidogen, additional laminins, type IV collagen and fibronectin to the lamina densa, and types I, III, and VII collagens to the sub-basal lamina densa [147, 148]. TGF-β secreted by fibroblasts has been shown to induce the synthesis of collagen types IV and VII by keratinocytes [149], [150]. Also the fibroblast density is a vital factor for the development of normal epidermal morphology and keratinocyte differentiation [151].

The importance of interactions between the dermal and subcutaneous layers is also well known. One of the most important functions of the dermis-

subcutaneous interactions is the maintenance of the overall skin elasticity. A recent study indicated that increment of subcutaneous adipose mass impairs dermal elasticity [152].

The development of adipose tissue is dependent on the growth and differentiation of fibroblast-like adipocyte precursor cells. Also, fibroblast growth factor receptors was shown to control epithelial-mesenchymal interactions that are necessary for alveolar elastogenesis [153].

1.6. Goals of Dissertation

The goal of this project is to estimate the potential health risk of gold nanoparticles with an inactive type of coating. This would allow us to determine the level of toxicity due strictly to the dimensionality of the particles. Dimensionality can play an important role in several processes associated with toxicity, and since chemical process are also involved it is important to design experiments where only one parameter, the particle size is varied and all other effects can be traced to the particle size. For example nanoparticle toxicity is due to (a) particle penetration into the cell; (b) adsorption of serum proteins onto the particle; (c) sequestration of the particle once inside the cell; (d) time of penetration. In each case, the surface chemistry of the particles may be modified by interactions with serum components, but even these interactions are controlled by the particle size.

Furthermore, the level of toxicity will also vary with cell type, and the dependence on particle size may also be cell type dependent, since different cell types secrete different types of proteins, which in turn will interact differently with the nanoparticles. Here again, the determining factor will be the particle diameter.

Hence the challenge of this thesis is to design experiments where I isolate the effect of dimensionality and be able to probe the interactions of these particles with different cell types, different proteins, different incubation conditions. Furthermore, by studying the effects of the particles on different cell types, which are interdependent within tissue, one may be able to use this data to predict the effects on an organ when exposed in vivo.

More specifically, the aims of the project are:

1) To investigate the mechanism of AuNPs penetration and interactions with different types of the skin cells.
2) To understand how the penetration rate of the nanoparticles into cells depend on the cell type, nanoparticle aspect ratio, and exposure time.
3) To find out how the location of the nanoparticle inside the cell depends on cell type and aspect ratio of the particle.
4) To verify the intracellular processes can be triggered by the nanoparticles.
5) To test whether cellular gene regulation and protein expression is enhanced or inhibited by the nanoparticles
6) To study the possibility of cell function recovery after the removal of the external nanoparticle source.

Successful completion of the research will make possible to describe the nature of the gold nanoparticle toxicity and will make the base for development of environmental and health regulations on gold nanoparticles.

As a result of this research it will be possible to develop general picture of the effect of gold nanoparticles on human skin cells, which make possible to formulate fundamental principles of toxicological evaluation.

CHAPTER 2

GOLD/CITRATE NANOPARTICLES SYNTHESIS AND CHARACTERISATION

2.1. Synthesis of gold nanoparticles stabilized with citric acid.

In this project two different size AuNPs were synthesized with an identical chemistry of the surface coating.

In general, to produce metal nanoparticles the reducing agents are reacting with a metal compound. For gold, the reducing agent is sodium citrate, and the starting gold compound is hydrochloroauric acid. When they react, the colloidal AuNPs are stabilized by a protective layer of citrate, chloride and sodium ions.

The simplified chemical reaction of the AuNPs formation process described above as follows:

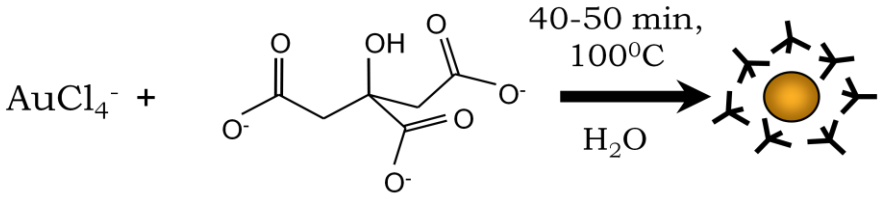

Where the citric acid plays the role of both a reducing and a stabilizing agent and therefore minimizes the amount of side products and contaminants.

To produce small 13nm Au/citrate nanoparticles the procedure of the Turkevich et al. [154, 155] was used. Briefly, $HAuCl_4$ (0.1ml, 30% wt solution in HCl (Aldrich)) in 95ml MilliQ water in a tree-necked flask equipped with condenser and thermometer was heated to boiling while stirring, after that sodium citrate (200mg, dehydrated, 99% (Aldrich)) in 5ml of water was added to the solution. Over a couple of minutes the color of the solution changed from yellow to grey and finally to purple. The solution was gently boiled for 40-50 minutes and then allowed to cool at room temperature.

To produce large 45nm Au/citrate nanoparticles synthesis was carried out in three-necked flask under condenser. 25 mg of $KAuCl_4$ was boiled in 98 ml MilliQ water following by addition of 2.5 ml of 1.5% sodium citrate under vigorous stirring. After the color changed from gray to purple, the nanoparticle solution was allowed to cool at room temperature.

In both cases the resulting particles were coated with negatively charged citrate and, therefore, were uniformly suspended (Figure 2).

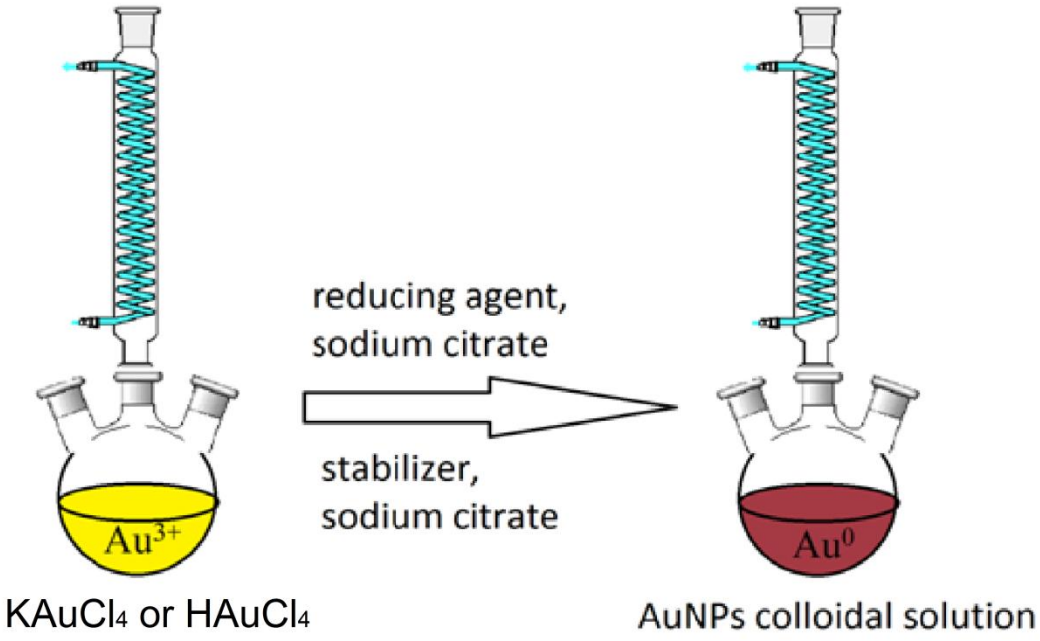

Figure 2. Synthesis of gold nanoparticles covered with citric acid.

2.2. AuNPs size measurement and size distribution.

The AuNPs were analyzed using Transmission Electron Microscopy (TEM) and Ultraviolet-visible spectroscopy (UV-vis).

TEM analysis:

TEM analysis was used to assess the size distribution of the AuNPs as well as the fate of internalized particles. One drop of the original AuNPs solution (0.95g/ml 13nm and 0.13g/ml 45nm particles) was placed on a 300 mesh copper grip, which was coated with formvar film. The sample was then dried at room temperature. Gaussian distributions of diameters were calculated from more than 170 nanoparticles (Fig. 3). Measurements shown by histograms (Fig. 3c and d) reveal that the average particles sizes were 13±1.1 nm and 45±3.2 nm.

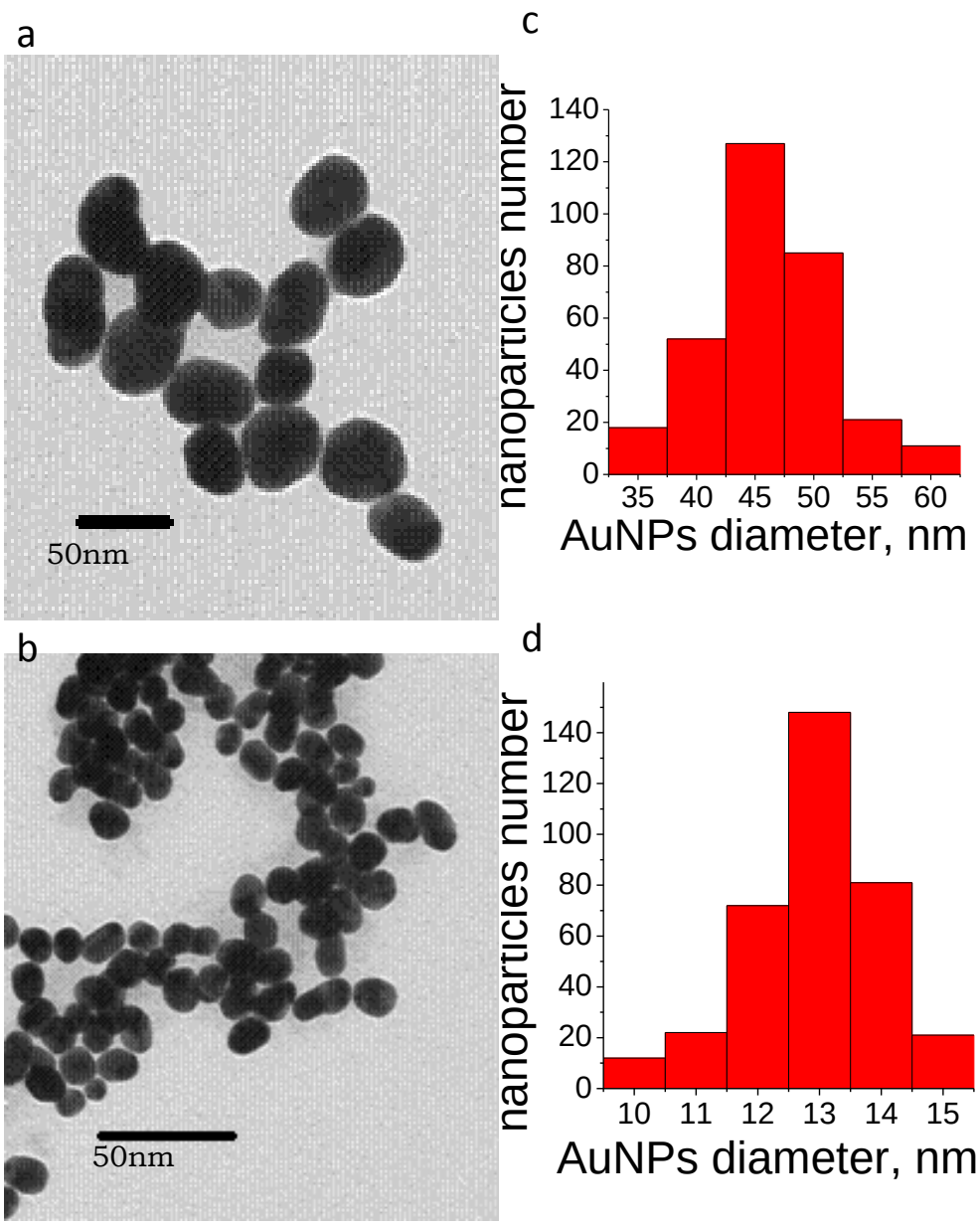

Figure 3. AuNPs imaged by TEM (on the left) and Gaussian size distribution histograms (on the right). a and c 45±5.1 nm particles, b and d 13±1.8 nm particles.

UV-vis Spectroscopy.

UV-vis spectroscopy is routinely used for AuNPs size and concentration determination [156-158]. It has been shown over the last decade that change in the wavelength of the Surface Plasmon Resonance (SPR) band provides information about particle size, shape and concentration as well as dielectric medium properties [25, 159-161]. This phenomenon is also called "gold nanoparticle red shift" and was originally described in the Mie theory [162] where a solution to the Maxwell equations was introduced, which made it possible to calculate the extinction and scattering efficiencies of small metal particles. The approach which was modified by Stratton [163] is used nowadays [164]. Recently Haiss et al. [156] published an elegant method to calculate the particle diameters from the UV-vis spectra. Haiss also showed how analytical relationships between extinction efficiency and diameter allow particle concentration to be calculated.

UV-vis spectras were acquired with a HP 8453 spectrophotometer. The spectra were obtained over the range of 190-860 nm. The characteristic absorbance peak was found around 500-550 nm and the data for both 13 nm and 45 nm are presented in Figure 4.

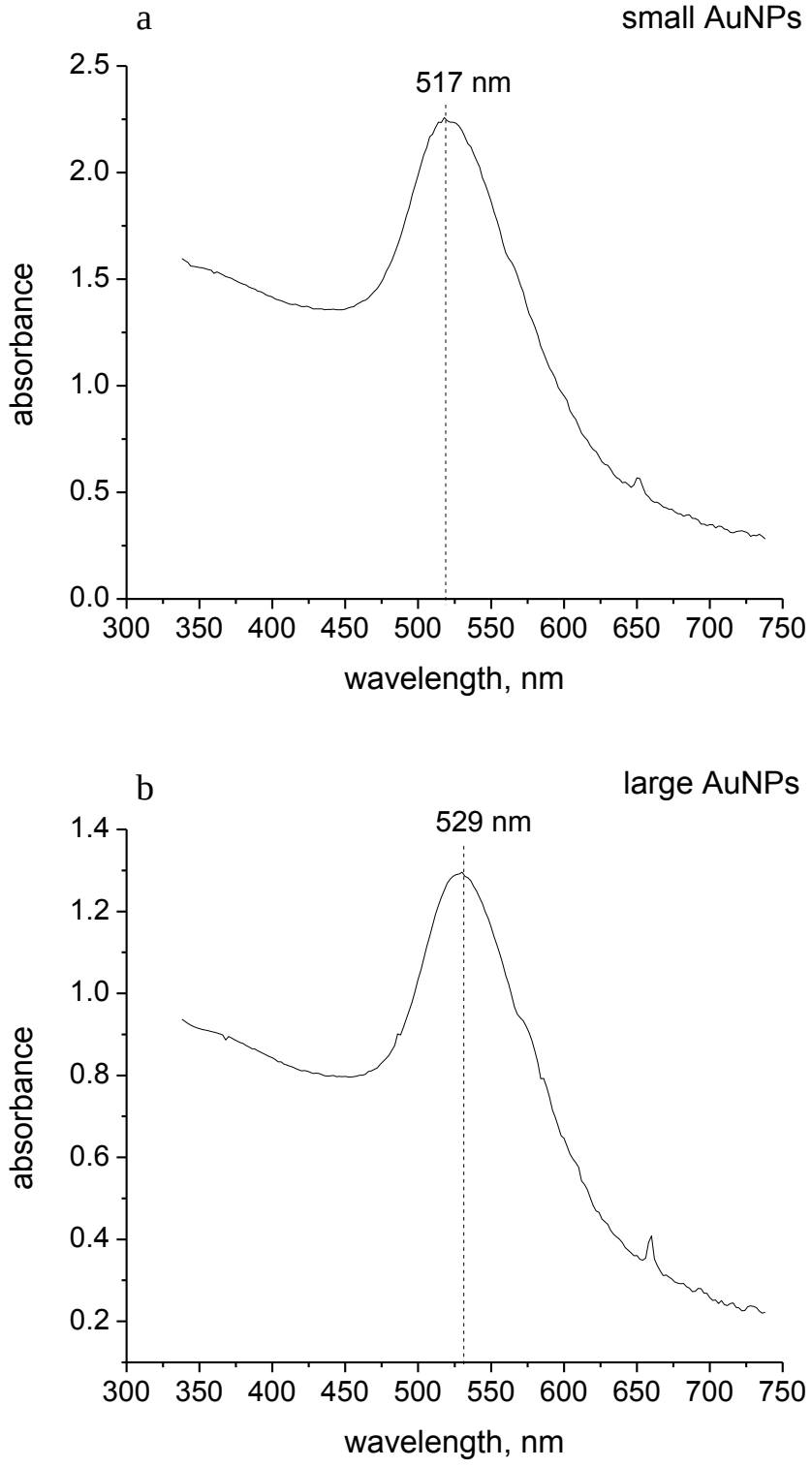

Figure 4. UV-vis spectras of the AuNPs of different sizes: (a) small (13 nm) AuNPs; (b) large (45 nm) AuNPs.

From the Figure 4a we can see that small AuNPs have an absorbance peak at 517nm. Using the Haiss at al. equation for particle size calculation when the expected diameter is less than 35 nm we can find the theoretical diameter of the nanoparticles (Equation 1):

$$d = exp(B_1 \cdot \frac{A_{spr}}{A_{450}} - B_2) \qquad (1)$$

Where d is nanoparticle diameter, A_{spr} is absorbance at the surface plasma resonance peak, A_{450} is absorbance at 450 nm, and B_1 and B_2 are fit parameters for the nanoparticle range 5-35nm: B_1=3.00; B_2=2.20.

Therefore the calculated nanoparticles diameter is:

$$d = exp(B_1 \cdot \frac{A_{spr}}{A_{450}} - B_2) = \exp\left(3.00 \cdot \frac{2.24}{1.38} - 2.20\right) = 14.23\, nm$$

The obtained diameter of the small AuNPs is 14.23 nm that is in a good agreement (less than 10% deviation) with the experimental data from TEM.

For the large AuNPs (Figure 4b) we observed the absorbance peak at 529 nm and we can calculate their size using the Haiss formula for the nanoparticles with an expected diameter 35-120nm:

$$d = \frac{\ln\left(\frac{\lambda_{spr} - \lambda_0}{L_1}\right)}{L_2} \qquad (2)$$

where d is a nanoparticle diameter, λ_{spr} is the wavelength at what the absorbance peak was observed, λ_0=512nm, L_1 =6.53 and L_2=0.0216 are the experimental fit parameters.

Therefore, the calculated diameter of the large AuNPs is:

$$d = \frac{\ln\left(\frac{\lambda_{spr} - \lambda_0}{L_1}\right)}{L_2} = \frac{\ln\left(\frac{529 - 512}{6.53}\right)}{0.0216} = 44.3\ nm$$

The calculated diameter of the large AuNPs is 44.3 nm that is in a good agreement (less than 3% deviation) with an experimental data from TEM.

According to Haiss et al. [156] the nanoparticle concentration (mole/L) can be calculated from the absorbance of the gold hydrosol because extinction efficiency at 450nm (ε_{450}) are perfectly fitted with Gauss function over large range of particles sizes.

$$c = \frac{A_{450}}{\varepsilon_{450}} \qquad (3)$$

Where c is the particles concentration, A_{450} is the absorbance at λ=450nm, and ε_{450} is the extinction at λ=450nm for the known particle diameter. For the small AuNPs we calculate:

$$c = \frac{1.36}{1.39 \times 10^8} = 9.78 \times 10^{-9} \text{ mole/L}$$

And therefore, the number density of AuNPs can be calculated from concentration of particles and Avogadro's number *n*:

$$N = c \times n = 9.78 \times 10^{-9} \times 6.022 \times 10^{23} = 5.89 \times 10^{15} \text{ particles/L}$$

that is comparable with the theoretical calculations of the particle number density from the initial concentration of gold in the reaction:

$$N = \frac{C_{Au}}{\left(\frac{4}{3}\right) \times \pi \times r^3 \times \rho} = \frac{0.96}{\left(\frac{4}{3}\right) \times 3.14 \times (6.5 \times 10^{-9})^3 \times 19320000}$$

$$= 5.12 \times 10^{15} \text{ particles/L}$$

where *r* is radius of the particle, C_{Au} is the initial concentration of gold in kg/L and ρ is the density of gold in kg/m^3.

For the large AuNPs the particle concentration is equal to:

$$c = \frac{0.8}{6.5\times10^{9}} = 1.23 \times 10^{-10} \text{ mole/L}$$

The number density of AuNPs is:

$$N = c \times n = 1.23 \times 10^{-10} \times 6.022 \times 10^{23} = 7.41 \times 10^{13} \text{ particle/L}$$

that is comparable with the theoretical calculations:

$$N = \frac{C_{Au}}{\left(\frac{4}{3}\right) \times \pi \times r^3 \times \rho} = \frac{0.13}{\left(\frac{4}{3}\right) \times 3.14 \times (22.5 \times 10^{-9})^3 \times 19320000}$$

$$= 6.72 \times 10^{13} \text{ particles/L}$$

Hence, the concentration and size of the AuNPs synthesized by the Turkevich method were estimated by two distinct techniques. The obtained results were in agreement within the 10% error.

2.3. AuNPs stability and supernatant toxicity

The stability of AuNPs dispersion depends upon the balance of repulsive and attractive forces that exist between particles as they approach one another. If all the particles have a mutual repulsion then the colloidal solution will remain stable. On the other hand, if AuNPs have little or no repulsive force then some instability mechanism such as flocculation or aggregation will eventually take place.

The Au particles in the colloidal solution are negatively charged, repel each other and stay in solution. However, salts, such as NaCl, shield the negative charges allowing the particles to clump together to form aggregates. To prevent aggregation the nanoparticles coated with sodium citrate. AuNPs colloidal solutions appear to be stable for more than 6 months, with no detectable precipitation or agglomeration of nanoparticles.

To estimate the stability of the AuNPs upon the storage we measured zeta potential for the samples of the different shelf life time, starting from freshly prepared and proceeding to the samples stored for 6 month. Zeta potential gives the degree of repulsion between nanoparticles, and therefore can be used as an indication of the long-term stability of the product. However, if the particles have low zeta potential values then there is no prevention technique for the particles flocculating. In Figures 4 and 5 we show experimental data for the freshly prepared 13 nm and 45 nm AuNPs. In all cases we observed the negative charge on the surface on the nanoparticles which indicates the presence of the citrate coating. We detected the decrease of zeta potential values for the samples with increasing storage time. From the Table 1 we can see that the zeta potential values for the 13 nm AuNPs decrease from the -51.94±1.27 mV to the -30.56±1.96 mV in 6 months.

In case of the 45 nm AuNPs the decrease is more rapid (Table 2) even though, the freshly prepared solution has a zeta potential comparable with the 13nm particles -44.75±1.8 mV it has a very fast decay with a zeta potential of -12.06±1.40 mV after 6 months of storage. Hence, the smaller nanoparticles appear to be more stable than the larger ones; the acceptable storage time for the samples is 2 months.

Table 1. Zeta potential and mobility values for the 13 nm AuNPs.

13nm AuNPs	Mobility	STD	Zeta Potential, mV	STD
Freshly prepared	-4.06	0.10	-51.94	1.27
2 month old	-3.92	0.14	-50.15	1.78
4 month old	-3.81	0.15	-48.77	1.89
6 month old	-2.45	0.21	-30.56	1.96

Table 2. Zeta potential and mobility values for the 45 nm AuNPs.

45nm AuNPs	Mobility	STD	Zeta Potential, mV	STD
Freshly prepared	-3.50	0.10	-44.75	1.26
2 month old	-2.53	0.16	-32.35	2.04
4 month old	-2.08	0.09	-26.66	1.10
6 month old	-0.94	0.11	-12.06	1.40

Measurement Parameters:

Mean Zeta Potential	= -51.94 mV	Liquid	= Water
Zeta Potential Model	= Smoluchowski	Temperature	= 25.0 °C
Mean Mobility	= -4.06 (μ/s) / (V/cm)	Viscosity	= 0.890 cP
pH	= 7.10	Refractive Index	= 1.330
Conductance	= 1650 μS	Dielectric Constant	= 78.54
Concentration	= 0.05 mg/mL	Particle Size	= 13.0 nm

Instrument Parameters:

Sample Count Rate	= 248 kcps	Voltage	= 4.00 volts
Ref. Count Rate	= 1104 kcps	Electric Field	= 7.64 V/cm
Wavelength	= 659.0 nm	User1	= 0.00
Field Frequency	= 2.00 Hz	User2	= 0.00
Target Residual	= 3.6000e-02		

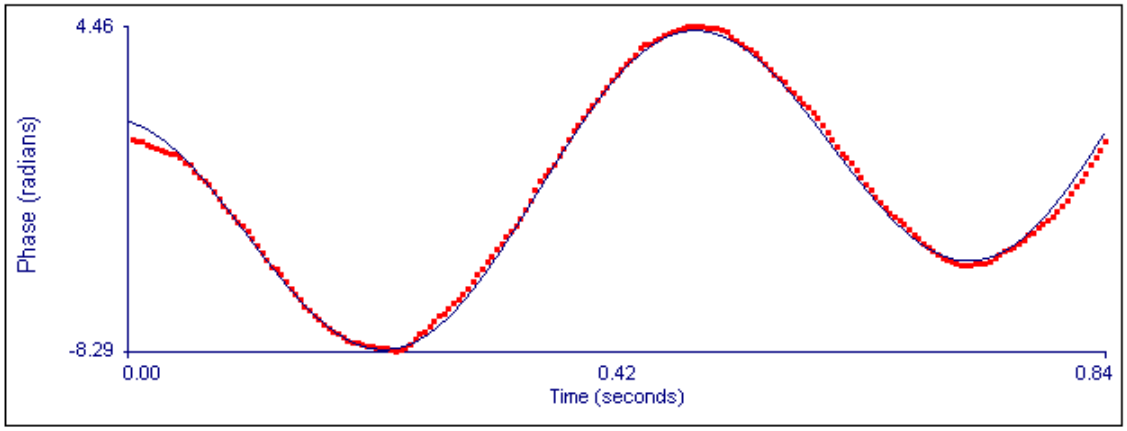

Run	Mobility	Zeta Potential (mV)	Rel. Residual
1	-4.30	-55.02	0.0335
2	-4.28	-54.75	0.0350
3	-4.22	-54.00	0.0323
4	-3.64	-46.64	0.0298
5	-3.68	-47.06	0.0329
6	-3.95	-50.51	0.0349
7	-4.44	-56.80	0.0357
8	-3.65	-46.77	0.0355
9	-4.40	-56.33	0.0337
10	-4.02	-51.50	0.0355
Mean	-4.06	-51.94	0.0339
Std. Error	0.10	1.27	0.0006
Combined	-4.05	-51.88	0.0152

Figure 5. Zeta potential and particle mobility measurement data for the 13 nm AuNPs.

Measurement Parameters:

Mean Zeta Potential	= -44.75 mV	Liquid	= Water
Zeta Potential Model	= Smoluchowski	Temperature	= 25.0 °C
Mean Mobility	= -3.50 (μ/s) / (V/cm)	Viscosity	= 0.890 cP
pH	= 7.10	Refractive Index	= 1.330
Conductance	= 357 μS	Dielectric Constant	= 78.54
Concentration	= 0.05 mg/mL	Particle Size	= 45.0 nm

Instrument Parameters:

Sample Count Rate	= 419 kcps	Voltage	= 4.00 volts
Ref. Count Rate	= 920 kcps	Electric Field	= 9.16 V/cm
Wavelength	= 659.0 nm	User1	= 0.00
Field Frequency	= 2.00 Hz	User2	= 0.00
Target Residual	= 3.7000e-02		

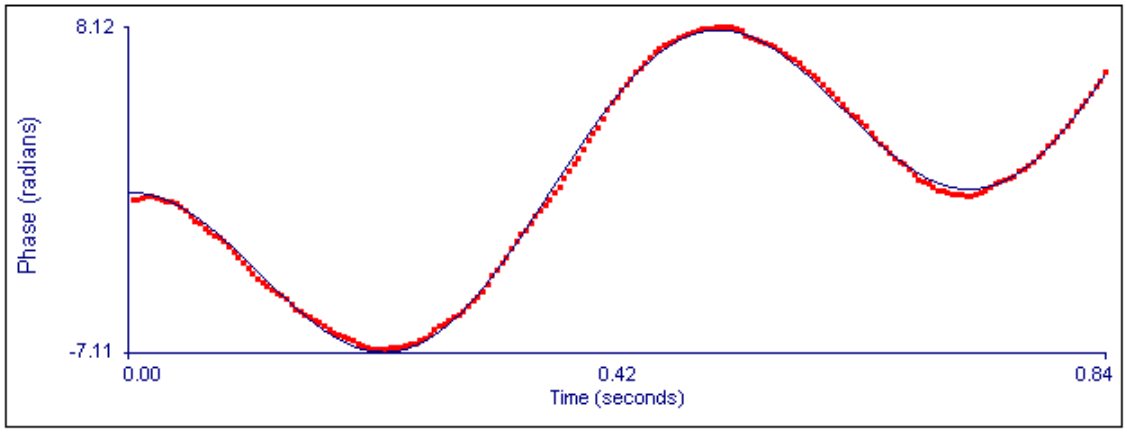

45nano_#27 (Combined)

Run	Mobility	Zeta Potential (mV)	Rel. Residual
1	-3.23	-41.33	0.0304
2	-3.48	-44.51	0.0368
3	-3.90	-49.89	0.0355
4	-3.56	-45.58	0.0369
5	-3.87	-49.48	0.0357
6	-3.15	-40.25	0.0345
7	-3.21	-41.15	0.0366
8	-3.84	-49.10	0.0318
9	-3.64	-46.56	0.0346
10	-3.10	-39.67	0.0369
Mean	-3.50	-44.75	0.0350
Std. Error	0.10	1.26	0.0007
Combined	-3.47	-44.36	0.0122

Figure 6. Zeta potential and particle mobility measurement data for the 45 nm AuNPs.

Metallic nanoparticles are known to dissolve in solvent during the storage [165]. Dissolution is one of the reasons causing toxicity of metallic nanoparticles solution in the environment and within the organisms. The dissolving rate depends on two factors: the metal solubility within a given environment and the concentration gradient between the particle surface and the bulk solution phase [166]. For example, widely used antibacterial and antifungal properties of Ag^0 and Cu^0 nanoparticles depend on the release of Ag^{2+} and Cu^{2+} ions in the solution caused by the [167].

To estimate the release of Au^+ ions from the AuNPs after different storage time human dermal fibroblasts were used as reporter cells. The aging of the colloidal gold solutions was determined in terms of supernatant toxicity due to release of the gold ions with respect to cell viability. The AuNPs solutions were stored for 1, 3 and 6 months at 4°C in the dark, after that an aliquot of the solution was centrifuged at 13000 rpm for 12 hours to ensure that all particles precipitated. The clear supernatant was separated from the sediment on the bottom of the test tube by pipeting. Human dermal fibroblasts were treated with 150 µl/ml dose of supernatant for 3 days, after that, cells were tripsynized and counted using the hemacytometer. Cell viability was measured as a function of cell number (Figure 7). From the figure we can see, that after the first month of storage the supernatants are not toxic to the cells, indicating the stability of the AuNPs and the slow rate of the nanoparticles dissolution. However, after 3 months of storage, cells treated with the supernatants showed decreases in viability of 40-50%, indicating an increasing concentration of positively charged gold ions Au^{3+}. The supernatant toxicity becomes more pronounced after 6 month of colloidal solution storage and cells treated for 3 days with half a year old supernatant have a viability less than

15%, indicating that the concentration of the gold ions in the solution have reached a critical level.

Hence, in this study all experiments were conducted with the freshly prepared AuNPs that have been stored for the duration of experiments but not longer than a month.

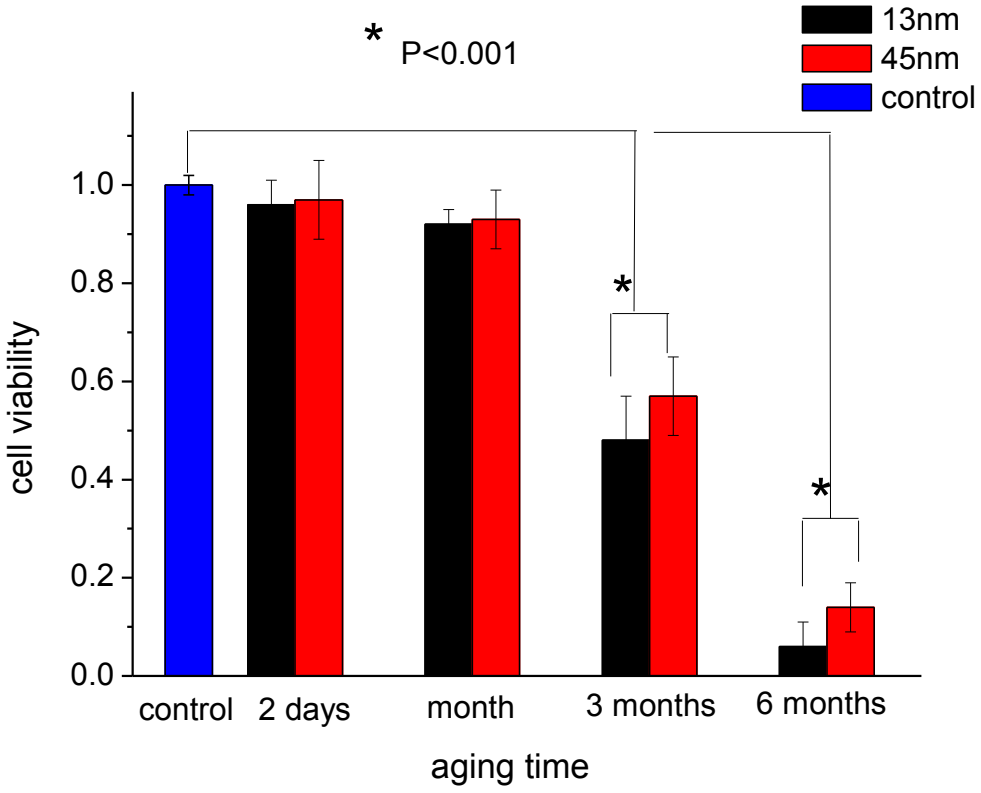

Figure 7. AuNPs supernatant toxicity vs. solution storage time.

CHAPTER 3

GOLD NANOPARTICLES INTERACTION WITH HUMAN SKIN CELLS

3.1. AuNPs effect on human keratinocytes

Even though it is not typical for the AuNPs to be topically applied to the skin, direct skin contact may occur during the manufacturing, handling and usage of the AuNPs. Keratinocytes are design as a protective cell layer for the entire organism; hence penetration rate for the nanoparticles is expected to be lower for the keratinocytes than for other cell types. However, even a small amount of nanoparticles inside the cell can lead to the significant changes and as a result affect the complete skin tissue by the disrupting cell protein expression and cell signaling.

3.1.1. Materials and Methods

Cell culture end exposure to AuNPs. Keratinocytes DO33 (Living Skin Bank, Stony Brook) were maintained in Dulbecco's Modified Eagle's Medium (DMEM) supplemented with 1% of Penicillin-Streptomycin (PS) and 10% of Fetal Bovine Serum (FBS) (all purchased from Sigma). Keratinocyte differentiation was carried out in the growth media KGM-2 supplemented with Bovine Pituitary Extract (BPE, 0.4%), human recombinant epidermal growth factor (rhEGF, 0.1%), insulin (0.1%), hydrocortisone (0.1%), transferrin (0.1%) epinephrine (0.1%) and gentamicin sulfate amphotericin-B (GA-1000, 0.1%) all purchased from Lonza.

Keratinocytes DO33 were exposed to the different concentrations of 13nm AuNPs (95 μg/ml, 145 μg/ml and 190 μg/ml) and 45 nm AuNPs (13 μg/ml, 20 μg/ml and 26 μg/ml) up to 6 days.

TEM analysis. TEM analysis was used to assess the fate of internalized particles. After exposure to AuNPs for 3 and 6 days at 142 μg/ml (13 nm) and 20 μg/ml (45 nm), the cells were fixed in a solution of 2% paraformaldehyde and 2.5% glutaraldehyde in 0.1M Phosphate Buffered Saline (PBS), stained in 2% uranyl acetate, dehydrated with ethanol, then embedded in Propylene oxide. The specimen was cut into ultrathin sections (90 nm) with Reichart UltracutE ultramicrotome and stained on the grid with uranyl acetate and lead citrate. The samples were imaged using a FEI Tecnai12 BioTwinG2 transmission electron microscope. Digital images were acquired with an AMT XR-60 CCD Digital Camera System and compiled using Adobe Photoshop program.

AuNPs uptake. 500,000 cells were plated in 75cm^2 tissue culture flasks. 24 hours after the plating AuNPs (13 μg/ml 45 nm and 142 μg/ml 13 nm AuNPs) were added and incubated with cells for 3 days. After that cells were harvested, counted and sent to Columbia Desert Analytical for gold content analysis by atomic absorption.

Cell counting. To determine the cell number during the growth curve experiments cells were plated at a density of 5000 cells per well and counted using hemacytometer at the specific time points (up to 8 days). Each condition had triplicates and all experiments were conducted three times. Cell suspensions were mixed for uniform distribution and were diluted enough so that the cells did not aggregate.

Cell Staining for Confocal Microscopy. Cell area and overall morphology as a function of time and concentration was monitored using a Leica confocal microscope. For these experiments, cells were fixed with 3.7% formaldehyde for 15 minutes, and stained with Alexa Fluor 488–Phalloidin to detect actin fibers and Propidium Iodide to detect the nuclei.

Western blotting. Proteins were extracted with Radioimmuno- presipitation Assay (RIPA) Lysis and Extraction Buffer (25 mM TrisHCl, pH 7.6, 150 mM NaCl, 1% NP-40, 1% sodium deoxycholate, 0.1% SDS, Pierce Biotechnology) and were separated by SDS-PAGE (0.9g of protein was applied per lane) and blotted onto nitrocellulose membrane (Millipore, Beverly, MA). The membranes were blocked with 5% non-fat milk and probed with diluted monoclonal antibodies (Anti-actin Clone AC-40, obtained from Sigma and Anti-human involucrin, gift from M. Simon, Living Skin Bank, Stony Brook) at 4°C for one hour. After washing, bound antibodies were detected with anti-mouse IgG coupled to HRP (1:10,000) at room temperature for 1h. The signal was visualized by using Enhanced Chemiluminescence (ECL) (Amersham Pharmacia Biosciences, Piscataway, NJ).

3.1.2. Results and Discussion

Since there is no agreement in the literature about whether or not nanoparticles penetrate cells, the first step in the investigating of AuNPs impact on human keratinocytes is the elucidating the ability of this nanoparticles to enter the cell.

Nanoparticles penetration and uptake were monitored by the Optical Microscopy, EDS/X-ray Microanalysis, TEM and atomic adsorption methods.

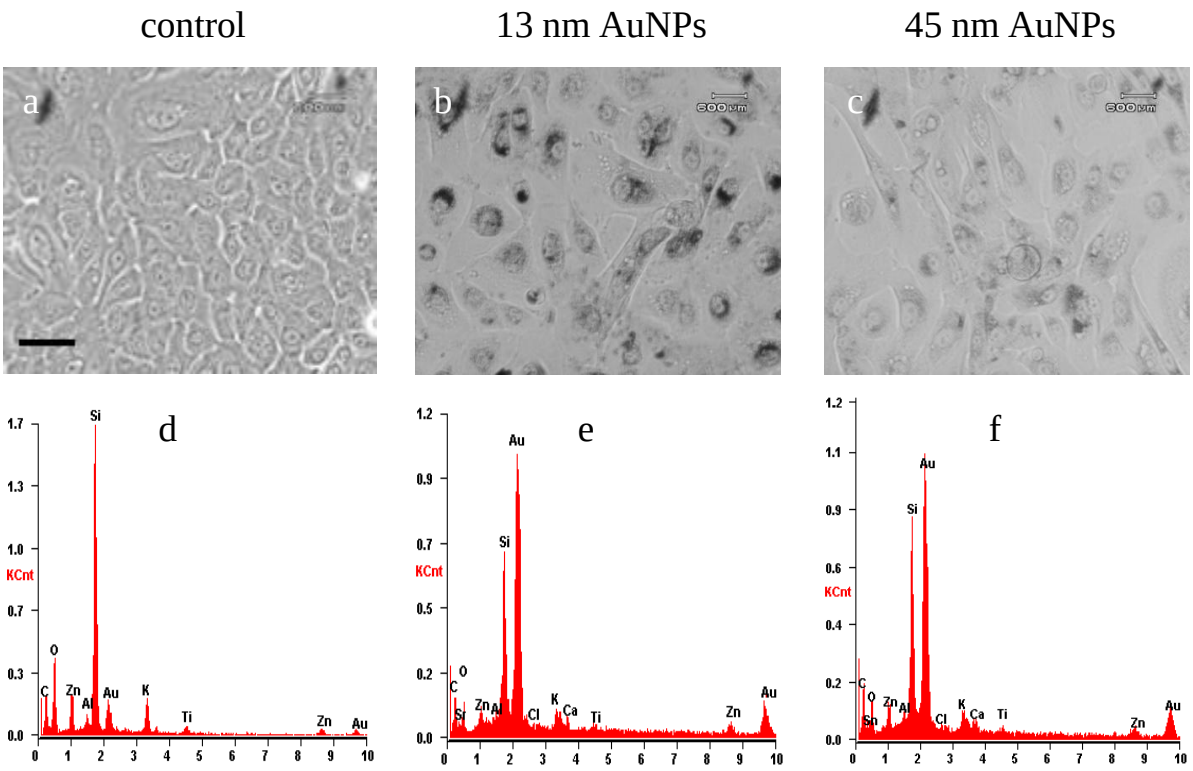

Figure 8. Human keratinocytes DO33 cultured with AuNPs for 3 days: Optical Microscopy pictures of the: (a) control; (b) 142 μg/ml 13 nm AuNPs; (c) 20 μg/ml 45 nm AuNPs; and EDS/X-ray Microanalysis for the same samples: (d) control; (e) 13 nm AuNPs; (f) 45 nm AuNPs.

The AuNPs penetration to the keratinocytes was visualized by the optical microscopy (Fig. 8a-c). As solid objects AuNPs block the light and therefore can be clearly seen under the optical light microscope. As we can see, control samples (Fig. 8a) have no NPs, however samples exposed to the 13 nm AuNPs (Fig. 8b) and 45 nm AuNPs (Fig. 8c) clearly have dark accumulations around the nucleus indicating nanoparticles entry to the cell. This observation was also confirmed by the EDS/X-ray microanalysis (Fig. 8d-f) that revealed a significant Au k_{α} peak at 2.3 keV only in the cells that were exposed to AuNPs (Fig. 8e-f) but not in the control samples (Fig.8 d).

The penetration rate for 13nm and 45nm AuNPs was found to be 2.5 fold different (Fig. 9). However, the concentration difference was approximately 7 folds indicating that AuNPs uptake into the cell is related to the particle penetration pathway.

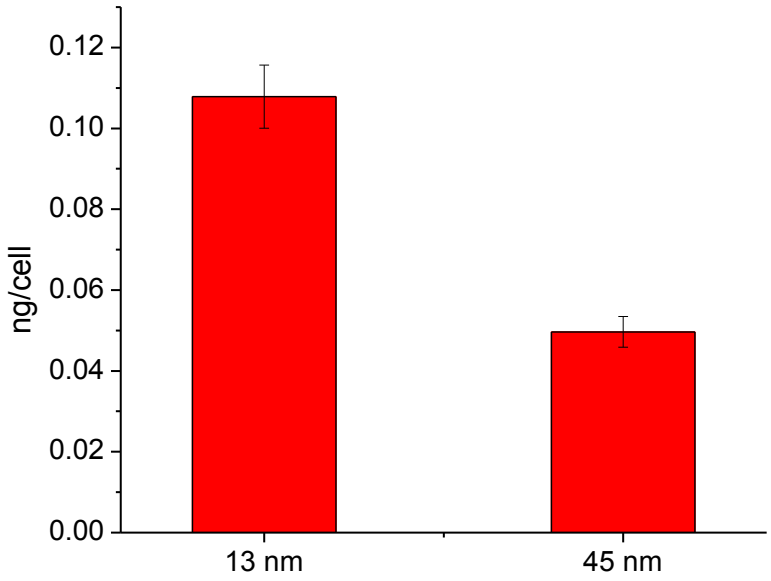

Figure 9. AuNPs uptake by the keratinocytes DO33. Cells were treated with 20 μg/ml 13 nm and 142 μg/ml 45 nm AuNPs for 3 days.

Intracellular fate of internalized AuNPs. The TEM data (Fig. 10) shows that both 13 nm and 45 nm AuNPs penetrate the keratinocytes and sequestered in vacuoles around the nucleus. No evidence of nucleic or mitochondrial penetration was found. Particles are agglomerated in large vacuoles that form a ring around the nucleus (Fig. 10b-c). Consistent with the atomic absorption results (Fig. 9) the density of the 13 nm AuNPs is significantly higher than that of the 45 nm particles.

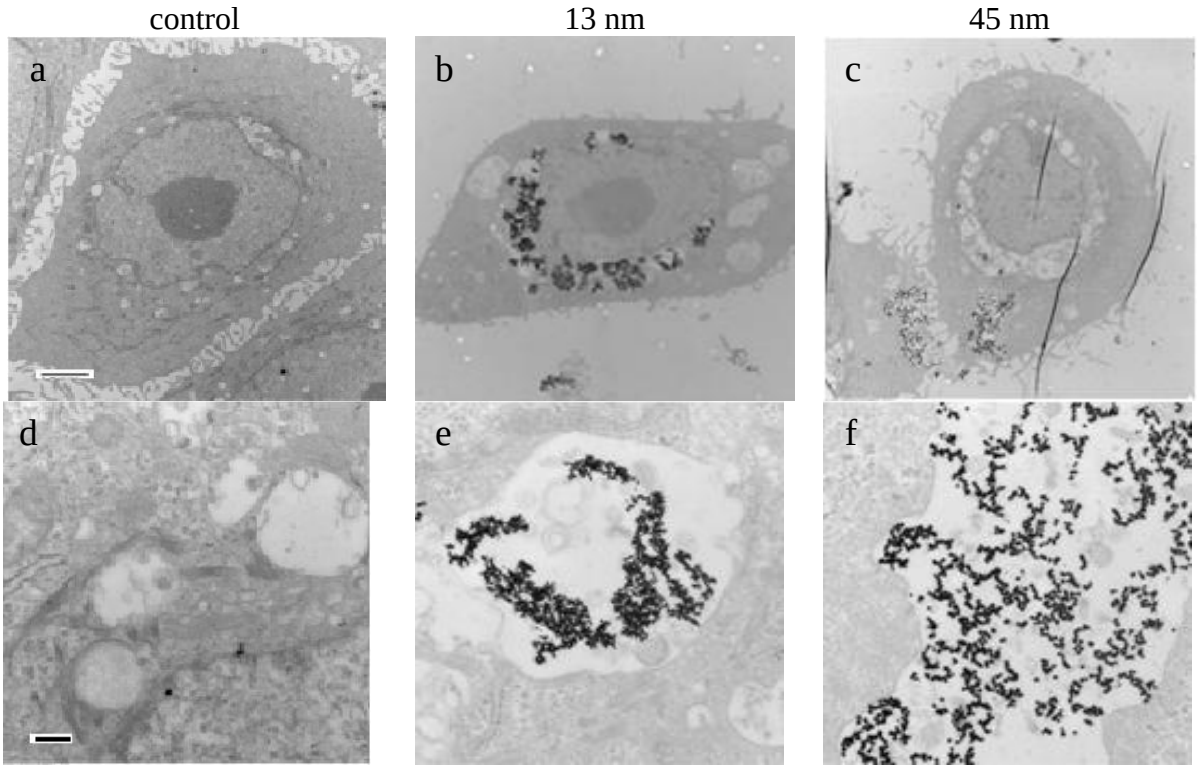

Figure 10. TEM images of the keratinocytes DO33. Cells were treated with 20 μg/ml 13 nm and 142 μg/ml 45 nm AuNPs for 3 days. (a) control; (b) 13 nm; (c) 45 nm; (d) HR TEM control; (e) HR TEM 13 nm; (f) HR TEM 45 nm AuNPs.

AuNPs impact on the cell proliferation and morphology. The growth curves in Figure 11 show that cell proliferation rates decrease with increasing AuNPs concentration. The decrease (for all concentrations) for 45 nm particles is much larger compared to the 13 nm particles, even though the concentration range of smaller AuNPs is approximately 7 times higher than the concentration of the 45 nm, indicating that large nanoparticles are more toxic. Specifically, our data indicates that on Day 1 the control cells as well as those that were exposed to 13 nm and 45 nm AuNPs for 24 hours showed almost the same number of cells (Fig. 11a and b). In contrast, at day 3, we can clearly see that those cells that were exposed to AuNPs showed a decrease of ~20-30% for the 13 nm and 45 nm

particles respectively. A much larger decrease of ~30-45% and 35-60% was observed, for the 13 nm and 45 nm particles at day 5 respectively. After 7 days, the damage become more pronounced showing the decrease in cell viability of up to 50% for the cells exposed to 13 nm nanoparticles and up to 70% when exposed to the 45 nm AuNPs.

We also addressed the question of possibility of cell recovery after the AuNPs removal from the cell environment. The recovery cell growth experiment was conducted in parallel with the experiment previously described (Fig. 10c-d), where cells were cultured with AuNPs for 3 days and after that allowed to recover for 5 days (Fig. 11). As we can see the cell number after recovery is draw alongside to control, indicating that the recovery process took place. The recovery rate is faster for the samples exposed to the 13 nm AuNPs compared to the 45 nm ones.

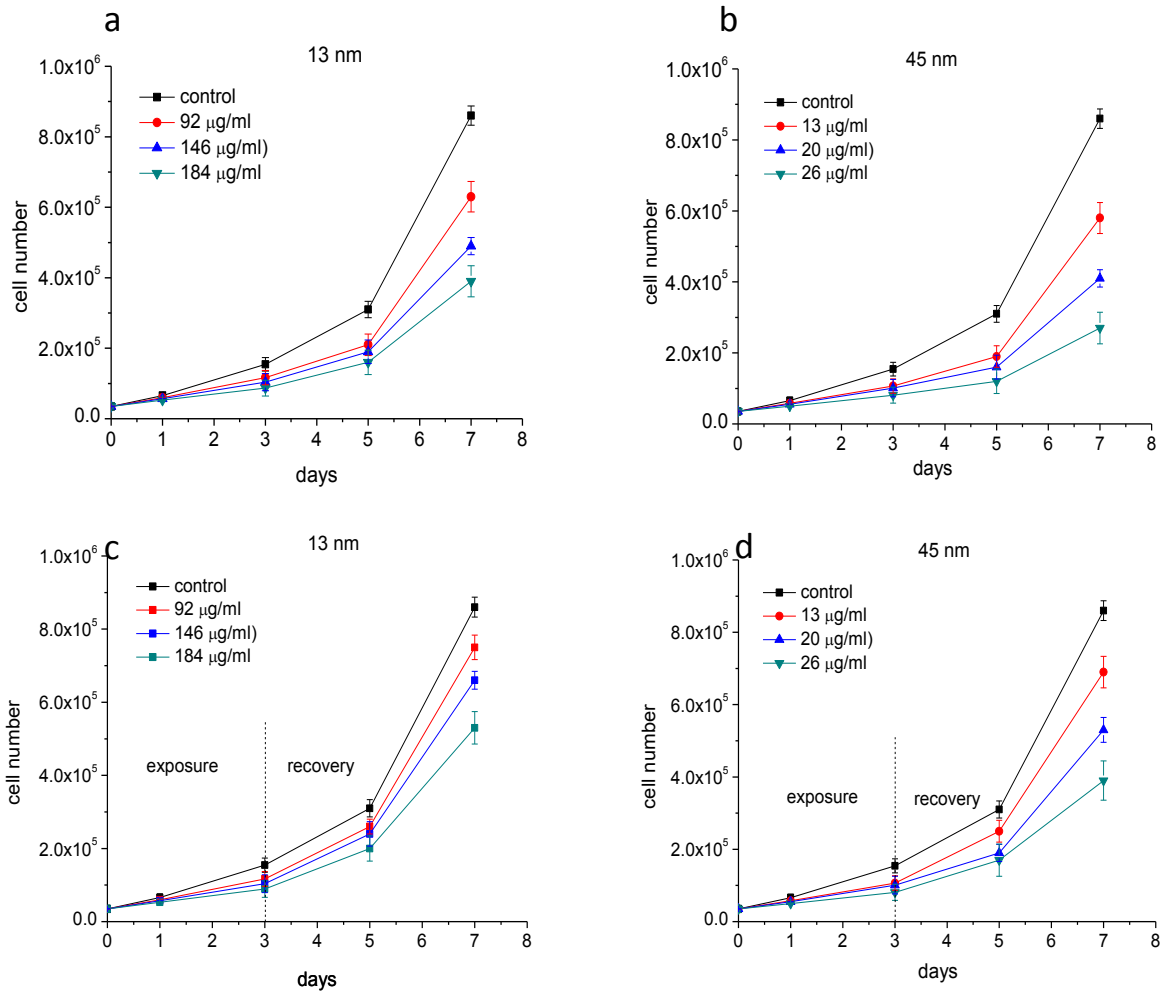

Figure 11. Growth curves of the human keratinocytes DO33 exposed to AuNPs and allowed to recover. (a-b) exposure for 8 days; (c-d) exposure for 3 days following by the recovery for 5 days.

Next we wanted to monitor the effects of the nanoparticles on the overall morphology of the keratinocytes. Using confocal microscopy, we show that 3 days after exposure, damage to the cells, as a function of size is not observable for the samples exposed to 13nm and 45nm (Fig. 12b and c) compared to control (Fig.12a). The cell number seems to be lower for the samples exposed to the both sizes of the AuNPs what is consistent with the previous observations. The damage become apparent 7 days after the exposure (Fig. 12e and f) were samples with AuNPs reveal the broken actin fibers. In all cases of exposure (13nm and 45nm) the cell number is reduced in the samples containing nanoparticles (absence of a uniform cell monolayer, Fig. 12d and f, compared to d). We also observed the change in morphology after the long exposure to AuNPs: cells did not form tight connections (Fig. 12e and f).

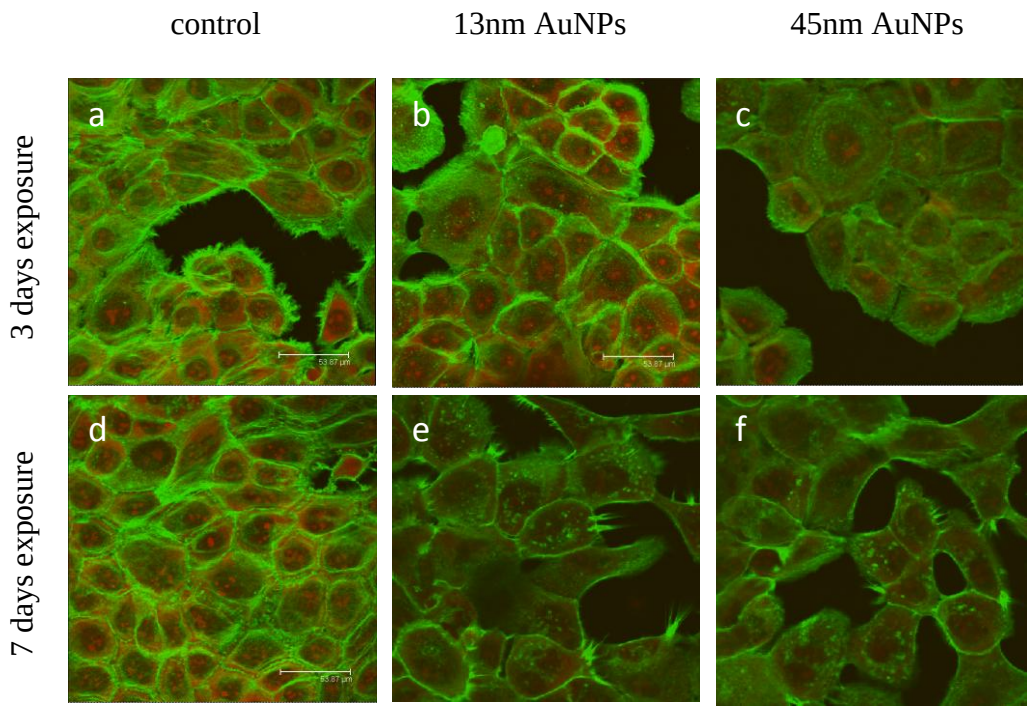

Figure 12. Confocal images of the human keratinocytes DO33 3 and 7 days after exposure to AuNPs. 3 days after: (a) control; (b) 20 μg/ml 13 nm; (c) 142 μg/ml 45 nm; 7 days after: (d) control; (e) 20 μg/ml 13 nm; (f) 142 μg/ml 45 nm.

Protein expression. Epidermal keratinocytes are extremely specialized epithelial cells designed to perform a very explicit function – the separation of organism from the environment. To accomplish that cells synthesize precursors and assemble them into two distinct structures: the cornified envelope and keratin intermediate filaments. The intermediate filaments are assembled from keratin monomers and the cornified envelope is assembled from different proteins including involucrin. Expression of involucrin and the keratins genes are regulated

as a function of the stage of keratinocyte differentiation [168]. Therefore, the expression of the differentiation marker protein involucrin was investigated.

One set of the DO33 keratinocytes were cultured with AuNPs for 3 days and after that differentiated for 3 days in the absence of nanoparticles. The parallel set of samples was differentiated for 3 days in the presence of AuNPs. Both experiments had a control – untreated cells that were differentiated for 3 days. From the Figure 13 we can see that no difference in the amount of the involucrin was detected by Western Blotting. Hence, AuNPs do not affect the differentiation ability of the keratinocytes.

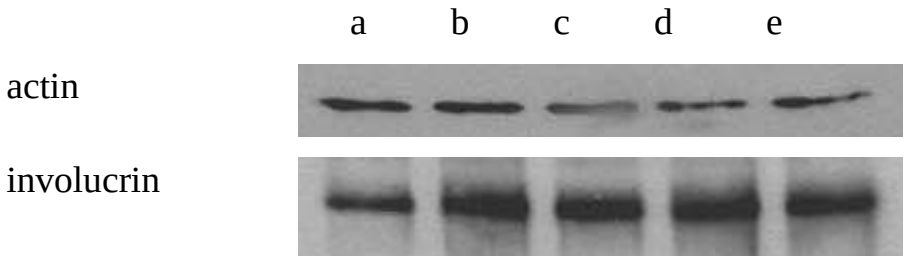

Figure 13. Protein expression by the human keratinocytes DO33 cultured with AuNPs. (a) control untreated cells; (b) cells treated with 142 μg/ml 13 nm AuNPs for 3 days prior to differentiation; (c) cells treated with 20 μg/ml 45 nm AuNPs for 3 days prior to differentiation; (d) cells differentiated with 142 μg/ml 13 nm AuNPs for 3 days; (e) cells differentiated with 20 μg/ml 45 nm AuNPs for 3 days.

3.2. AuNPs effect on Human Dermal Fibroblasts

The next skin layer subjacent to the epidermis is called dermis and consists on the human dermal fibroblast cells. These cells have no mechanism of protection from invasion of external objects or viruses. Therefore, the question of the effect of AuNPs on this type of cells has to be thoroughly investigated.

3.1.1. Materials and Methods

Cell culture. Primary human dermal fibroblasts (CF-31, Caucasian female, 31 years old, National Institute on Aging (NIA) Bank, passage 7-14 only) were plated at cell density 2,500 cells per well and cultured in 24-well dishes. Dulbecco's Modified Eagle's Medium (DMEM) was used with 1% of penicillin-streptomycin (PS) and 10% of fetal bovine serum (FBS) (all purchased from Sigma). 1 ml of medium containing AuNPs (with concentrations in the range of 0-189 μg/ml in case of 13 nm and 0-26 μg/ml in case of 45 nm) was added to each well 24 hours after plating. The wells were incubated with AuNPs for the chosen time points (up to 6 days) and then counted or fixed, stained and imaged. All incubations were performed at 37^{o}C and 5% CO_2. Each experiment had a control (cells grown in medium without AuNPs), and was performed in triplicate and repeated at least three times.

Cell counting. To determine the cell number during the growth curve experiments cells were plated at an initial density of 2,500 cells per well and counted using hemacytometer at the selected times (up to 8 days). Each condition had triplicates and all experiments were conducted three times. Cell suspensions were mixed for uniform distribution and were diluted enough so that the cells did not aggregate.

Cell Staining for Confocal Microscopy. Cell area and overall morphology as a function of time and concentration was monitored using a Leica confocal microscope. For these experiments, cells were fixed with 3.7% formaldehyde for 15 minutes following exposure to AuNPs for 3 and 6 days. Alexa Fluor 488–Phalloidin was used for actin fiber staining and Propidium Iodide for nuclei staining. In addition, a set of images was obtained using an Hg lamp with the excitation filter of 450-490 nm and the emission filter at 515nm.

TEM. TEM analysis was used to assess the size distribution of the AuNPs as well as the fate of internalized particles. One drop of the original AuNPs solution (95 μg/ml 13 nm and 13 μg/ml 45 nm particles) was placed on 300 mesh copper grip, which was coated with formvar film. The sample was then dried out at room temperature. Gaussian distributions of diameters were calculated from the samples with more than 170 nanoparticles. After exposure to AuNPs for 3 and 6 days at 142 μg/ml (13 nm) and 20 μg/ml (45 nm), the cells were fixed in a solution of 2% paraformaldehyde and 2.5% glutaraldehyde in 0.1 M Phosphate Buffered Saline (PBS), stained in 2% uranyl acetate, dehydrated with ethanol, and then embedded in Propylene oxide. The specimen was cut into ultrathin sections (90nm) with Reichart UltracutE ultramicrotome and stained on the grid with uranyl acetate and lead citrate. The samples were imaged using a FEI Tecnai12 BioTwinG2

transmission electron microscope. Digital images were acquired with an AMT XR-60 CCD Digital Camera System and compiled using Adobe Photoshop program.

SEM. SEM analysis was used to assess the uptake of particles by exposing cells to 20 μg/ml 45 nm AuNPs and to 142 μg/ml 13 nm AuNPs for 3 days, following by fixing (3.7% formaldehyde in PBS) and then multi step ethanol dehydration. Samples were coated with a thin layer of atomic Au for conductivity and imaged by SFEG SEM LEO 1550.

Apoptosis induction and quantification. Apoptosis was induced by the use of Recombinant Human Tumor Necrosis Factor-alpha (RH TNF-α, Biosource). An anti-ACTIVE Caspase-3 pAb (Promega) and Cy3 conjugated secondary antibody was used to determine whether cells underwent apoptosis after exposure to AuNPs for 3 and 6 days at different concentrations (13 nm AuNPs : 95 μg/ml, 142 μg/ml and 190 μg/ml: 45 nm AuNPs: 13 μg/ml, 20 μg/ml and 26 μg/ml). Cells were also stained with DAPI to reveal the nuclei (Invitrogen). The percentage of apoptotic cells per sample was determined using the images captured during fluorescent microscopy. For this experiment, 15 random images were captured for each sample (samples were in triplicate and the experiment was repeated twice).

Western blotting. Proteins were extracted with RIPA Lysis and Extraction Buffer (25mM TrisHCl, pH 7.6, 150mM NaCl, 1% NP-40, 1% sodium deoxycholate, 0.1% SDS) and were separated by SDS-PAGE (50 μg of protein was applied per lane) and blotted onto nitrocellulose membrane (Millipore, Beverly, MA). The membranes were blocked with 5% non-fat milk and probed with diluted monoclonal antibodies (Anti-actin Clone AC-40, obtained from Sigma and anti-β-tubulin (E7) developed by Klymkowsky and obtained from the Developmental Studies Hybridoma Bank (The University of Iowa, Department of Biological

Sciences, Iowa City, IA 52242) at 4°C for one hour. After washing, bound antibodies were detected with a goat anti-rabbit IgG or anti-mouse IgG coupled to HRP (Sigma, 1:10,000) at room temperature for 1 h. The signal was visualized by using ECL (Amersham Pharmacia Biosciences, Piscataway, NJ).

Clathrin mediated endocytosis inhibition. Cells were cultured in 24-well dish for 24 hours, after that PAO [44] solution in 1% DMSO was added to obtain a final concentration 2.0 M. After 20 minutes of pre-treatment with PAO, the AuNPs were added to medium and the cells were cultured for another 2hrs, rinsed with PBS, and fixed for TEM as described above.

Endocytosis inhibition. Cells were plated in tissue culture flasks ($75cm^2$) under normal conditions (37^oC, DMEM, 5% CO_2) for 24 hours. The cells were then exposed to AuNPs for 24 hours either at low temperature (4^oC, DMEM, 5% CO_2) or at 37^oC as control. The cells were then counted and sent to Columbia Analytical Inc. for gold content analysis by atomic absorption spectroscopy.

Collagen and Fibronectin expression. Collagen and fibronectin were analyzed in supernatants of cultured CF-31 cells by Procollagen Type I C-Peptide EIA Kit (Takara, MK101) and human Fibronectin EIA Kit (Takara, MK115) as described in instructions provided by the manufacturer. Samples with high concentrations of collagen and fibronectin were appropriately prediluted with Sample Diluent.

Cell migration. Cell migration was evaluated using the agarose droplet assay. The agarose gel was prepared by dissolving 2% (w/v) agarose stock solution in DMEM to the final concentration of 0.2% (w/v). Then, the 0.2% (w/v) agarose was added to the cell pellets and the cells were re-suspended to a concentration of 1.5×10^7 cells/ml. 1.25µl were then loaded on the prepared hyaluronic acid (HA)

and fibronectin- functional domains (HA/FNfd) hydrogel surfaces in a 24-well dish. The whole dish was than placed at 4ºC for 20 minutes to allow the agarose droplet to gel before the addition of 400µl of DMEM into each well. Following a 24 hr incubation at 37ºC, the cells were visualized under a microscope. To quantify cell migration, the area of agarose droplets and the area covered by the leading edges of the migrating cells were measured using imageJ software. The cell migration distance was defined as the distance of the outward cell migration from the agarose droplets edge.

Collagen gel contraction. Cells were grown and exposed to 13 µg/ml 45 nm and 142 µg/ml 13 nm AuNPs for 3 days. After that cells were trypsinazed, counted and suspended in prepared collagen solution (1.8 mg/ml purified collagen, 2% BSA, 100ng/ml PDGF in DMEM with P/S/G) at 3.5×10^5 cells/ml. Cell/collagen gels were loaded into a BSA coated 24-well dish with 0.7 ml/well. After preincubation for 2 hours to gel the mixture, collagen gels were gently detached by slight tapping on the wells and 500 µl DMEM with 2% BSA and 100 ng/ml PDGF were added. After 5 hours at 37°C, images of gels were taken and analyzed by measuring the gel area.

3.1.2. Results and Discussion

Size and time dependent uptake of AuNPs. Since gold is more electron dense than the surrounding organic material it was clearly visible under SEM (Fig. 14). The images shown in Figure 14 clearly reveal the outline of the cell. The brighter regions are indicative of gold, outside the nuclei (Fig. 14a-d). This observation was confirmed by EDS/X-ray Microanalysis, which shows the Au Kα peak at 2.3 keV, indicating the presence of AuNPs clusters inside the cells (Fig. 14e). In the control cells (not exposed to AuNPs), the Au peak is very small, probably resulting from the gold thin film coating used for conductivity (Fig. 14g).

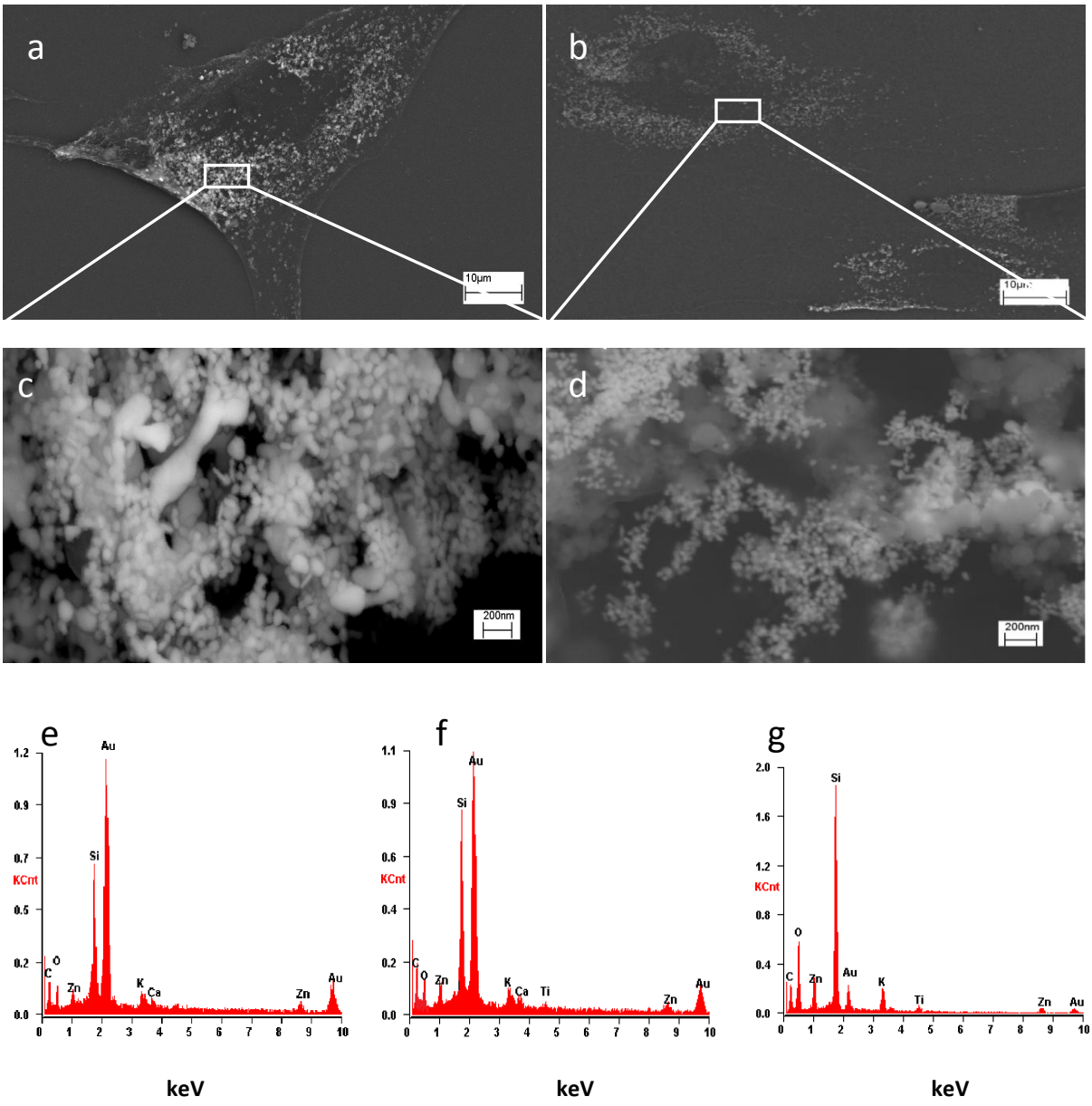

Figure 14. SEM and EDAX pictures of cells being exposed to AuNPs for 3 days. a and c. SEM images of cells exposed to 20 µg/ml 45 nm AuNPs; b and d SEM image of cells exposed to 142 µg/ml 13 nm AuNPs; e, f and g EDAX spectrum of cells with 13 nm, 45 nm and without any AuNPs, respectively.

The impact of AuNPs on cell proliferation. Results in Figure 15 show that for both particle sizes, the cell doubling time increased with higher AuNPs concentration and longer exposure. If we compare the concentrations for which the cell doubling time increases from 35 to 45 hours, we find that the concentration of the 13 nm particles, on average, is seven times higher than that of the 45 nm particles (at day 2 and 4) and increases to nearly a factor of 10 after 6 days of incubation. The inset graphs show that the doubling time increases as a function of time for both particles sizes suggesting that saturation is not occurring, and for a specific concentration of AuNPs (20 μg/ml 45 nm and 142 μg/ml 13 nm), the effect is almost equivalent at day 4 and 6. In attempt to directly compare the effects of the 13 nm and 45 nm size AuNPs, we chose exposure concentrations based on their effect on doubling time (Fig. 15). We observed that for a 2-6 day time interval, the concentration difference for two nanoparticle sizes (for the same doubling time increase) varies by 6-13 folds. This significant variation occurs because of the concentration-doubling time non-linearity over time. The average concentration that causes the same increase in cell doubling time for cells exposed to 13 nm particles is larger than the concentration of the 45 nm particles by roughly a factor of eight. Therefore, a set of 3 concentrations 13 μg/ml, 20 μg/ml and 26 μg/ml was chosen for 45 nm AuNPs and a set of 95 μg/ml, 142 μg/ml and 190 μg/ml for 13 nm AuNPs.

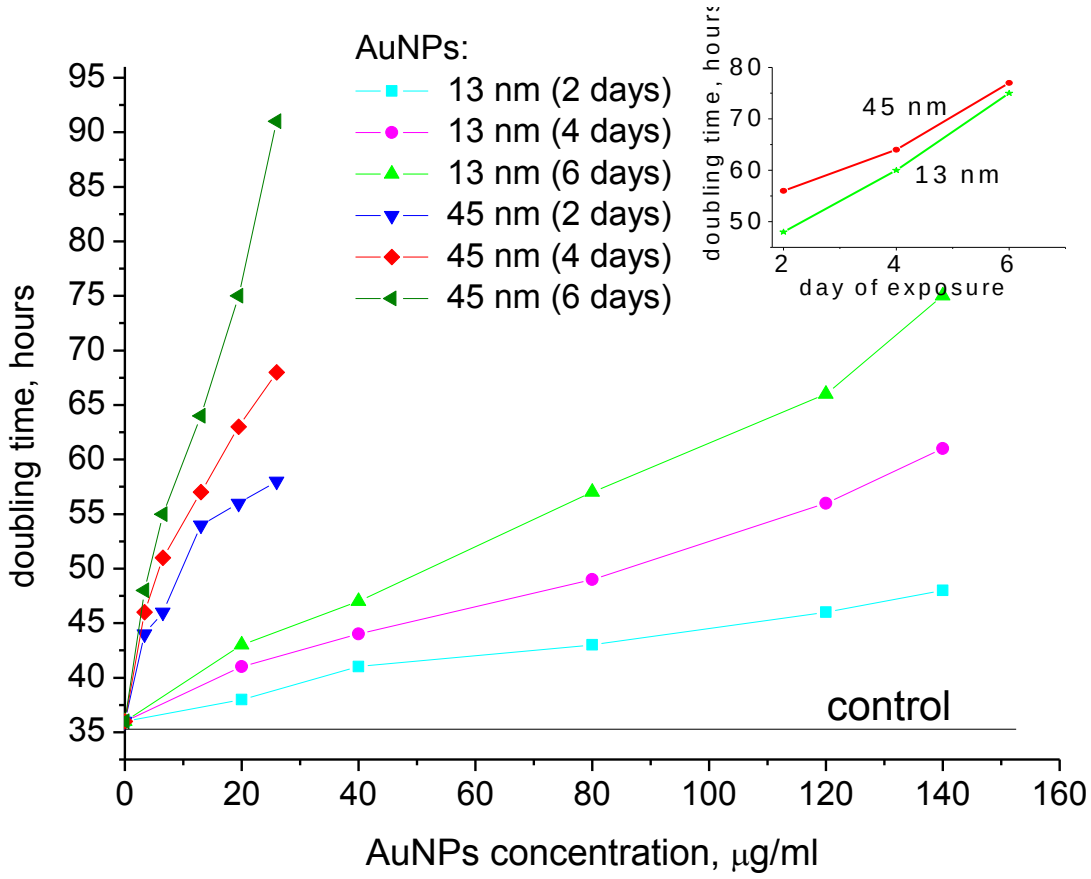

Figure 15. Doubling time for samples exposed to different concentrations of AuNPs 13nm and 45nm for 2, 4 and 6 days, inset: doubling time versus time of exposure for samples exposed to 20 μg/ml 45 nm and 142 μg/ml 13 nm AuNPs.

Intracellular fate of internalised AuNPs. The data clearly shows that for both particle sizes the AuNPs are sequestered inside large vacuoles and do not penetrate either the nucleus or the mitochondria (Fig. 16 and 17). The vacuoles are distributed uniformly across the cytoplasm (Fig. 16 and 17), consistent with the particle distribution observed in the dry samples imaged with SEM (Fig. 14). Closer examination also shows that even after 6 days, no particles were detected inside the nucleus or mitochondria (Figure 16c and 17c). We also present higher magnification images revealing that neither the 13 nm nor the 45 nm particles are uniformly distributed within vacuoles. Rather, we find that both types of particles are accumulated along the vacuole membrane, leaving the interior almost empty (Figure 16e and 17e). In the case of the 13 nm particles, their density around the membrane is greater and we can see sections of the membrane protruding inside the vacuole with particles still attached to it (Figure 16e). In contrast, with the 45 nm particles, only a "monolayer" string of particles covers the membrane surfaces and no particles were seen attached to the thinner tendrils.

The vacuoles appear to be "full" when available membrane surfaces are covered with particles. As a result, the concentration of AuNPs that they can hold is inversely proportional to the cross sectional area of the particles. Comparing cross sections obtained from cells incubated for 3 and 6 days, we find that the mean diameter of the vacuoles increases by approximately a factor of 2 while the number of particles per vacuole increases by a factor of 4-5. Hence the number of particles within a vacuole increases in a manner proportional to the available increased area which the particles could subtend on the membrane surface.

Further, with increasing incubation time additional AuNPs (both sizes) enter the cell, causing the formation of greater number of vacuoles as well as increasing the diameter of the existing vacuoles (Fig. 18a and b). Specifically, we find that the number and diameter of vacuoles per cell increases at the same rate for both types

of AuNPs (average of 7 cells for each conditions were examined). The major difference between samples exposed to the two AuNP sizes is the number of particle clusters per vacuole, which is roughly 5 times greater with the 13 nm particles (Fig. 18c).

On the other hand, the size of the vacuoles is similar for the two types of particles after equivalent incubation times, and the number of vacuoles is nearly the same after 6 days of incubation. Thus, it is the number of vacuoles, rather than the absolute concentration of particles within the cell, that plays the largest role in disrupting normal cellular function. However, we do observe "loose" particles that are visible in the cytoplasm of cells exposed to 45 nm AuNPs for 6 days. This observation might be the result of vacuole structural instability at certain local particle concentrations. In essence, it is more difficult for the inner surface of a vacuole to equilibrate larger 45 nm AuNPs, leading to vacuole collapse and nanoparticle release in the cytoplasm. Therefore, our observations that toxicity correlates with vacuole number must be qualified by the fact that some vacuoles ruptured when exposed to 45 nm AuNPs, and thus were not counted. With the same intact vacuole number, the higher toxicity of cells exposed to the 45 nm AuNPs probably arises from additional vacuoles that collapsed and release the AuNPs in the cytoplasm leading to interference with normal cellular function and ultimately damaging the cell.

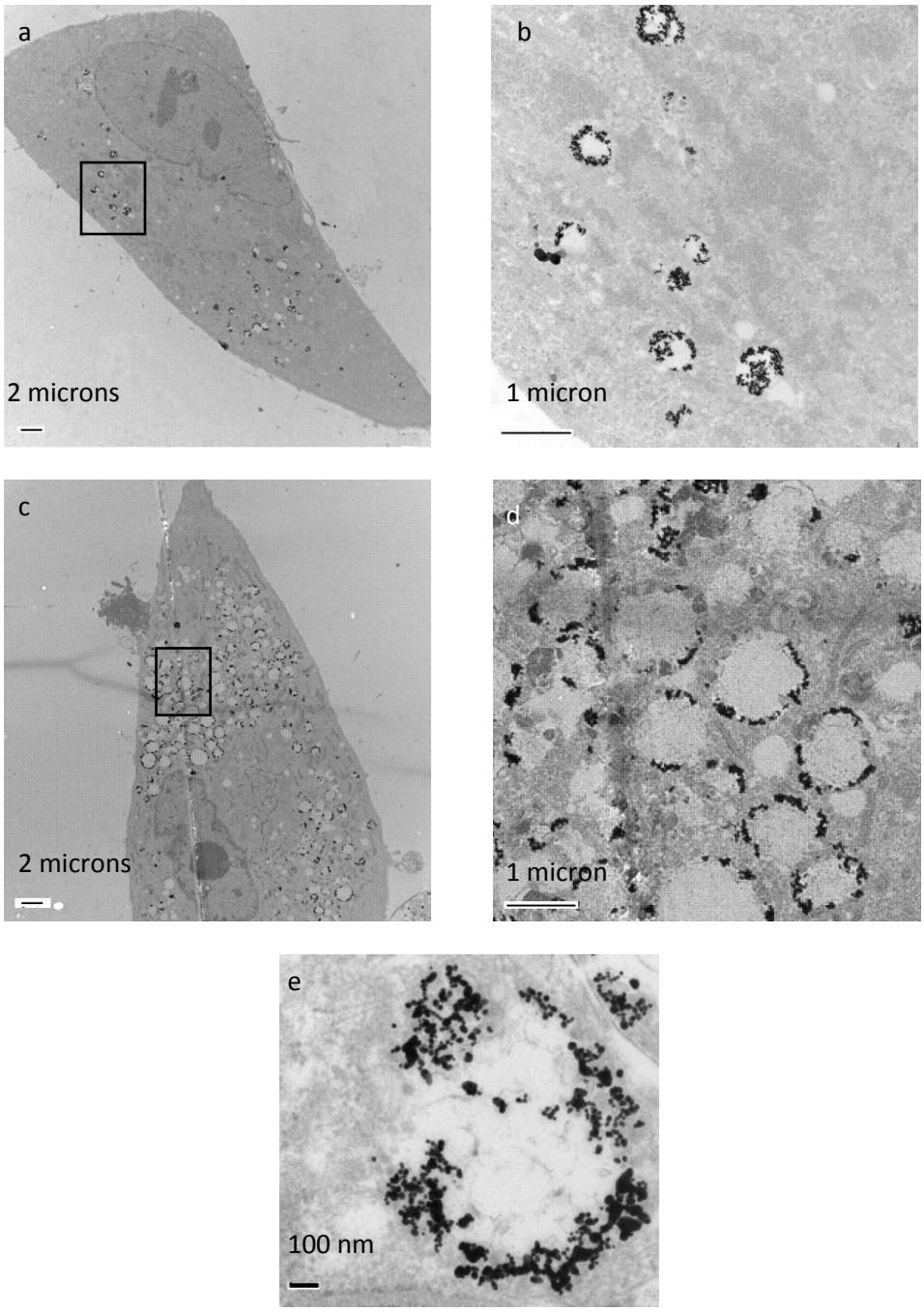

Figure 16. TEM section of cells exposed to 13nm AuNPs at different magnification, a and b – 142 μg/ml 13 nm nanoparticles 3 days exposure, c and d – 142 μg/ml 13 nm nanoparticles 6 days exposure, e - high magnification of cell vacuole exposed to 13 nm.

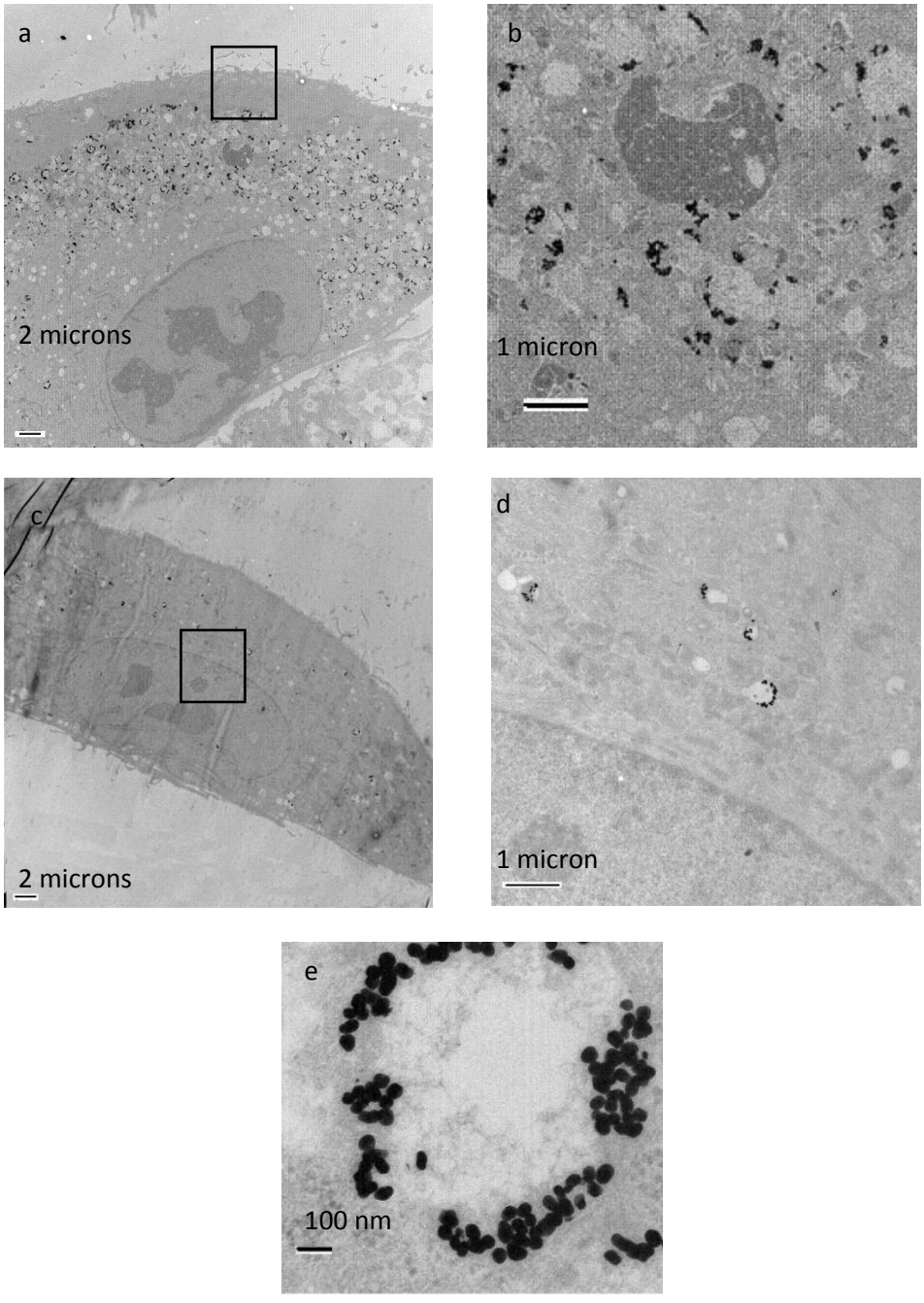

Figure 17. TEM section of cells exposed to 45nm AuNPs at different magnification, a and b – 20 μg/ml 45 nm nanoparticles 3 days exposure, c and d – 20 μg/ml 45 nm nanoparticles 6 days exposure, e - high magnification of cell vacuole exposed to 45 nm.

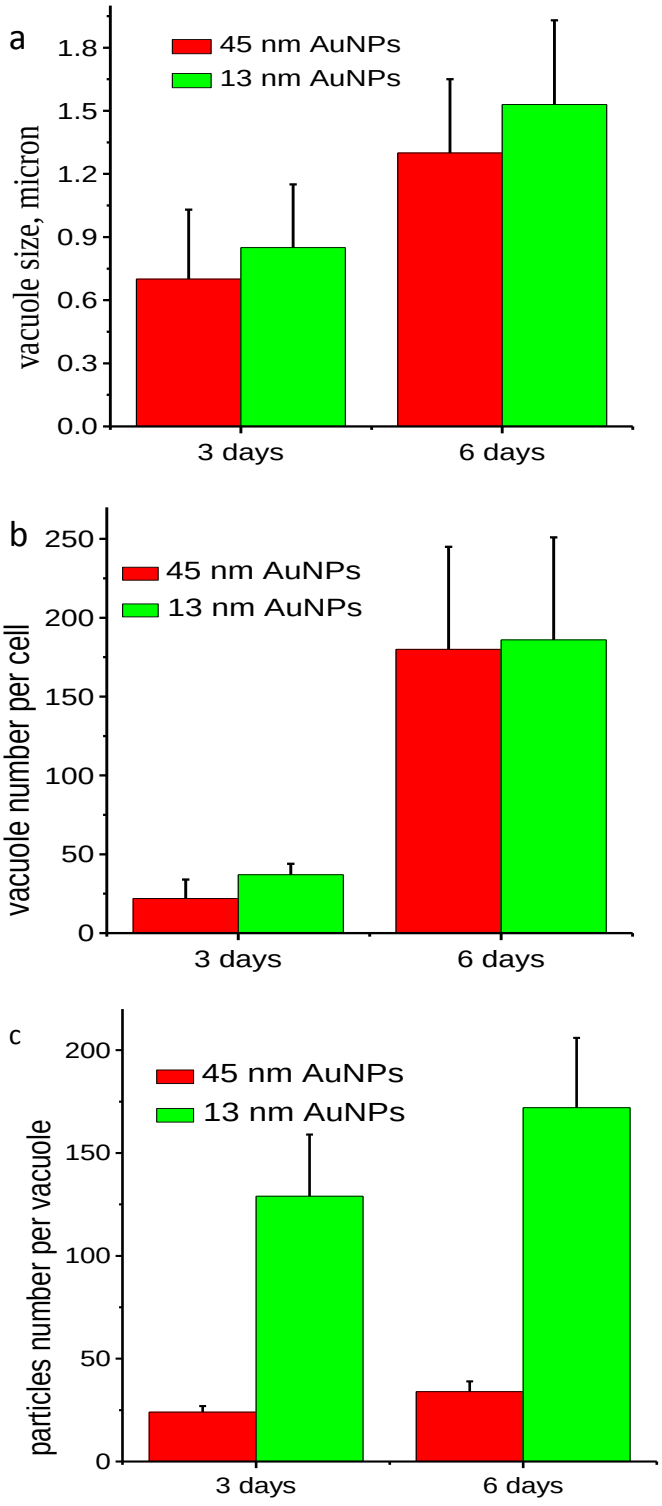

Figure 18. Inner cell morphology after AuNPs exposure. a – vacuole size distribution, b – number of vacuoles per cell, c – number of particles/clusters per vacuole.

In order to determine whether the mode of penetration of the AuNPs in the cells is a function of particle size, i.e. do some particles penetrate by passive diffusion through the cell membrane [169] or do they enter via endocytosis [139], clathrin mediated endocytosis was inhibited using PAO [170]. Following treatment of cells with PAO prior to AuNP exposure, the cells were fixed, sectioned, and examined with TEM (Fig. 19). The results were quantified by measuring the ratio of AuNPs adjacent to the cell membrane versus the number in the cytoplasm. Figure 19 shows that the number of AuNPs clustered in the vicinity of the cell membrane, and the number that penetrated the cells in the absence of PAO is nearly the same for both particle sizes. With exposure to PAO the ratio is nearly unchanged for the 13 nm particles (Fig. 19e), indicating that clathrin mediated endocytosis is not the predominant particle penetration pathway. In Figure 19f-i we show cross sections for cells treated with and without PAO and exposed to 45 nm AuNPs, revealing that almost no particles are present inside the cytoplasm of the treated cells, while a significant number is present in the untreated control cells. In fact, a strong accumulation of AuNPs is clearly seen outside of the membrane in the treated cells (Fig. 19i) and as a result, the ratio is reduced to nearly zero for the 45 nm particles, as compared to that of the control cells (Figure 19k), indicating that clathrin mediated endocytosis is the predominant mode of entry.

To further investigate if the major pathway for 13 nm AuNPs penetration is diffusion through membrane driven concentration gradients or non-receptor mediated endocytosis (phagocytosis), we utilized an approach involving temperature. Also, the dependence of the uptake on temperature will help to clarify whether non clathrin mediated endocytosis is responsible for particle penetration. Sudhakaran et al [171] have shown that endocytosis in human dermal fibroblasts decreases to approximately 15% with decreasing the temperature to 16^{o}C. A similar decrease was observed by Mamdouh et al [172] in epithelial cells, also they

found that at 4^{o}C endocytosis in epithelial cells is reduced nearly 95%. Our results show that with both small and large AuNPs, their uptake was inhibited. Specifically, when we decreased the incubation temperature to 4^{o}C, almost 90% of 13nm AuNPs cell penetration was inhibited (Fig. 19j). In contrast, only 70% of penetration was inhibited in case of 45 nm AuNPs (Fig. 19l), indicating that phagocytosis appears to be the prime mode of 13 nm AuNPs penetration, and also is partly responsible for the cell penetration of the 45 nm AuNPs. Though the amount of inhibition is significant, it is still smaller that that reported for endocytosis, indicating that other pathways may also play a role in overall particle uptake.

The data described herein supports pathway of AuNPs cell penetration in dermal fibroblasts; for 45 nm nanoparticles clathrin mediated endocytosis is the major pathway, while for the 13 nm it is phagocytosis. Another possibility may be that the particle size affects the amount of protein adsorbed, which in turn can affect the recognition pathway triggered when the particles attach to the cell membrane. Since the radius of gyration of albumin is approximately 3.5 nm, more molecules are likely to be adsorbed on the larger particles, with radii of 22 nm and surface area of ~1200 nm than on the smaller particles with radii of 6nm and surface area ~120 nm. Lastly, the ratio of particles inside and outside the cell, in the untreated control cells is an indication of the efficiency of the particular penetration mechanism used by the cells to bring the AuNPs across the cell membrane to the interior of the cell (PAO data).

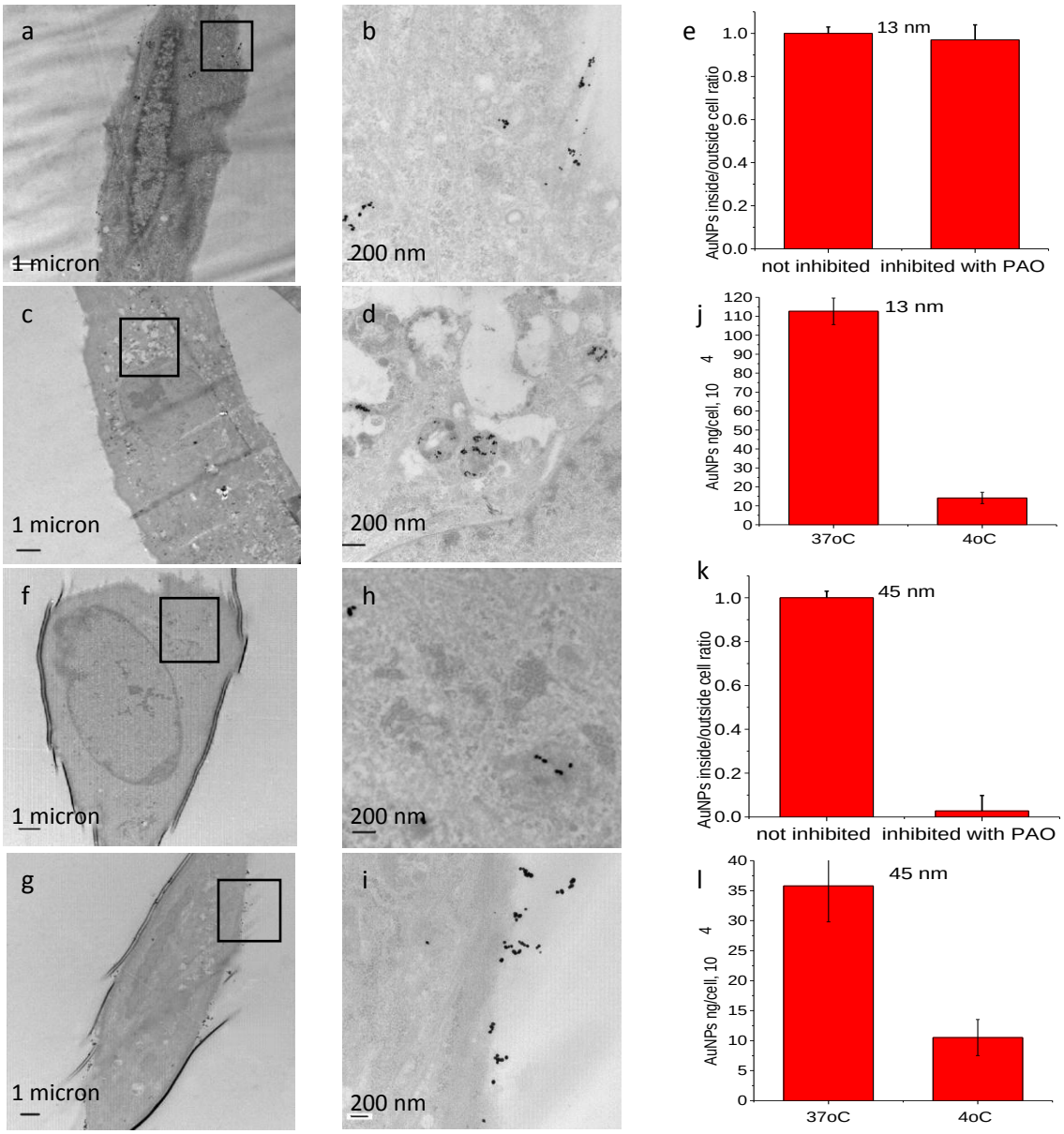

Figure 19. TEM sections of dermal fibroblast exposed to AuNPs for one hour, a-b. cells exposed to 142 μg/ml 13 nm gold, c-d. cells treated with PAO (give concentration) and exposed to 142 μg/ml 13 nm AuNPs, e. 13 nm AuNPs ratio inside and outside of the cell with PAO and without inhibition, f-h. cells exposed to 20 μg/ml 45 nm nanoparticles, g-i. cells treated with PAO and exposed to the same concentration of 45 nm gold, j. 45 nm AuNPs ratio inside/outside cell.

Cell recovery. Based on these results, an interesting question arises: do cells have a mechanism for eliminating AuNPs and thereby recover from their adverse

effects? In the simplest scenario the cells can pass the nanoparticles to daughter cells, therefore in the absence of particles in the media, the AuNPs concentration inside the cell becomes increasingly diluted. Hence, if the nanoparticles are removed from the environment, can the cells eventually recover from AuNP exposure? Thus, we tried to address these questions by specifically investigating whether cells containing AuNPs are still capable of dividing and passing the particles to the daughter cells.

In Figure 20 images of cells immediately before the removal of the particles, and 5 days later show that after 3 days of incubation, AuNPs uptake is greater for the 13 nm particles (Fig. 20b) than for 45 nm (Fig. 20e). After 5 days of incubation without AuNPs, a drastic reduction in the average amount of particles per cell is observed in cells exposed to both particle sizes (Fig. 20c and f). Thus, the major mechanism for AuNPs reduction appears to be cell division (Fig. 20d), where the particles are divide between the two daughter cells.

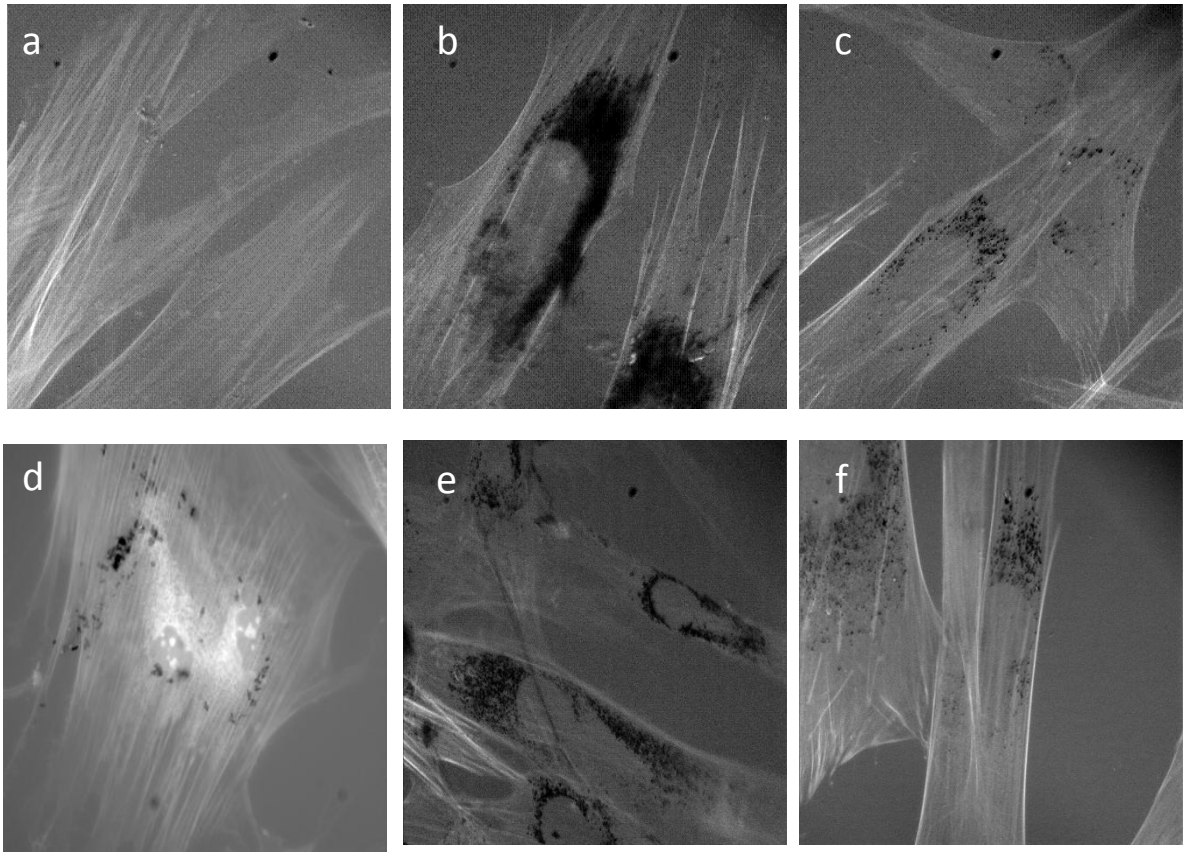

Figure 20. a. Control, b. Cells exposed to 20 μg/ml of 13 nm AuNPs after 3 days, c. Cells for the same concentration of 13 nm AuNPs after 5 days recovery following 3 days exposure, d. Cell transmitting nanoparticles to daughter cell upon dividing, e. Cells exposed to 142 μg/ml of 45 nm AuNPs after 3 days, f. Cells for the same concentration of 45 nm AuNPs after 5 days recovery.

Particle mediated apoptosis. To investigate whether exposure to AuNPs leads to detrimental effects for the cells, we examined the rate of apoptosis. Figure 21 shows the percentage of cells undergoing apoptosis exposed to different AuNPs concentrations and incubated for three and six days. We measured the fraction of cells undergoing apoptosis by assaying the production of caspase 3, which is a protein produced in the early stage of apoptosis. Cells producing this protein are adherent, but no longer divide, therefore for obtaining the precise doubling time, the number of cells have to be corrected by subtraction of apoptotic cells. AuNPs were previously reported to have no toxic effects [131], but others found that they induce apoptosis in certain cell types [131, 173, 174] clearly indicating cell type dependence of AuNPs cytotoxicity. However, even though Patra et al. [131] and Pan et al. [174] reported apoptosis in melanoma, fibroblast and macrophage cell lines, they did not test it with apoptosis specific assays. Further, we found that for the 13 nm particles, the fraction of cells undergoing apoptosis increases linearly with concentration at both incubation at 3 and 6 days, however, for 45 nm AuNPs it increases in exponential fashion with higher concentration for 3 days and almost 100% for all concentrations tested for 6 day exposure. Specifically, we find that in the presence of the 45 nm AuNPs there is a higher rate of apoptosis with either longer exposure or higher particle concentrations in comparison to that with the 13 nm AuNPs. Whereas the apoptotic rate for cells exposed to 13nm AuNPs at day 3 starts at 23% and increases to 42% at the highest concentration, with the 45nm AuNPs, it ranges from 44% to 75%. Similarly, after 6 days, apoptosis further increases to 61% with the lowest and increases to 97% with the highest concentration of 13 nm, whereas with the 45nm AuNPs the rate is 91-100% at the different concentrations (Fig. 21). It is clear that for the 45 nm AuNPs that apoptosis 1) occurs at nearly one tenth of the concentration of that of the 13 nm particles, 2) increases steeply with higher concentration and 3) is nearly 100% for

all concentrations after 6 days of incubation. Hence, even though the damage may appear to be equivalent, i.e. approximately 40% for 142 μg/ml of 13 nm particles, versus 13 μg/ml for the 45 nm particles, the rate of increase with concentration and incubation time is much faster with the larger AuNPs.

Further, determined apoptotic rates for cells exposed to different AuNPs sizes and concentrations also showed that the previously reported decrease in cell proliferation was erroneously interpreted as an increase in doubling time.

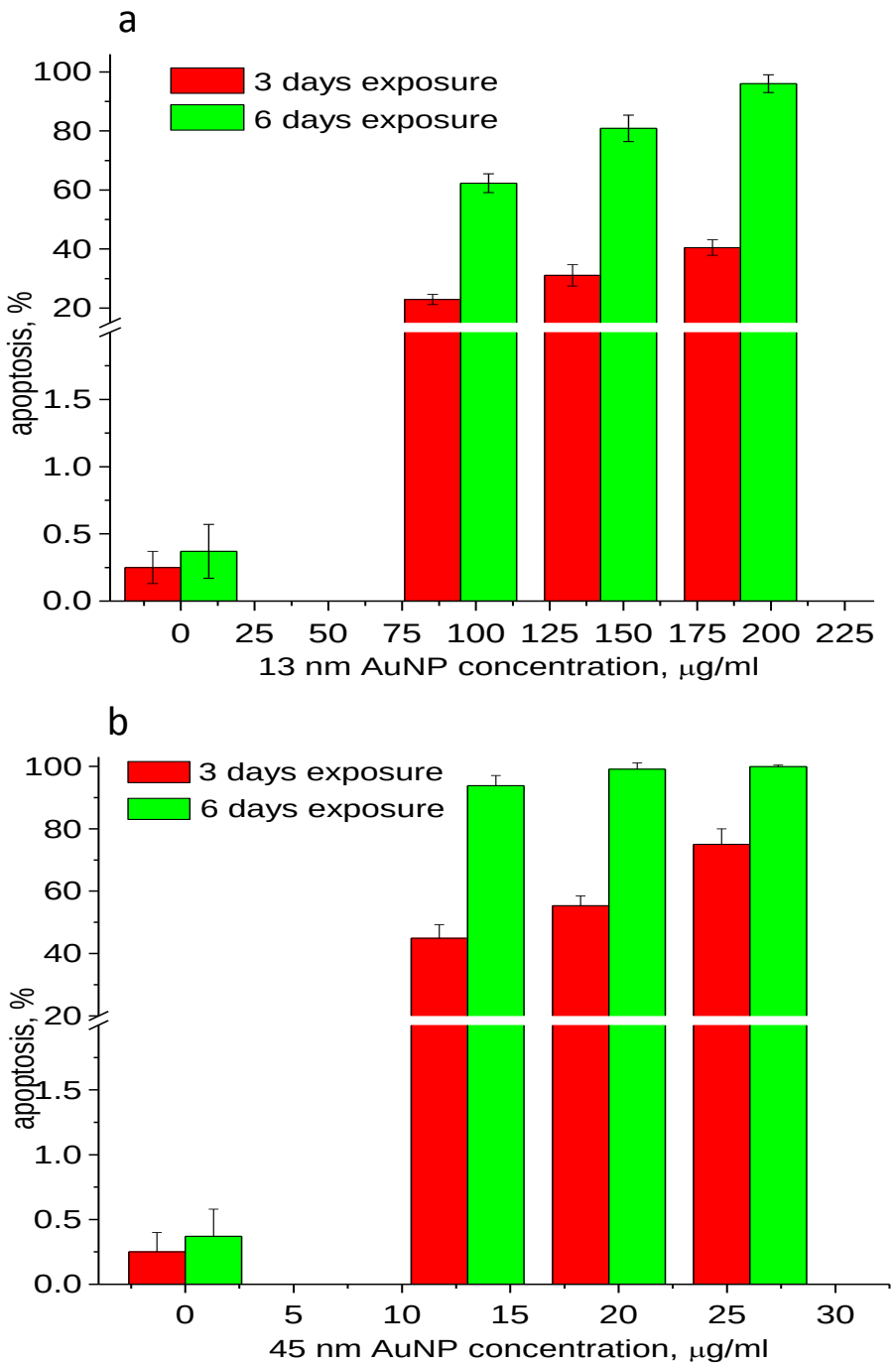

Figure 21. Apoptosis rate for cells exposed to AuNP for 3 and 6 days at different concentrations. (a) 13 nm AuNP (concentrations: 0 μg/ml, 95 μg/ml, 142 μg/ml, 190 μg/ml); (b) 45 nm AuNP (concentrations: 0 μg/ml, 13 μg/ml, 20 μg/ml, 26 μg/ml).

Next we tested to see if removal of AuNPs can rescue the cells from apoptosis. Figure 22 shows that even after removal of the AuNPs, the rate of cell growth in the exposed cells is slower than that of the control unexposed cells, with the slowest being in cells exposed to the 45 nm particles. In the inset we plotted the percent recovery after a total of an 8 day incubation (3 days with AuNPs incubation, 5 days of recovery), which is calculated by defining control as undergoing 100% recovery. With the 13 nm AuNPs the rate of cell proliferation increases immediately after removal of the particles and recovery reaches 61%, 48% and 37% for increasing concentration (Fig. 22a inset).

With the 45 nm AuNPs, the rates of recovery are much slower with respect to increasing particle concentrations (42%, 22% and 11%). Even though numerous papers have explored the effects of AuNPs exposure in different cell culture systems [125, 127, 131, 132, 139, 173, 175, 176], no data has been reported on the ability of any cell type to recover once the particles have been removed from the media. Our data for cell proliferation where we found a decrease in growth rate with increasing AuNPs concentration are in agreement with other studies [124, 127, 173, 176] regardless of nanoparticle coating.

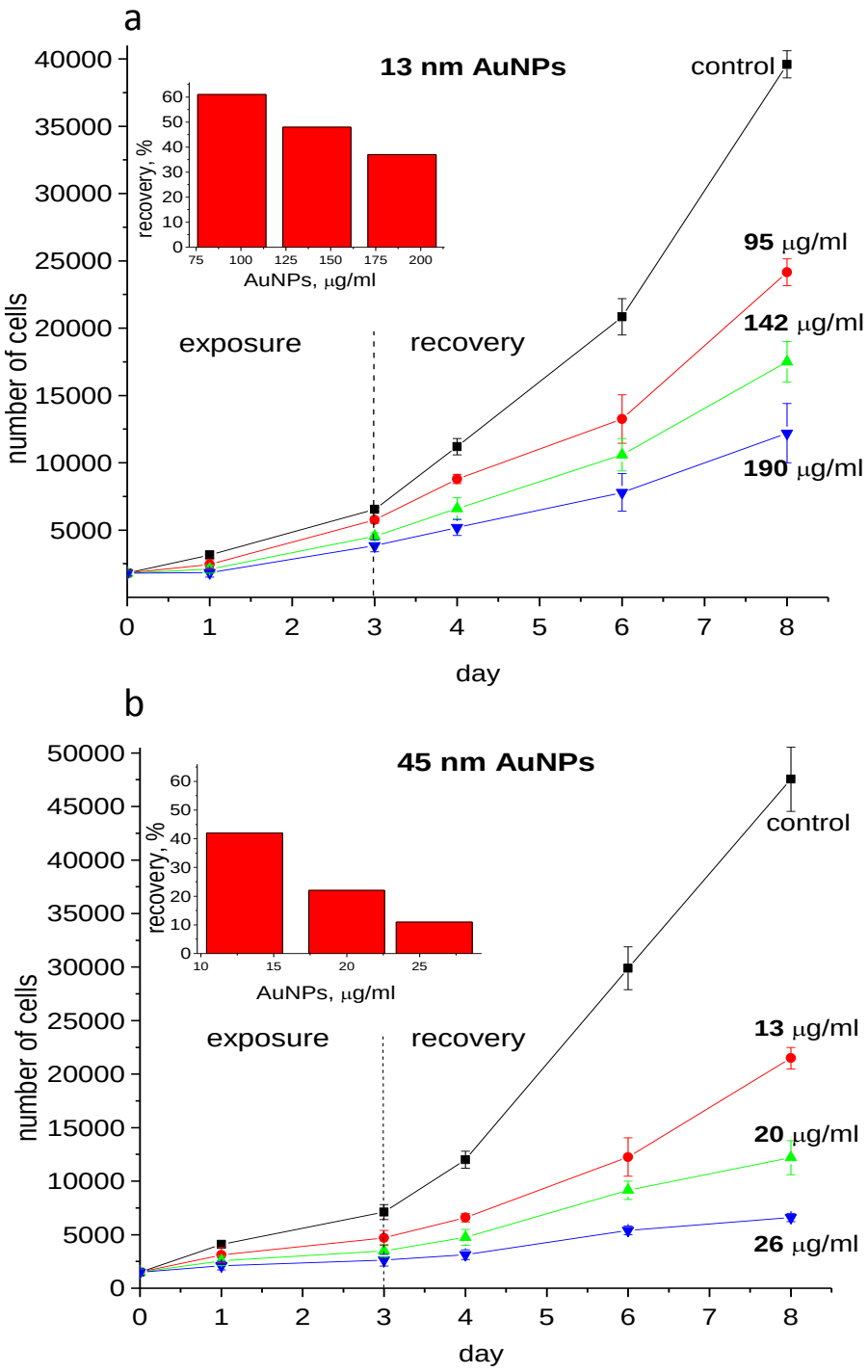

Figure 22. Cell recovery. Dermal fibroblasts (strain CF-31) were exposed to different AuNPs concentrations for 3 days and then allowed to recover for 5 days. (a) 13 nm AuNPs (b) 45 nm AuNPs.

Since no division occurs during apoptosis, recovery is also not possible, and thus the number of AuNPs in the cells is not reduced. Therefore, we re-plotted the data by subtracting the fraction of cells that have undergone apoptosis after three day incubation, and thus no longer divide (Fig. 23). The data shows that the cell number (as a function of incubation time after correcting for the fraction of non-dividing apoptotic cells on day 3) for both types of particles is nearly identical to that of the control cells indicating that the doubling time of the exposed cells is similar, even if they still contain nanoparticles.

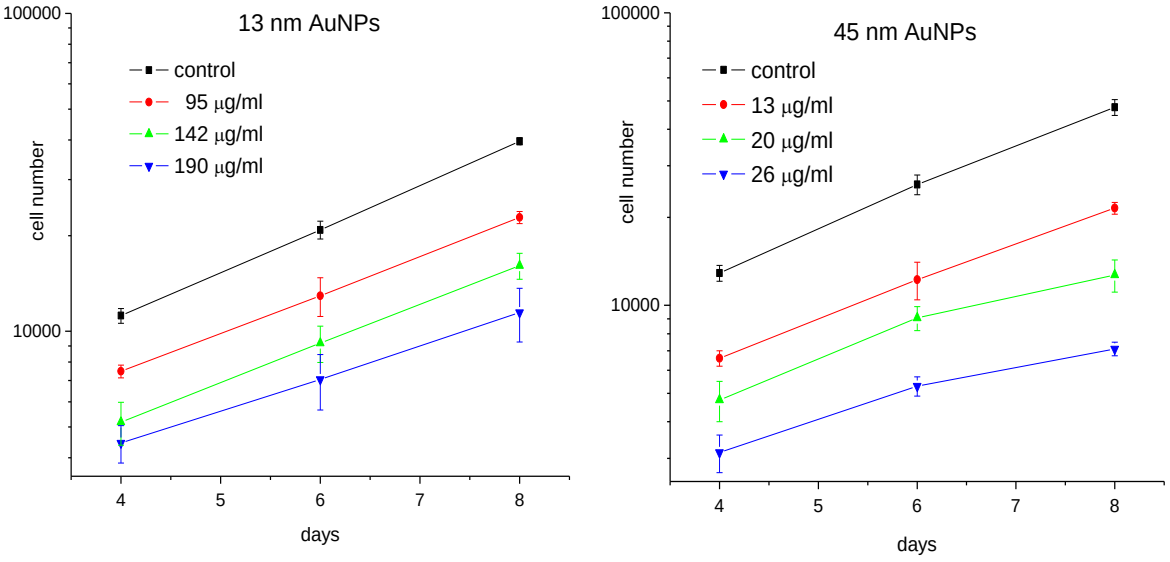

Figure 23. Cell recovery. Growth curves for the 5 days after AuNP exposure (counted after apoptotic cell subtraction on day 3).

Particle mediated microfilament disruption. We observed that consistent with previous result cell area was reduced [127]. In order to try to provide a possible explanation for this reduction in cell area we looked at the integrity of the cytoskeleton. Actin fibers are responsible for distributing internal forces by attaching one end the integrin receptors expressed on the cell membrane, which adhere to proteins secreted by the cell in the extra cellular matrix. In Figures 24(a-d) and 25(a-d) we show confocal images of cells after exposure to different concentrations of both 13 nm and 45 nm AuNPs for 3 and 5 days and following recovery (Figs. 24e-h and 25e-h). Figure 26 shows the average cell aspect ratio corresponding indicating that it is bigger in the exposed cells than control. Further, we can clearly see that there are fewer cells for the samples exposed to 45 nm AuNPs (Fig. 24), which are also more elongated and appear ready to "lift off" the substratum, as compared to cells exposed to the 13 nm AuNPs (Fig. 24). Removing the AuNPs and allowing the cells to recover for another five days, has a dramatic effect; the 13 nm AuNPs exposed cells have the same appearance as the unexposed control cells even at the highest concentration. In contrast, for the larger particles, the recovery is much slower, and even after five days many cells still appear not attached on the edges and their density remains low (Fig. 25f-h).

This type of fiber disruption due to the presence of AuNPs can occur either due to down regulation of cytoskeletal proteins or triggering a signaling pathway which somehow interferes with the self assembly of the actin, possibly due to physical interference by the large amounts of vacuoles.

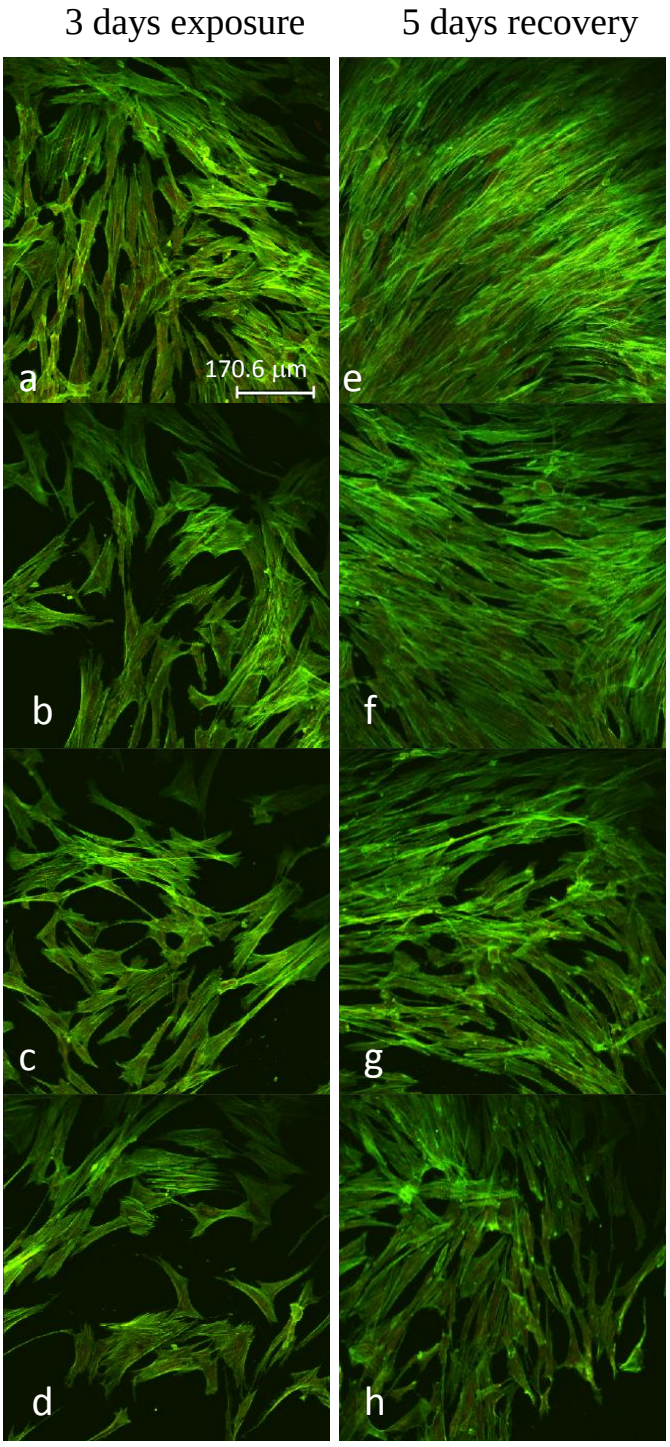

Figure 24. Human dermal fibroblasts CF-31 imaged with confocal microscopy after 3 days. (a) control; samples exposed to 13 nm AuNPs (b) 95 µg/ml, (c) 142 µg/ml and (d) 190 µg/ml. And following recovery for 5 days of AuNP removal (f-h), compared to control (e).

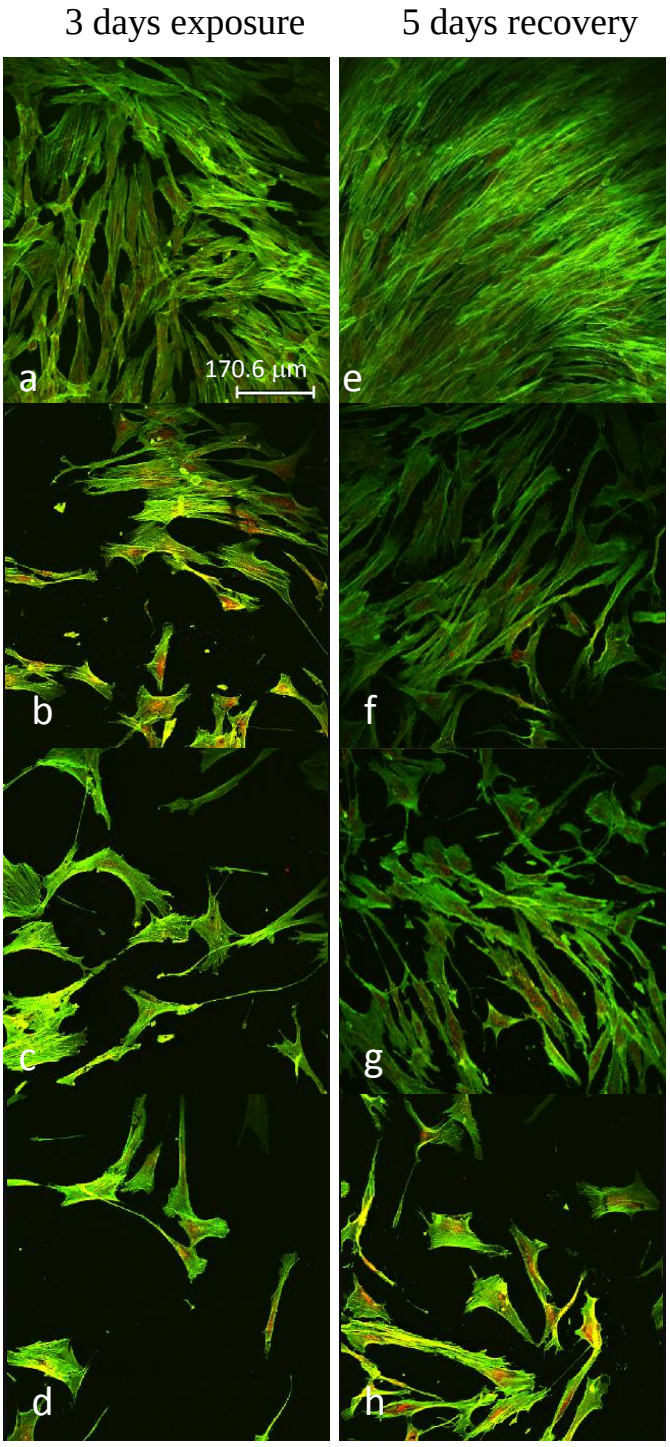

Figure 25. Human dermal fibroblasts CF-31 imaged with confocal microscopy after 3 days. (a) control; samples exposed to 45 nm AuNPs (b) 13 µg/ml, (c) 20 µg/ml and (d) 26 µg/ml. And following recovery for 5 days of AuNP removal (f-h), compared to control (e).

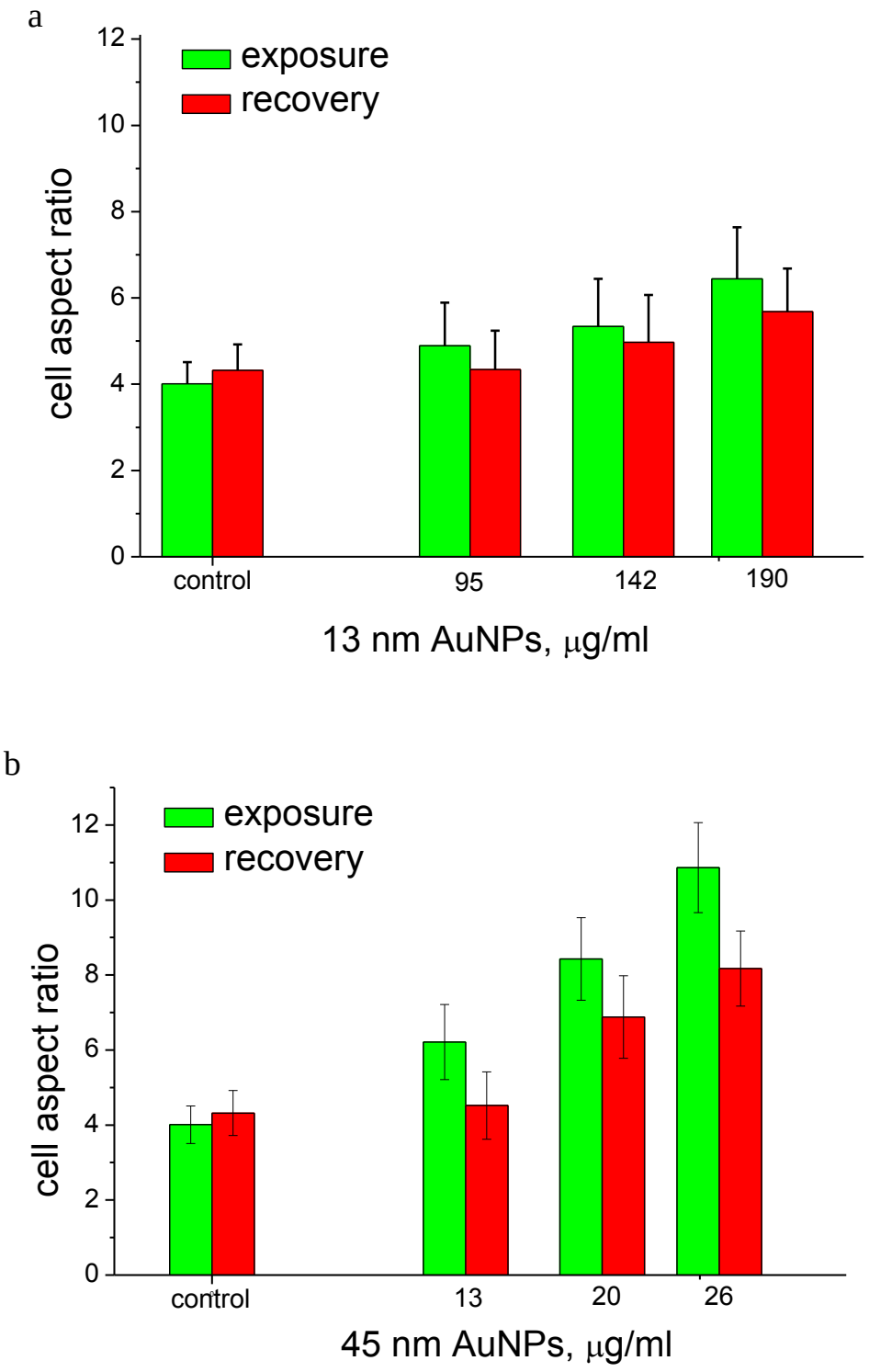

Figure 26. Cell aspect ratio after 3 days exposure to AuNPs and following recovery for 5 days. (a) 13 nm AuNPs, (b) 45 nm AuNPs.

We further show a magnified view of cells, that shows how the actin fibers are well extended across the cell cytoplasm in the control conditions (Fig. 27a-c). On the other hand, after 3 days of AuNPs exposure to either 13 nm or 45 nm AuNPs, the actin filaments appear disrupted, thinner, and broken (Fig. 27d and g). After 5 days of recovery the disruption of the actin filaments are less obvious in the case of 13 nm AuNPs (Fig. 27e) as compared to those still present with the 45nm particles (Fig. 27h). Stretched actin filaments were observed again with the 13 nm AuNPs indicating that the cells are in the process of recovery and cells appear to generate large and strong actin fibers while for the larger particles, the significant amount of disrupted actin filaments was still visible, even though some stretched filaments were also observed. We also find, that following 14 days of recovery, the cytoskeleton of the cells exposed to both size particles completely recover with an intact actin cytoskeleton (Fig. 27f and i) and resemble that of the control cells (Fig. 27c).

We show that the actin fibers are well extended across the cell cytoplasm in the control cells, where as in those exposed to both 13 nm and 45 nm particles, actin filaments were disrupted and appear as small dots.

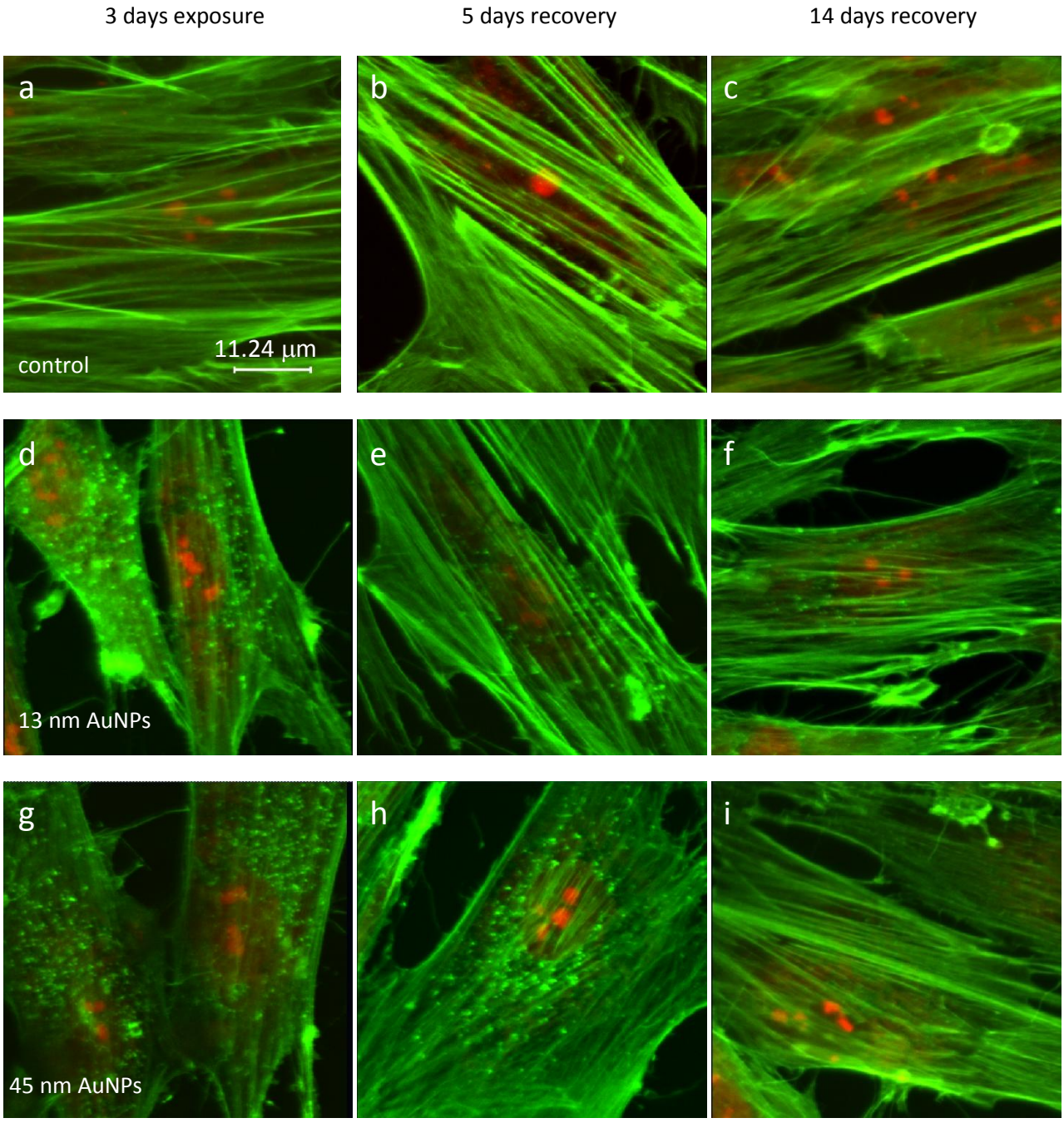

In order to examine whether these effects on the cytoskeleton were a direct result of less production of actin or tubulin, we examined the expression of these proteins from the particle exposed and control cells. Figure 28 shows no difference

between the control and any of the exposed samples, indicating that the amount of actin and beta tubulin is unaffected.

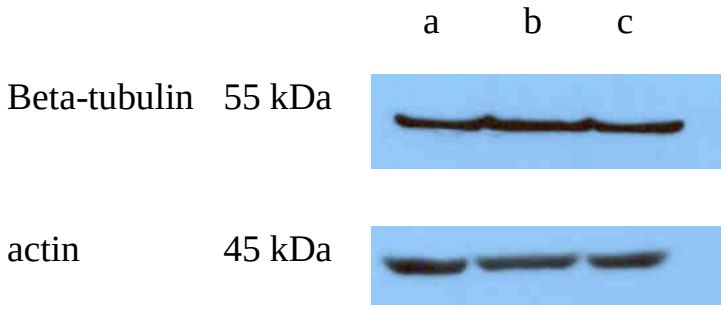

Figure 28. Western blot. (a) – control, cells cultured for 3 days with AuNPs (b) – 142 μg/ml 13 nm, c – 20 μg/ml 45 nm.

Another possible cause for the observed change in cell area may be a decrease in the expression of ECM proteins. Therefore, we measured the amount of collagen (type I) and fibronectin expressed by the cells after incubation for three days with 20 and 142 μg/ml of 13 nm and 45 nm AuNPs, respectively, and then after recovery for 5 and 14 days. The magnitude of the reduction after 3 days of exposure for both proteins is within one standard deviation for the two particle sizes and appears to be mostly a function of the exposure conditions (Fig. 29). It is also important to notice, that collagen is reduced more than fibronectin and indicates that extra cellular matrix (ECM) proteins produced after exposure to AuNPs is altered to a low collagen and higher fibronectin composition (a ratio contains 20% less collagen than fibronectin when compared with control composition for cells exposed to 13nm AuNPs and 35% less collagen in case of cells exposed to 45nm particles). Furthermore, the data shows that the production

of fibronectin partially recovers after five days and fully recovers after 14 days, whereas the production of collagen only slightly recovers after 5 days and is still not fully recovered after 14 days. These results are consistent with those of the actin fibers, shown in Figure 27.

In order to carry proper tension, the actin fibers must also be anchored to integrins that are bound to Arg-Gly-Asp (RGD) domains found on the secreted ECM proteins. Therefore, the lack of tension in the fibers may also be caused by a disruption in the expression of the ECM proteins, which for fibroblasts are primarily collagen and fibronectin. When we investigated this possibility, we found that significantly less collagen and fibronectin were expressed by the cells exposed to nanoparticles, which may explain the observed drastically reduced cell area. Furthermore, since collagen reduction is higher than fibronectin, the composition of the ECM is altered. Loss of collagen is generally associated with increased ECM rigidity and aging. Hence, this shift in composition may explain the increased modulus of the fibers previously reported by Pernodet et al. [127] while the decreased overall quantity is consistent with the smaller and thinner fibers for cells cultured with AuNPs.

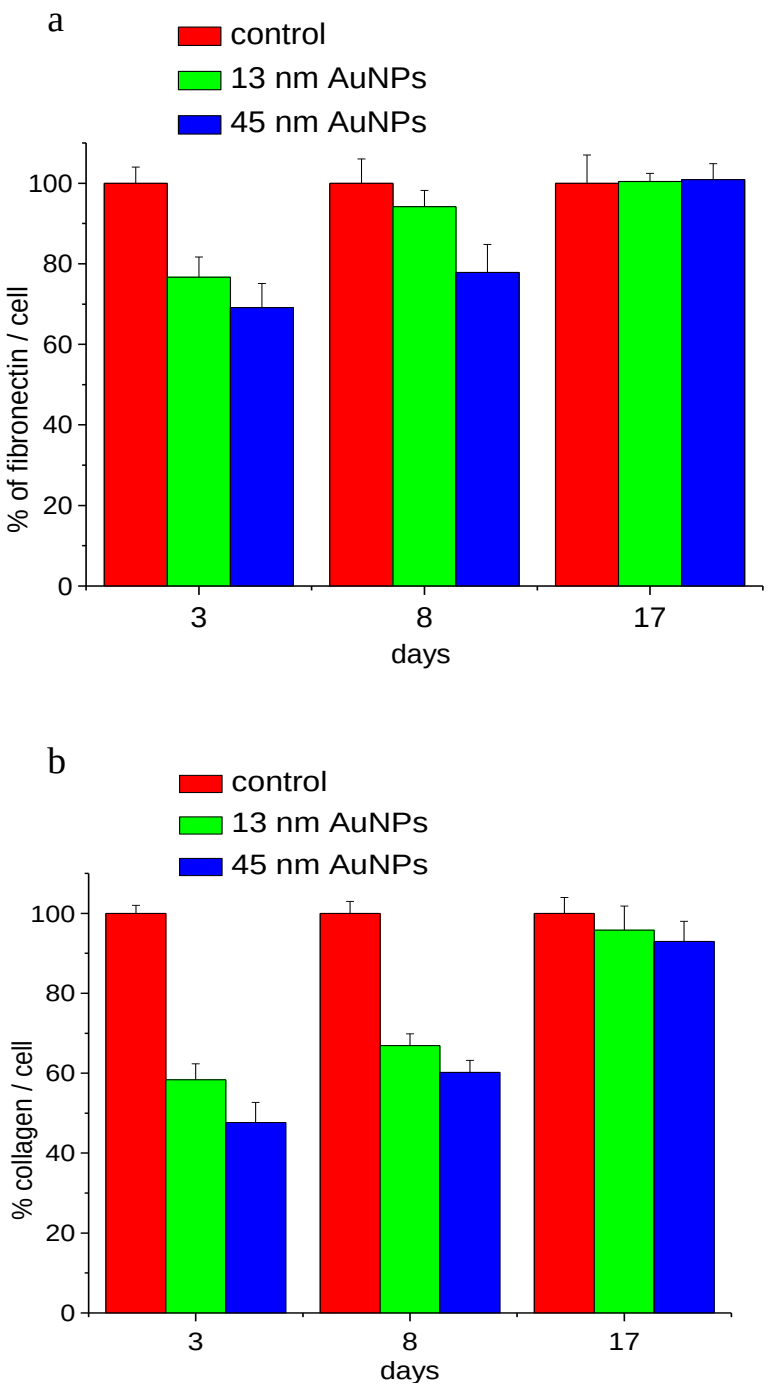

Figure 29. Fibronectin (a) and collagen (b) expression, cells treated with 142 μg/ml 13 nm and 20 μg/ml 45 nm AuNPs for 3 days, recovered for 5 and 14 days after exposure and control.

We also investigated the effect of exposure to the AuNPs to other primary functions of dermal fibroblasts such as collagen contraction and migration. From the Figure 30 we can see that for the cells exposed to nanoparticles for 3 days, their migration velocity decreases about ~10-15%. We also observe that for the samples exposed to 45 nm AuNPs, migration velocity is slower than for the cultures exposed to 13 nm AuNPs.

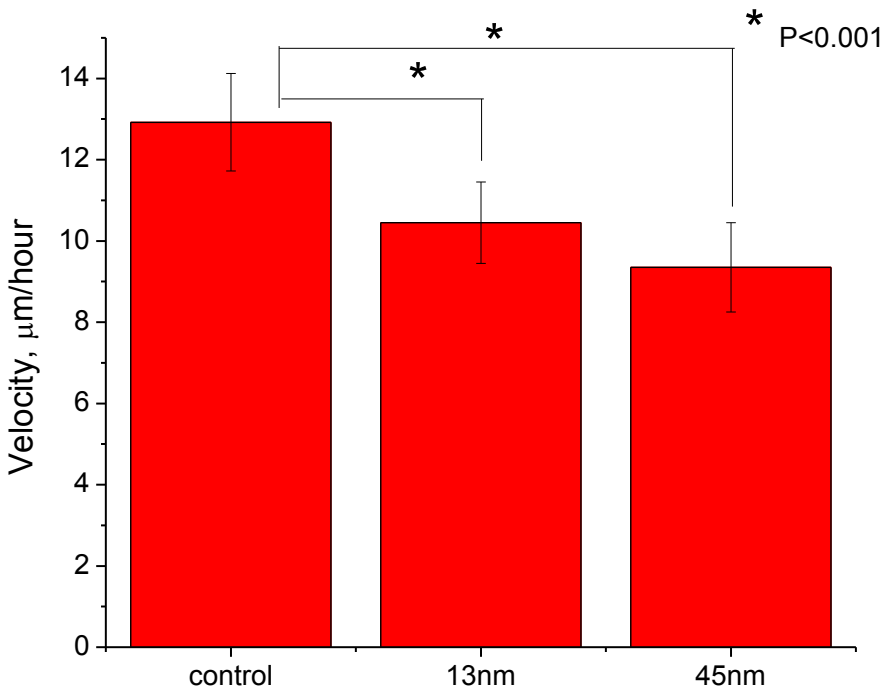

Figure 30. CF-31 dermal fibroblast cell migration after the exposure to the 142 μg/ml 13 nm and 20 μg/ml 45 nm AuNPs for 3 days and control.

Collagen fiber contraction is another important function of dermal fibroblasts we studied. A decrease in the degree of contraction is frequently associated with skin damage and premature aging. Exposure to the AuNPs reduces the ability of dermal fibroblast to contract the collagen gels by 53% relative to the

unexposed control samples (Fig. 31). For cells incubated with 45nm particles, the decrease is larger comparing to the cells exposed to 13nm particles and are 76%.

Dermal fibroblast ability to migrate and contract collagen fibers is the most important feature of the wound healing process. First cells migrate into the wound site and the tissue repair begins when they contract the collagen fibers allowing keratinocytes to differentiate and form the subsequent layers of the new skin tissue. Our results indicate that both processes are affected by exposure to the AuNPs. The influence of the slower migration velocity on wound healing is clear and result in the insufficient recovery, also inability to contract collagen is probably related to damage to the cell's machinery.

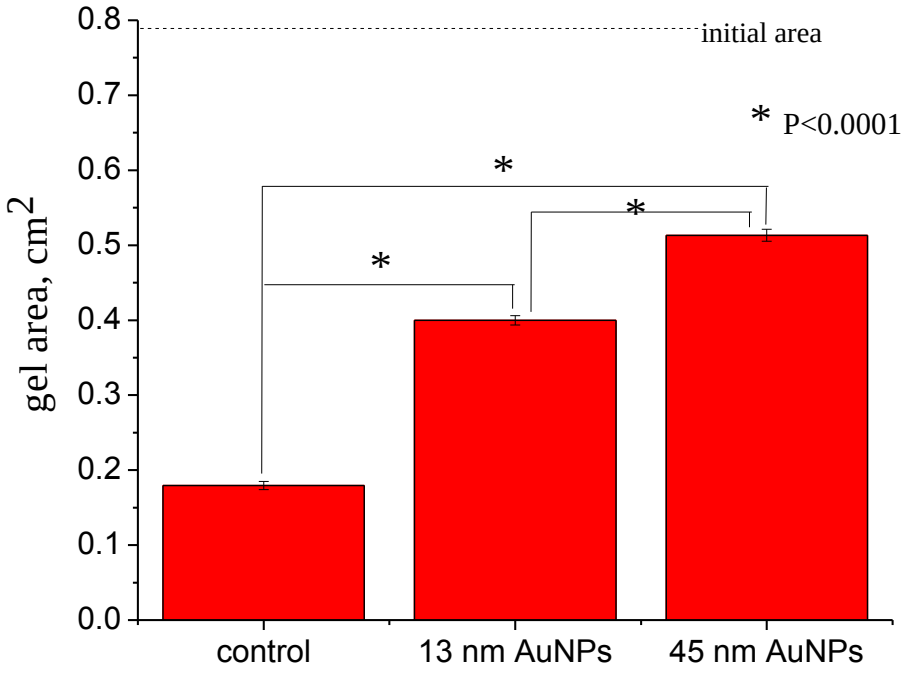

Figure 31. Collagen gel contraction for the CF-31 dermal fibroblasts cells exposed to the 142 μg/ml 13 nm and 20 μg/ml 45 nm AuNPs for 3 days.

3.2. AuNPs influence on Adipose Derived Stromal (ADS) cells

3.3.1. Materials and Methods

Cell culture. Primary human ADS cells (strain CW, obtained from Marcia Simon, Living Skin Bank, under the SBU IRB # 20022283, exempt) were cultured with Dulbecco's Modified Eagle's Medium (DMEM) supplemented with 1% of *penicillin*-streptomycin (PS) and 10% of fetal bovine serum (FBS) (purchased from HyClone laboratories, Logan, Utah). Differentiation of the ADS cells was carred out in the DMEM supplemented with 1% PS, 10% FBS, 0.1% 3-isobutyl-1-methylxanthine (IBMX), 0.01% insulin, 0.04% Indomethin, 0.033% Biotin, 0.01% Dexamethasone and 0.001% Pantothenic acid. Medium containing AuNPs (with concentrations in the range of 0-189µg/ml in case of 13nm and 0-26µg/ml in case of 45nm) was added to each culture plate 24 hours after plating. The samples were incubated with AuNPs for the chosen time points (up to 6 days) and then counted or fixed, stained and imaged. All incubations were performed at 37^{o}C and 7.5% CO_2. Each experiment had a control (cells grown in medium without AuNPs), and was performed in triplicate and repeated at least three times.

Cell counting. To determine the cell number during the growth curve experiments cells were plated at an initial density of 2,500 cells per well and counted using hemacytometer at the specific time point (up to 8 days). Each condition had triplicates and all experiments were conducted three times. Cell suspensions were mixed for uniform distribution and were diluted enough so that the cells did not aggregate.

Cell Staining for Confocal Microscopy. Cell area and overall morphology as a function of time and concentration was monitored using a Leica confocal microscope. For these experiments, cells were fixed with 3.7% formaldehyde for 15 minutes following exposure to AuNPs for 3 and 6 days. Alexa Fluor 488–Phalloidin was used for actin fiber staining and Lipid TOX red (Sigma) was used for the lipid droplets staining.

TEM. TEM analysis was used to assess the fate of internalized particles. One drop of the original AuNPs solution (95µg/ml 13nm and 13µg/ml 45nm particles) was placed on 300 mesh copper grip, which was coated with formvar film. The sample was then dried out at room temperature. After exposure to AuNPs for 3 and 6 days at 142 µg/ml (13 nm) and 20 µg/ml (45 nm), the cells were fixed in a solution of 2% paraformaldehyde and 2.5% glutaraldehyde in 0.1M Phosphate Buffered Saline (PBS), stained in 2% uranyl acetate, dehydrated with ethanol, then embedded in Propylene oxide. The specimen was cut into ultrathin sections (90 nm) with Reichart UltracutE ultramicrotome and stained on the grid with uranyl acetate and lead citrate. The samples were imaged using a FEI Tecnai12 BioTwinG2 transmission electron microscope. Digital images were acquired with an AMT XR-60 CCD Digital Camera System and compiled using Adobe Photoshop program.

AuNPs uptake. 500,000 cells were plated in 75 cm^2 tissue culture flasks. 24 hours after the plating AuNPs (13 µg/ml 45 nm and 142 µg/ml 13 nm AuNPs) were added and incubated with cells for 3 days. After that cells were harvested, counted and sent to Columbia Desert Analytical for gold content analysis by atomic absorption. Another set of samples was kept for 3 weeks to differentiation and after that cells were harvested, counted and sent for gold content analysis.

Lipids accumulation. Lipid buildup was monitored with Oil Red O staining and measuring the absorbance intensity at 500 nm. Cells were fixed with 3.7% formalgehyde, washed with 60% isopropanol and let dry completely and stained for 10 minutes with Oil Red O working solution (4 parts of DI water, 6 Parts of Oil Red stock solution, filtered through 0.2 μm filter). After that cells were washed 4 times with water and eluated with 100% isopropanol. Absorbance was red at 500nm in a microplate reader (BioTek EL800).

Migration. Cell migration was evaluated using the agarose droplet assay. The agarose gel was prepared by melting 2% (w/v) agarose stock solution and diluting it with DMEM to the final concentration of 0.2% (w/v). Then, the 0.2% (w/v) agarose was added to the cell pellets and the cells were re-suspended to a concentration of 1.5×10^7 cells/ml. 1.25 μl were then loaded on the prepared hyaluronic acid (HA) and fibronectin- functional domains (HA/FNfd) hydrogel surfaces in a 24-well dish. After that, the whole dish was placed at 4ºC for 20 minutes to allow the agarose droplet to gel before the addition of 400 μl of DMEM into each well. Following 24hr incubation at 37ºC, the cells were visualized microscopically. To quantify cell migration, the area of agarose droplets and the area covered by the leading edges of the out-migrating cells were measured using imageJ software (NIH). The cell migration distance was defined as the distance between the edge of the outward cell migration minus the edge of the agarose droplet.

Collagen gel contraction. Cells were grown and exposed to 13 μg/ml 45 nm and 142 μg/ml 13 nm AuNPs for 3 days. After that cells were trypsinized, counted and suspended in prepared collagen solution (1.8 mg/ml purified collagen, 2% BSA, 100ng/ml PDGF in DMEM with P/S/G) at 3.5×10^5 cells/ml. Cell/collagen gels were loaded into a BSA coated 24-well dish with 0.7 ml/well. After

preincubation for 2 hours to gel the mixture, collagen gels were gently detached by slight tapping on the wells and 500 μl DMEM with 2% BSA and 100 ng/ml PDGF were added. After 5 hours incubation, the images of gels were taken and analyzed by measuring the gel size.

Adiponectin release. Conditioned media were collected at medium change at the day 7, 14 and 21. A cocktail of protease inhibitors was added and media were stored at -20°C until assays. Adiponectin was directly measured from secretion media using the human adiponectin ELISA kit (Insight Genomics). Samples were prepared as described in the protocol from the manufacturer and the absorbance was read at 450nm.

Collagen and Fibronectin expression. Collagen and fibronectin were analyzed in supernatants of cultured CF-31 cells by Procollagen Type I C-Peptide EIA Kit (Takara, MK101) and human Fibronectin EIA Kit (Takara, MK115) as described in instructions provided by the manufacturer. Samples with high concentration of collagen and fibronectin were appropriately prediluted with Sample Diluent.

3.3.2. Results and Discussion

Size and media dependent uptake of AuNPs.

It was investigated whether the size and/or culture conditions affect the uptake of the AuNP's by two different cell types, ADS and dermal fibroblasts. In Figure 32 we show the results obtained from the atomic absorption experiments regarding the uptake of the AuNPs. From the figure we find that, after 3 days of incubation with 142 μg/ml and 20 μg/ml for the 13 nm and 45 nm particles,

respectively, for ADS cells in non-induced media, the uptake of the 13 nm particles is roughly 7 times larger than that of the 45 nm particles, consistent with the difference in their concentration in the incubation media (Fig. 32a).

When these cells were cultured in induced media, on the other hand, the uptake of the 13 nm particles after three days was reduced by a factor of six, while that of the 45 nm particles was reduced by a factor of three (Fig. 32a). Hence the uptake of the larger particles is increased relatively to that of the smaller particles when normalized by the concentration.

In order to understand weather this effect is the result of a chemical interaction between the cell membrane and the media or an aspect connected with differentiation of the ADS cells, we preformed two types of experiments:

(a) We compared the uptake between cells cultured in non-induced media with those cultured in media where only one component of the induced media was added.

(b) We also performed the analogous experiment with dermal fibroblasts, where no adipogenic differentiation could be induced by the media. In Figure 32b we show the results for the both media, where similar reduction in the uptake is observed in the induction media. Since dermal fibroblasts do not differentiate, this pathway can now be ruled out.

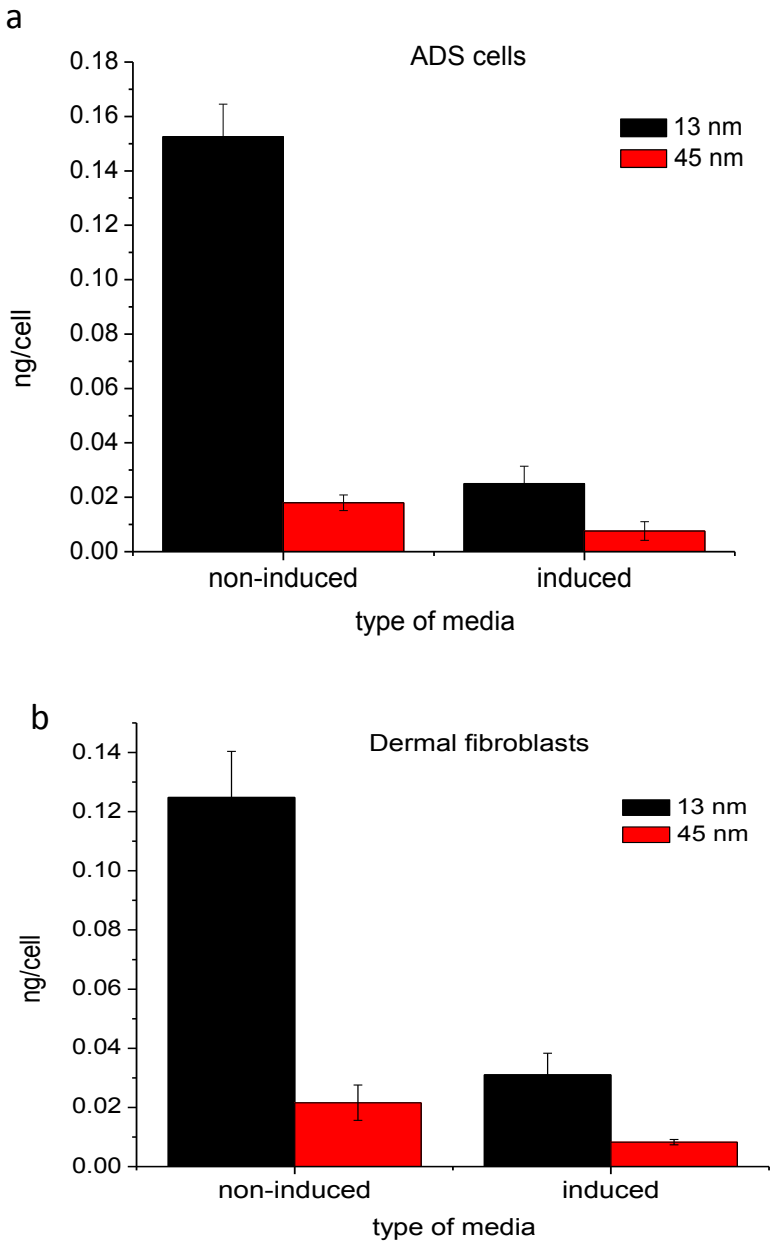

Figure 32. AuNPs uptake by (a) ADS cells and (b) dermal fibroblasts in non-induced and induced media incubated for 3 days with 142 μg/ml 13 nm and 20 μg/ml 45 nm AuNPs.

.

Intracellular fate of internalized AuNPs. The data clearly shows that in both medium (DMEM and adipogenic medium) human ADS cells sequester AuNPs inside large vacuoles and do not penetrate either the nucleus or the

mitochondria (Fig. 33) which is consistent with previous observation for the human dermal fibroblasts CF-31. The vacuoles are distributed uniformly across the cytoplasm (Fig. 33a-h). The major difference between the two types of cells is that in dermal fibroblasts particles are mainly localized along the vacuole membrane, and the center portion is mostly vacant. In the case of the ADS cells, the particles are sequestered in another type of organelle, which is more electron dense than the surrounding cytoplasm, and the particles are uniformly distributed. The sequestration of the 13 nm particles in dermal fibroblasts which were cultured in induction media, also occurred within vacuoles, but in this case most of the particles could be seen in the interior of the vacuole. This is a more efficient method of packing and hence fewer vacuoles are produced. The phenomenon is similar, though less pronounced, for the 45 nm particles, which may explain the much larger effect of the media on the sequestration. From this data we can conclude that the manner of sequestration of particles is specific for each type of cell, and for a given type of cell, may depend on the incubation media.

The induction media makes different types of cells less accessible for nanoparticles indicating the significant alteration of the membrane. However we did not identified single media component that might be responsible for that change suggesting that the effect is due to the combination of different induction media components. That is in agreement with data published by Sundelacruz et al. [177] who found that in induced media cells exhibit approximately 3 times more negative cell membrane potential compared to non-induced media. Since AuNPs are negatively charged by the stabilizing agent (citric acid) the observed increase in the membrane potential may decrease particle adsorption to the membrane and as a result decrease overall particle internalization rate. Also, another group [178] recently published that cell membrane upon adipogenesis became stiffer with the peak after 7 days which is gradually decreases to the initial (non-induced media)

level by the day 21. The membrane stiffness may also be partly responsible for the decreased AuNPs uptake by cells in the induced media. As we previously observed 45nm AuNPs penetrate dermal fibroblast via clathrin mediated endocytosis while 13 nm AuNPs mostly via phagocytosis, therefore we can speculate that observed 3 fold decrease in uptake of 45nm particles correlates with 3 times increase in the membrane negative potential while for the 13nm gold the uptake inhibition is approximately 6 fold and may be caused by combination of cell membrane potential increase and stiffening of the membrane.

After 3 weeks of incubation in induced medium to differentiate ADS cells to adipocytes AuNPs were found to be located in the same type of the small organelles, however, the overall number of the nanoparticles or clusters inside the organelle was significantly lower. From the figure we can clearly see that some the cells which have differentiated and accumulated large amounts of lipids (Fig. 33b and c), while other cells have not (Figure 33j and k), in a manner similar to the control. Close examination shows that the cells which have large lipid accumulation also have significantly fewer particles. Figure 3d-f are high magnification images of the particles in the vicinity of the lipid droplets, where we cans see that they are stored in the same type of organelles as in the non differentiated cells, and they do not penetrate into the areas of lipid storage. Regardless of the media type, once inside the cells, AuNPs are sequestered in subcellula organelles, where they tend to fill up the interior. On the other hand, control cells displayed their typical structure with well-define plasma membrane, cytoplasm and random inclusions of organelles and vacuoles and nuclei with clear nucleolus. Further, the AuNPs are usually incorporated in the perinuclear region of the cell and do not penetrate mitochondria or nuclei. They are also rarely found in cytosol and do not enter into lipid droplets in mature adipocytes. Most likely, as it

was hypothesized by Yi et al [179], AuNPs penetrate mesenchymal stem cells by membrane adsorption followed by internalization via endocytosis.

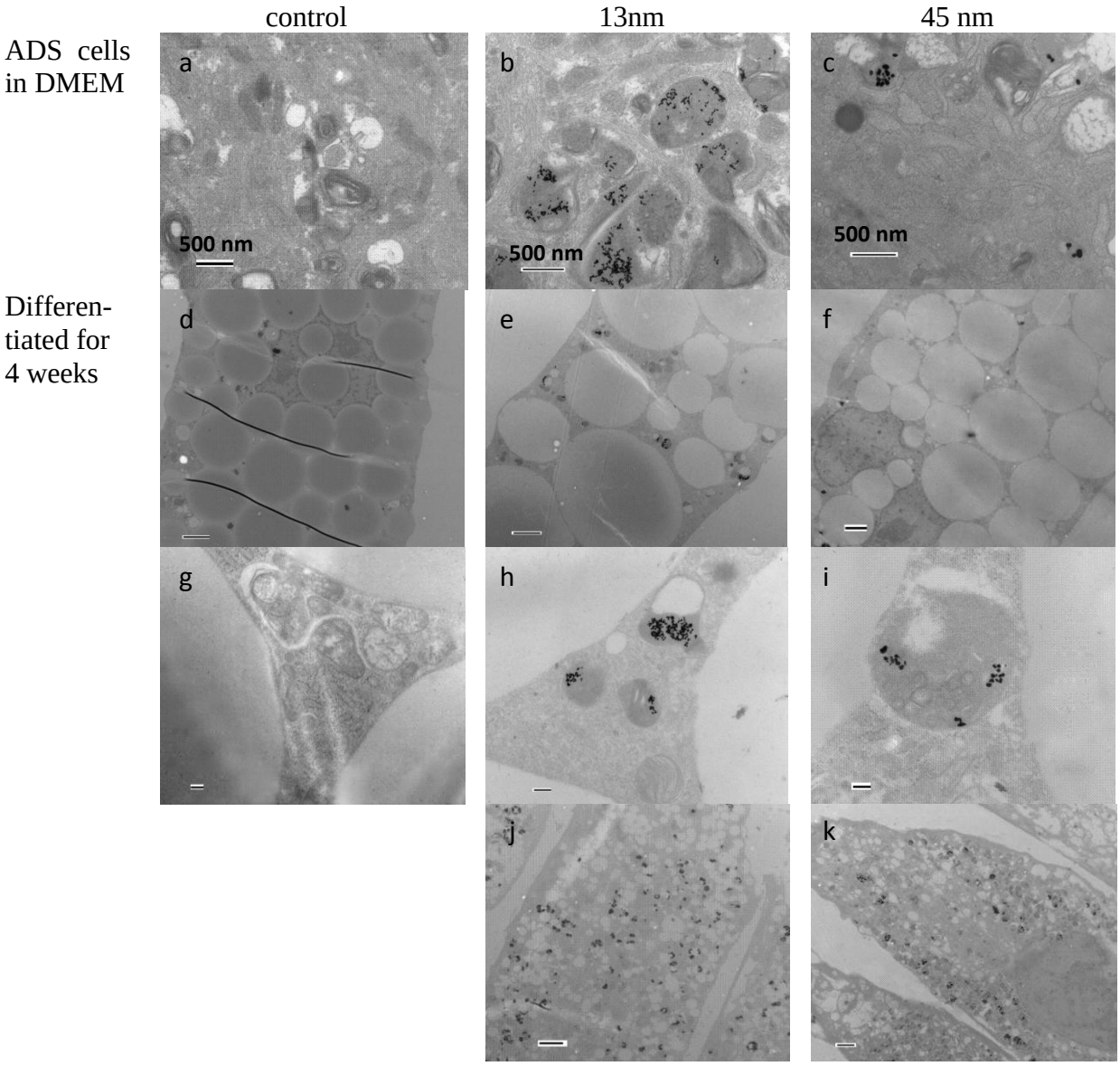

Figure 33. Pictures of TEM sections of ADS cells, a - control in normal media, b and c – ADS cells exposed to 142 μg/ml 13 nm and 20 μg/ml nanoparticles for 3 days in normal media, TEM section of ADS cells differentiated for 3 weeks in adipogenic media containing AuNPs, d, g – control, e and f –exposed to 142 μg/ml 13 nm and 20 μg/ml nanoparticles, h and i – high magnification of cells exposed to AuNPs, j and k - ADS cells exposed to AuNPs for 3 weeks that did not differentiated.

Before the differentiation ADS cells exhibit the properties and the phenotype of the dermal fibroblasts. In this state ADS cells are expected to be affected by the AuNPs in the similar manner as dermal fibroblasts discussed previously. Therefore, to confirm our hypothesis we carried out a number of the experiments on ADS cells to identify their response to the AuNPs treatment.

The impact of AuNPs on ADS cell proliferation. Results in Figure 34 show that similar to the dermal fibroblasts ADS cell proliferation rates decrease with increasing particle concentration and exposure time for both particle sizes. The impact is more severe for the 45 nm AuNPs and is roughly equivalent to the 7 fold concentration of 13 nm gold particles indicating the non-concentrational nature of the damage. These results also shows that ADS cells are more sensitive to the AuNPs comparing to the human dermal fibroblasts, leading to the conclusion that nanoparticles impact is cell specific.

We also investigated whether recovery from the AuNPs is possible when the source of the particles is removed (Fig. 34d and e). Similar to our previous findings for dermal fibroblasts we observed that if AuNPs is removed from the cell media 3 days after the exposure and cells are allowed to recover for 4 more days the proliferation rates are increasing compared to the cultures with AuNPs. 45 nm particles have slower recovery rate compared to 13 nm and for the highest concentration 26 μg/ml recovery does not occur at all, indicating that all cell population underwent apoptosis.

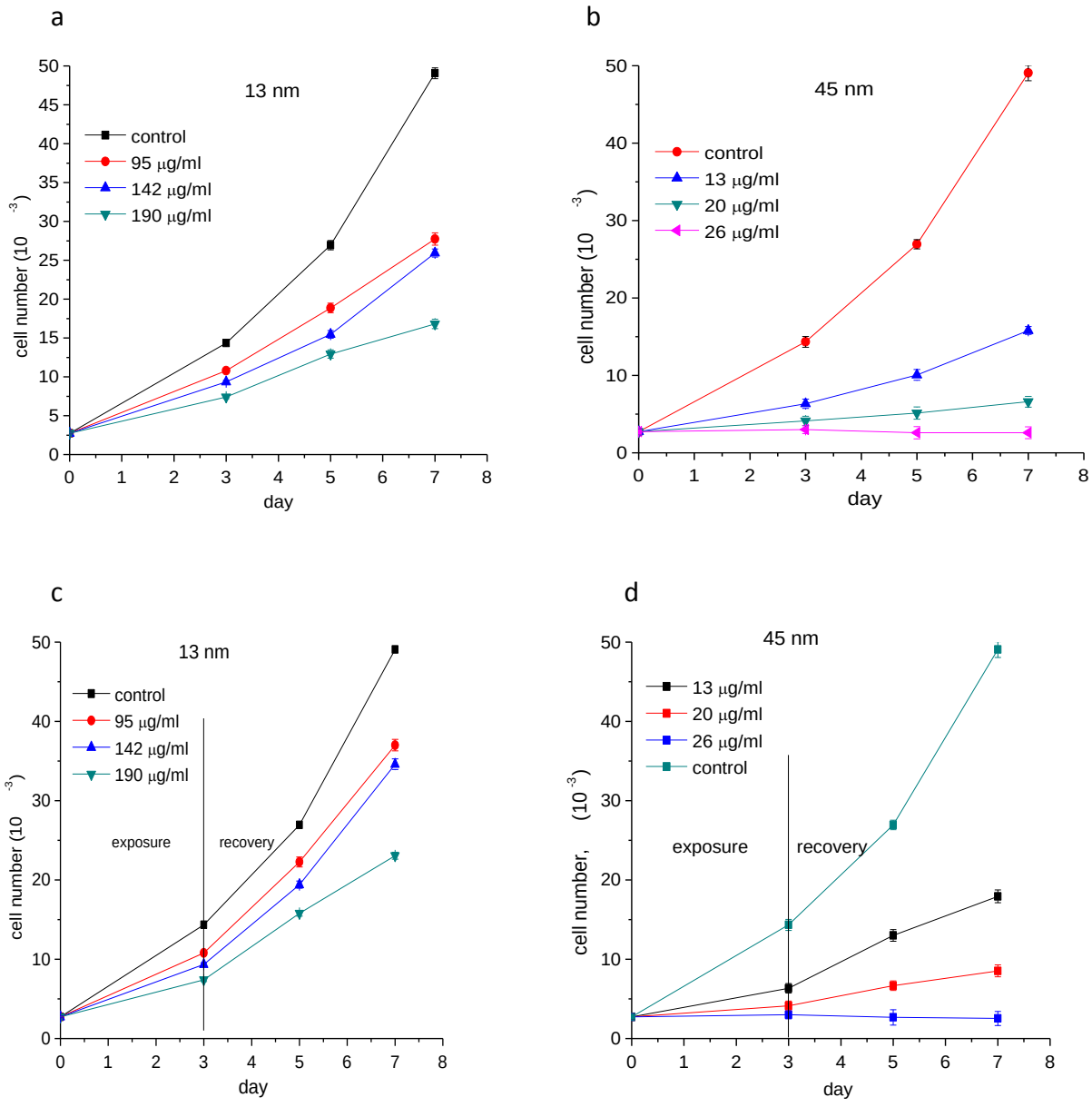

Figure 34. Cell growth and recovery. ADS cells were exposed to different AuNPs concentrations for 3 days (a and b) in non-induced media and then allowed to recover for 4 days (c and d).

Migration and Collagen gel contraction. Two other important characteristics of the ADS cells functions are the ability to differentiate and create an adipose tissue and the ability to migrate and contract collagen fibers in the wound healing process. Similar to the dermal fibroblasts, ADS cells incubation with AuNPs leads to the decrease in cell migration velocity. In Figure 35 samples that were exposed to the 13 nm AuNPs have a modet but statistically significant reduce in migration velocity (17%, P<0.001). The effect of the exposure to the 45 nm AuNPs is greater and resulted in a 25% decrease in the cell migration speed.

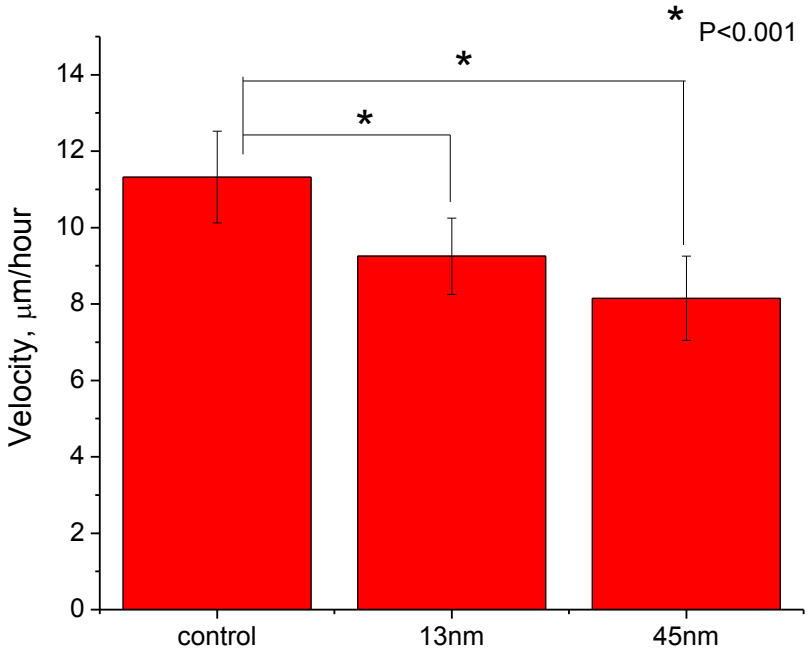

Figure 35. ADS cell migration after the exposure to 142 μg/ml 13 nm and 20 μg/ml 45 nm AuNPs for 3 days and control.

Collagen contraction is another important function of ADS cells we studied. Several groups [180-183] explored the importance of the collagen secretion as well as collagen fibers formation for the differentiation of ADS cells. It was found that the constitution and distribution of the ECM are altered during differentiation,

suggesting that the organization of each ECM component into a suitable structure is a requirement for the differentiation and maintenance of unilocular adipocytes.

We found that exposure to the 13 nm AuNPs reduces the ability of ADS cells to contract the collagen gels by 56% relative to the unexposed control samples (Fig. 36). For cells incubated with 45 nm particles, the decrease is larger compared to the cells exposed to 13 nm particles and are approximately 65%.

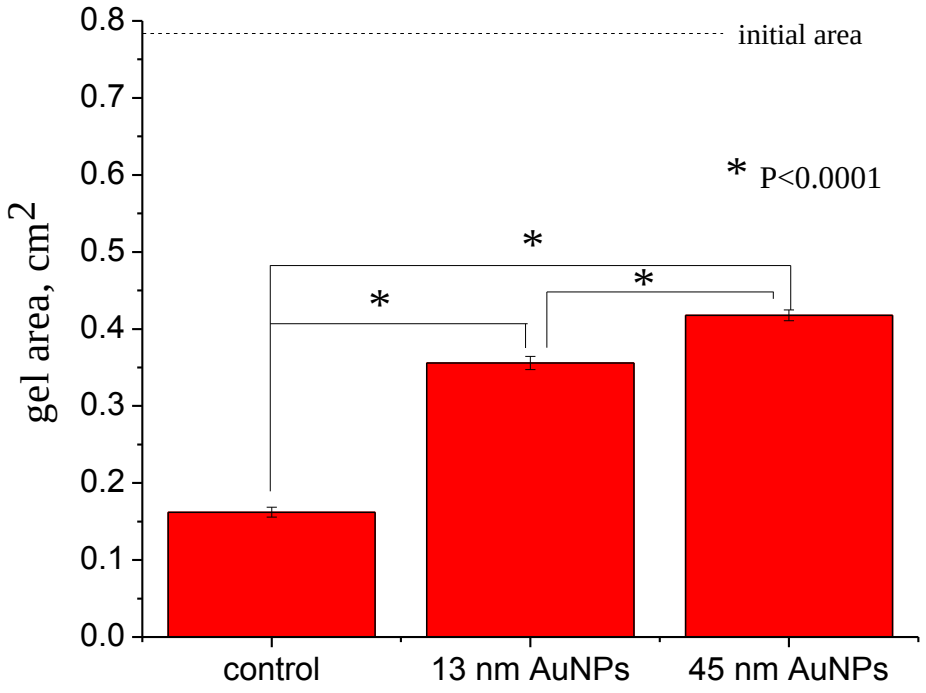

Figure 36. ADS cells collagen gel contraction after the exposure to 142 μg/ml 13 nm and 20 μg/ml 45 nm AuNPs for 3 days and control.

Dermal wound healing is an extremely synchronized biological process where skin fibroblasts interact with surrounding cells such as keratinocytes, fat cells and mast cells. During the process of skin repair, fibroblasts produce ECM, glycoproteins, adhesive molecules and various cytokines [184]. Because of all these and cell-to-cell, and cell-to-ECM interactions, skin fibroblasts contribute to

the fibroblast-keratinocyte-endothelium complex that not only repairs wounds, but also maintains the integrity and viability of skin. In the early phase of wound healing, fibroblasts migrate into the affected area and move across fibrin-based matrix. Since this matrix is relatively devoid of fibroblasts, the processes of migration, proliferation and ECM production are the vital steps in the regeneration of a functional dermis [185]. Fibroblasts produce ECM that replace the provisional fibrin-based matrix and help reorganize wound edges through their contractile properties.

In deep skin wounds, the underlying adipose tissue is exposed in the wound bed and the dermis at the wound borders. As a result of such injury, both cell types, dermal fibroblasts and ADS contribute to the wound healing process. Recently the possible roles of ADS cells in skin wound healing, especially in the aspect of fibroblast activation and proliferation, as well as collagen synthesis and migratory properties was investigated [186]. In this study ADS cells were found to have effects on human dermal fibroblasts by increasing type I collagen and fibronectin synthesis, increasing mRNA expression of ECM proteins and by activating proliferation and migration of fibroblasts. In addition, in an animal model, ADS cells were found to reduce the wound size and accelerate the re-epithelialization from the edge. Lastly, other research groups [187, 188] also showed that ADS cells stimulate cutaneous wound healing and improve scar thickness *in vivo* by secretion of various cytokines and chemokines.Therefore, the observed loss of migration and collagen contraction ability of the ADS cells exposed to AuNPs can result in delayed wound repair.

The impact of AuNPs on ADS cells differentiation. Unlike dermal fibroblasts, whose main function lies with migration and contraction, the main function of the ADS cells is to differentiate into adipocytes which are capable of

lipid accumulation and storage. Therefore, another measurable effect on ADS cells differentiation in the presence of AuNPs is lipid accumulation. In figure 37 we plot the absorption after one, two and three weeks of incubation in adipogenic media without particles, and incubated with 142 μg/ml and 20 μg/ml of 13nm and 45nm particles respectively. Cells in the presence of the AuNPs do not show any difference after one week in the induction medium. A slight difference becomes apparent after second week, where approximately 15% less lipid is produced in the cultures with nanoparticles. In contrast, sever decreases in lipids accumulation is clearly present in the samples exposed to the AuNPs after 3 weeks of incubation; samples exposed to the 13 nm and 45 nm AuNP's exhibit approximately a 50% and ~35% decrease, respectively. On the contrary to the effects previously measured on the undifferentiated cells, which were more severe for the 45 nm particles, it is interesting to note that the reduction in lipid production is larger for the 13 nm particles.

These results were also confirmed by the confocal microscopy (Fig. 38). From the images we can see that in all cases the cells have well extended actin fibers, with no effect on their structure observable due to the presence of the nanoparticles. As we can see in the figure 38a-c no difference in lipid accumulation is observed after 7 days of differentiation for the samples incubated with AuNPs or control. A similar pattern is seen after 14 days of differentiation (Fig. 38d-h), but after 21 days a significant delay in lipid accumulation is observed in the samples cultured with 13 nm AuNPs and a less pronounced effect with the 45 nm. Specifically, only the droplets in the control sample have increased in average diameter and number, while significantly fewer droplets, with smaller diameters are seen in those cultured in the presence of the nanoaprticles. Hence the presence of nanoparticles in the culture is seen to impair the ability of ADS cells to accumulate lipids.

When the ADS cells were treated with AuNPs for 3 days prior to inducing differentiation, lipid accumulation was inhibited after 7 days of differentiation (25% for 13 nm and 20% for 45 nm) (Fig. 39). But the cells recover and reach the levels of lipid accumulation in the control cells after 14 days and are equal at 21 days of differentiation. Same pattern is also observed by confocal microscopy, where the only statistically significant difference is in the lipid droplet density and size in the samples pre-treated with AuNPs after 7 days of differentiation as compared to control (Fig. 40a-c). This difference becomes undetectable for all samples containing NP's after 14 and 21 days of incubation (Fig. 40d-i).

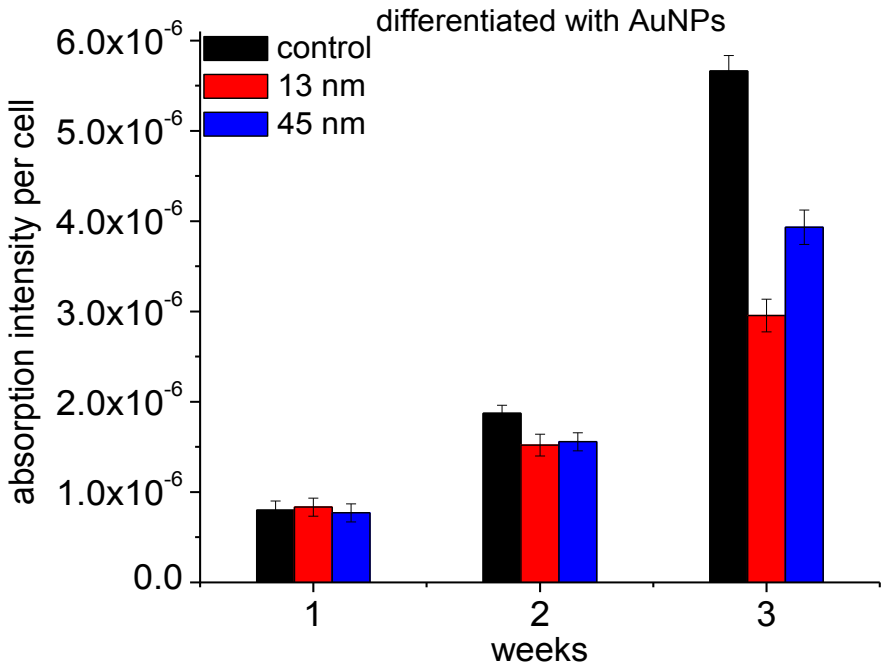

Figure 37. ADS cells lipid accumulation. Cells were differentiated for 3 weeks in the presence of nanoparticles (142 μg/ml 13 nm and 20 μg/ml 45 nm AuNPs).

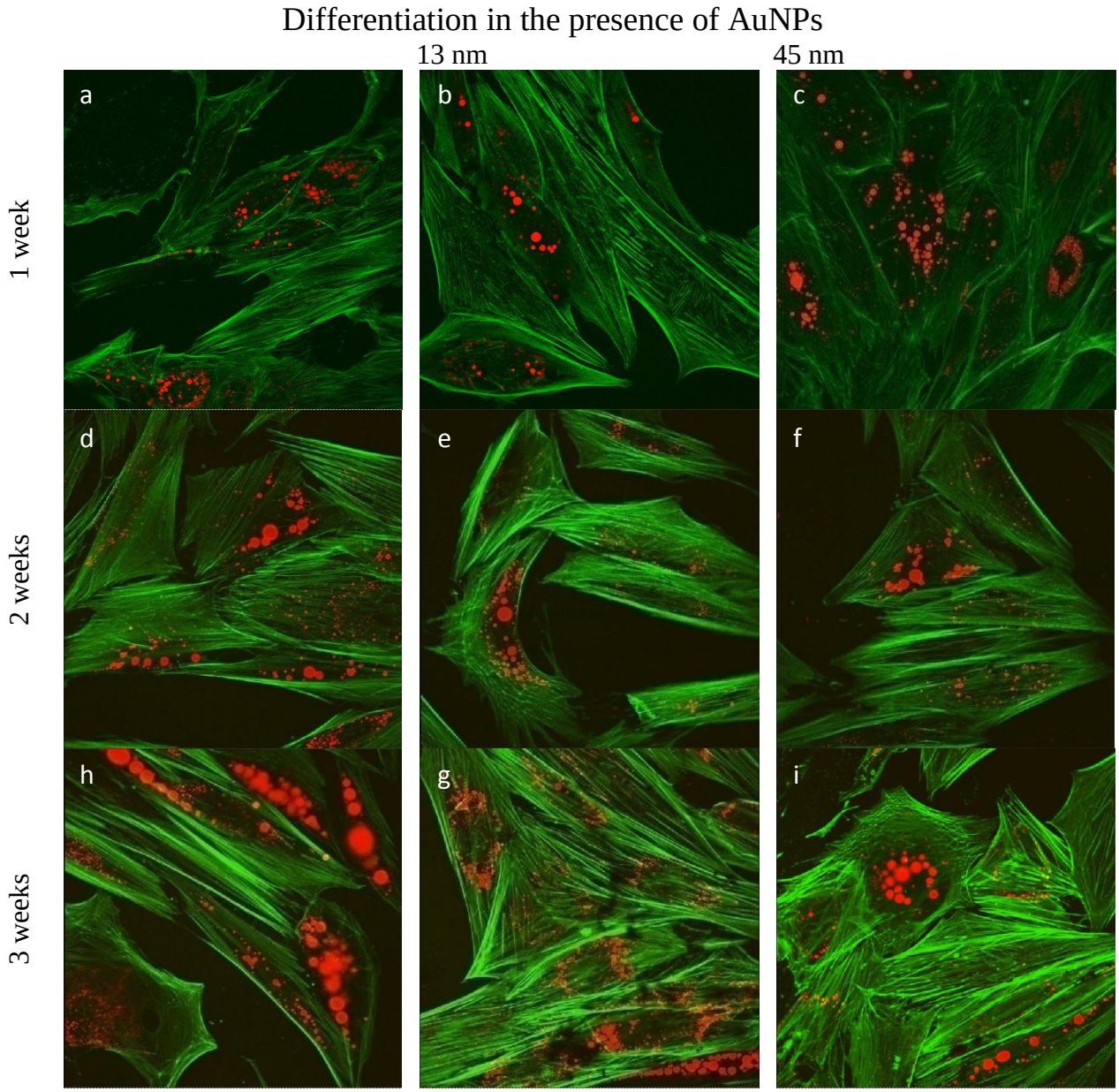

Figure 38. Confocal microscopy images of ADS cells differentiated for 3 weeks in presence of AuNPs. a, d and h – controls; b, e and g – exposed to 142 μg/ml 13 nm AuNPS; c, f and i-exposed to 20 μg/ml 45 nm AuNPs.

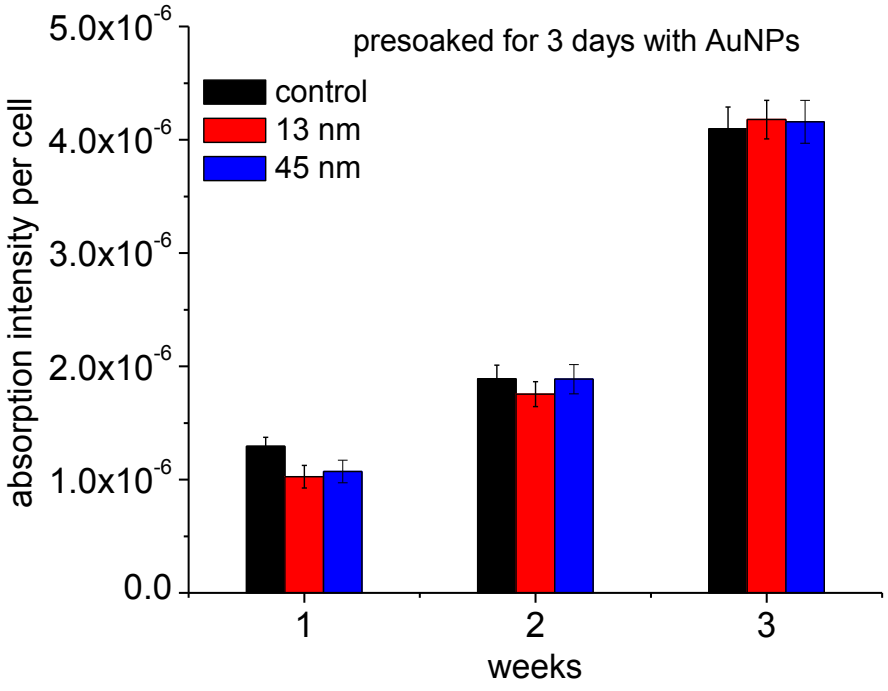

Figure 39. ADS cells lipid accumulation. Cells were exposed to AuNPs for 3 days in non-induced media and differentiated for 3 weeks (142 μg/ml 13 nm and 20 μg/ml 45 nm AuNPs).

.

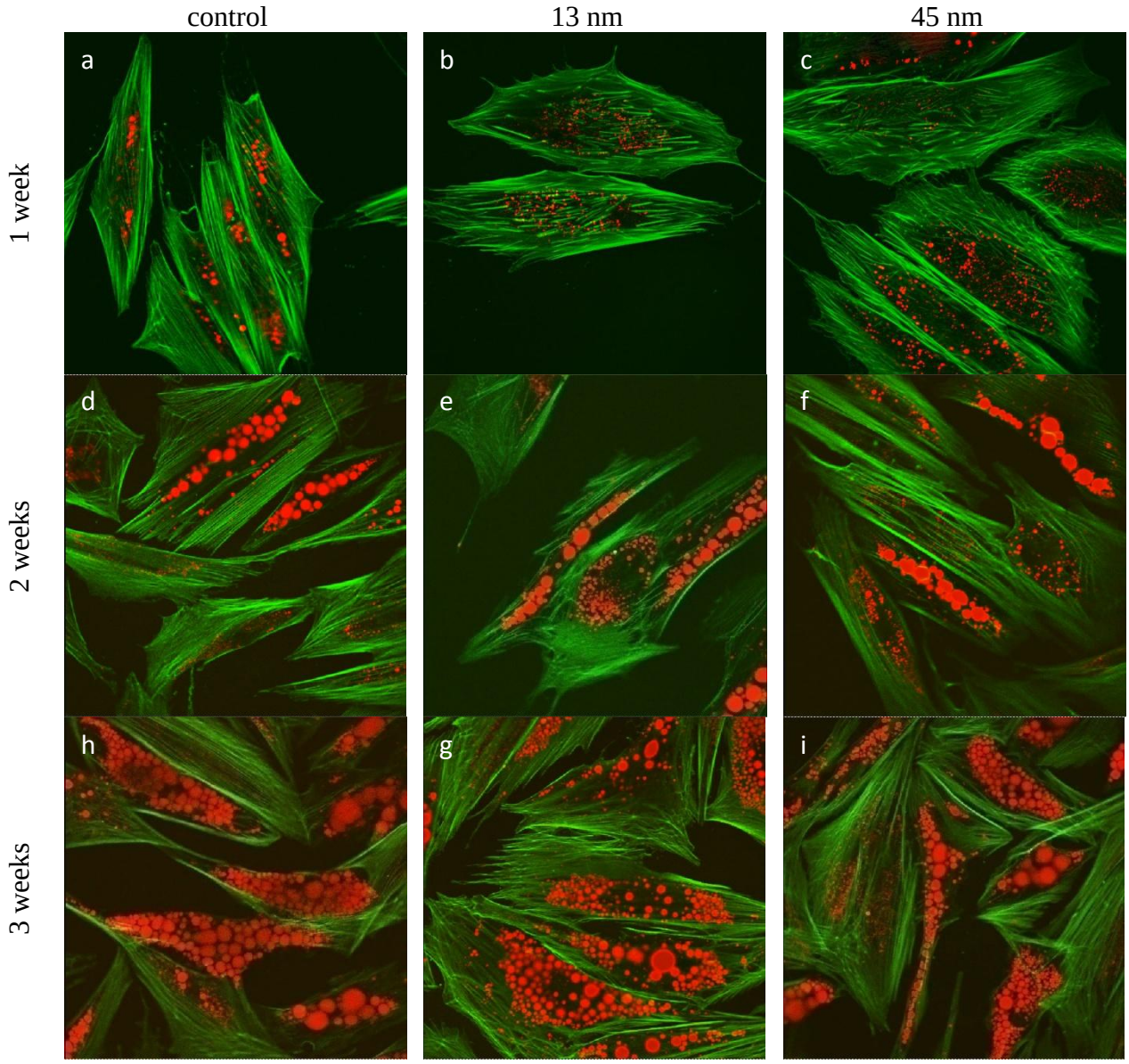

Figure 40. Confocal microscopy images of ADS cells exposed to 142 μg/ml 13 nm and 20 μg/ml 45 nm AuNPs for 3 days in non-induced media and then differentiated for 3 weeks in induced media. a, d and h – controls; b, e and g – exposed to 13 nm AuNPS; c, f and i-exposed to 45 nm AuNPs.

Adiponectin release. Adiponectin (ACRP30, adipoQ, apM1, or GBP28) is the product of a gene induced during adipocytes differentiation [189-191] and has been found to be exclusively expressed in adipose tissue and shows important peripheral effects. It is a 30-kDa protein that is synthesized and secreted from adipocytes. It has an N-terminal collagenase domain followed by a C-terminal globular domain that can undergo homotrimerization [190]. Adiponectin levels are known to be very high in plasma (compared to other adipokines), where it circulates as either a trimer, a hexamer (called the low-molecular-weight form), or as multimeric forms of 12–18 subunits (called the high-molecular-weight form) [192].

After secretion, adiponectin/ACRP30 plays an insulin-sensitizer role in liver and skeletal muscles by an increase in fatty acid oxidation [193-199] similar to the action of leptin. Interestingly, insulin resistance might be fully reversed by a combination of physiological doses of adiponectin and leptin, but only partially by either adiponectin or leptin alone [196] suggesting that adiponectin and leptin work together to sensitize peripheral tissues to insulin.

Serum concentrations of adiponectin have been shown to directly reflect the amount of adipose tissue present. Therefore, the affect of the AuNPs on the ADS cells differentiation was monitored by the expression of the differentiation markers adiponectin (an adipose tissue-specific adipocytokine) and leptin, as well as by overall lipids accumulation inside the cell.

In figure 41 we show adiponectin concentration per cell at one, two, and three weeks following differentiation for the control and samples with 13 and 45nm particles. From the figure we see that adiponectin is not detected after the first week in any of the samples. An abrupt increase is seen in the control sample

after the second week, followed by a slight increase in the third week. A much smaller initial increase is seen in the samples cultured with nanoparticles, where the amount of adiponectin is approximately 35% of the control value in both 13 and 45nm samples. At week three, the increase in adiponectin in the control sample is only 10% of the value in week two, as compared with increases of 40% and 65% for cells cultured with the 13 and 45 nm particles.

As we already shown, adipocytes that were differentiated in the presence of the nanoparticles produced fewer lipids. These findings were also consistent with a reduced expression of adiponectin, a known marker of adipogenesis which correlates directly with lipid formation [189-191]. Adiponectin was also found to be exclusively expressed in adipose tissue and shows important peripheral effects such as energy expenditure. Our results are also consistent with those of Yi et al., [179] who made similar observations of lipids accumulation inhibition in mesenchymal stem cells treated with AuNPs. Further, the decrease in adiponectin concentration observed after 21 days of differentiation is consistent with the previous data that show that two weeks in adipogenic conditions cells can lead to an accumulation of enough lipids and a plateau of adiponectin levels [200]. Therefore, our results showing the decrease in the difference between control and exposed samples may be due to the fact that samples exposed to AuNPs did not reach the plateau in adiponectin levels whereby the controls did. Taken together, these results indicate that the uptake of the AuNPs inhibits the accumulation of lipids during the adipogenic differentiation. This conclusion is in agreement with results published by Yi et al [179] where they found that mesenchymal cells treated with AuNPs exhibit down-regulation of adipogenic specific genes and proteins. They also found activation of the p38 MAPK signaling pathway switched toward osteogenesis as appose to adipogenesis during exposure to AuNPs. It was also

previously reported that AuNPs, can inhibit adipogenesis in mesenchymal stem cells [201, 202].

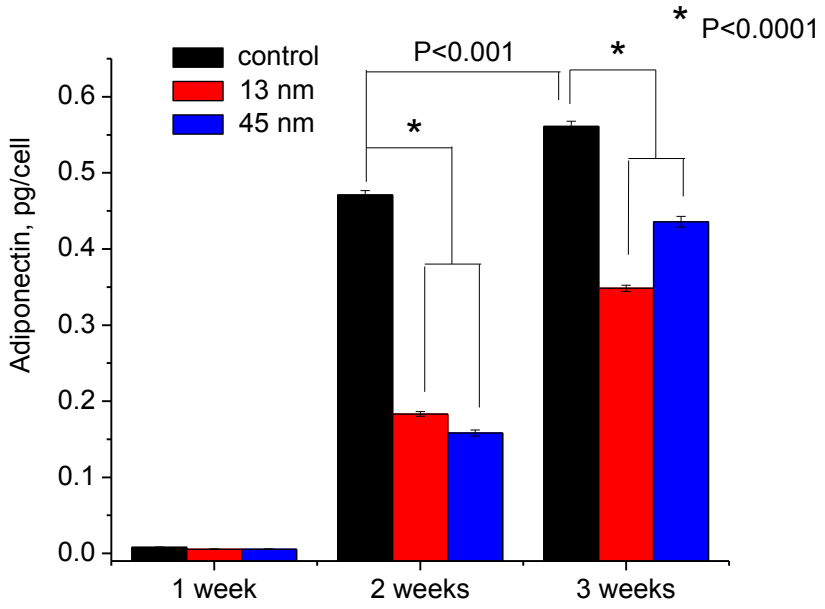

Figure 41. Adiponectin secretion per cell after one, two and three weeks of differentiation with 142 μg/ml 13 nm and 20 μg/ml 45 nm AuNPs and control.

Changes in ECM. During adipocyte differentiation, cells convert from a fibroblastic to a round shape, and significant changes occur in cell morphology, cytoskeletal components, and the level and type of extracellular matrix components [203, 204].

Thus, we decided to look for collagen I and fibronectin expression changes during the differentiation process in cultures with and without exposure to AuNPs. From the Figure 42 we can see, that the only statistically significant decrease for

the collagen secretion was observed after 3 weeks in the adipogenic conditions for all samples. We did not detect any additional changes for the samples exposed to the AuNPs even though in all cases samples exposed to nanoparticles seem to have slightly lower level of the collagen I. In case of fibronectin secretion (Fig. 43) we clearly observe the decrease for samples exposed to AuNPs 21 days after the switching in to adipogenic media.

Many of the studies on the effects of cytoskeletal and ECM components during adipocyte differentiation predate the characterization of adipocyte transcription factors. Previously, it was found that during the adipocyte differentiation, the expression of type I and type III collagens decrease [201, 202], while the synthesis and secretion of type IV collagen increase [205]. On the other hand, the amounts of pericellular and cellular synthesis of fibronectin was found to decrease [206]. These results are in agreement with our findings of the gradual decrease in the fibronectin and collagen expression during differentiation. In addition, we found that exposure to AuNPs have no effect on collagen I production in contrast to dermal fibroblasts [207], while fibronectin production was reduced by ~35% indicating ECM softening unlike human dermal fibroblasts. Since the degradation of fibronectin in the ECM is one of the steps during adipogenesis [208] the fibronectin-poor ECM in the samples treated with AuNPs promotes cell differentiation and therefore partially masks the observed inhibition of differentiation as a function of the lipid accumulation and adiponecting release.

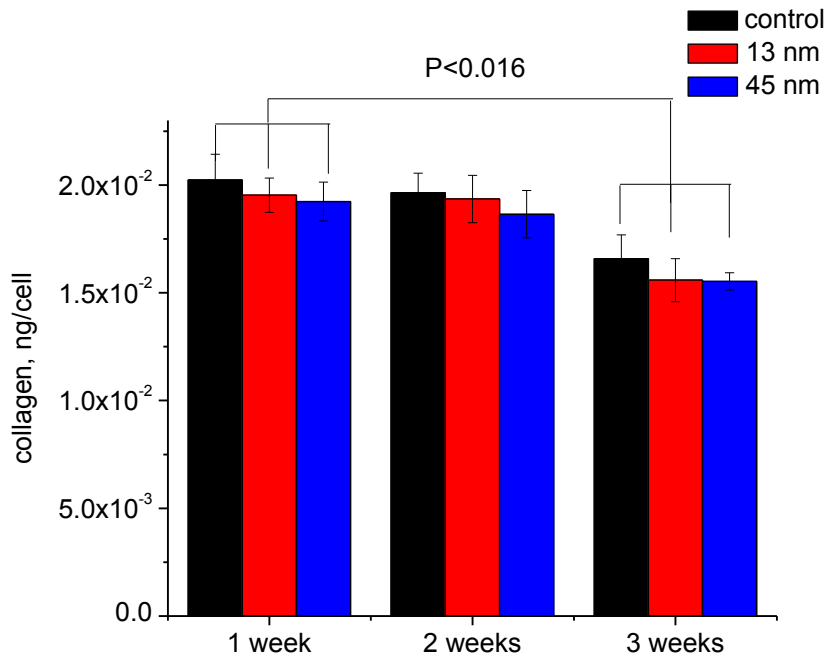

Figure 42. Collagen type I secretion per cell after one, two and three weeks of differentiation with 142 μg/ml 13 nm and 20 μg/ml 45 nm AuNPs and control.

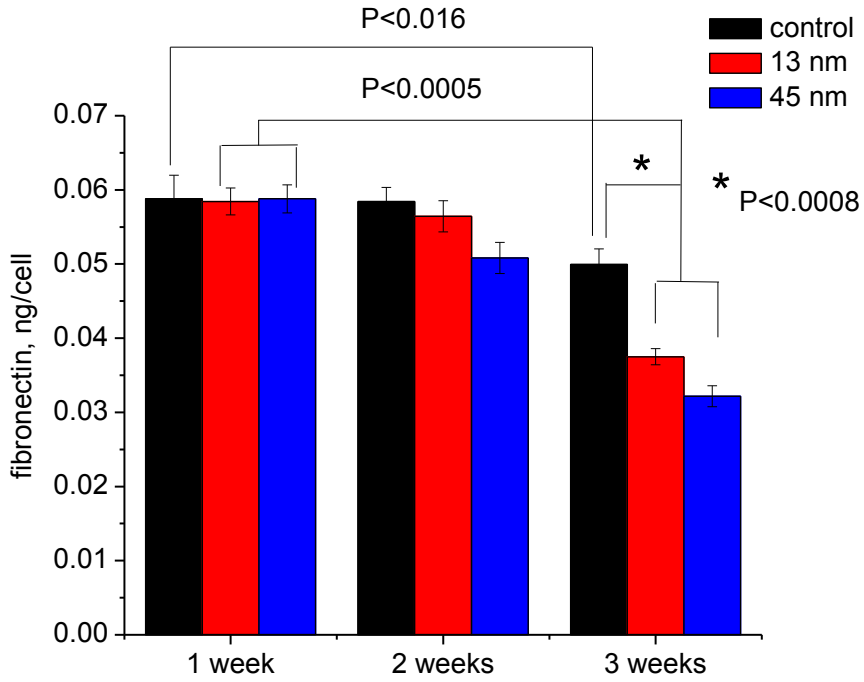

Figure 43. Fibronectin secretion per cell after one, two and three weeks of differentiation with 142 μg/ml 13 nm and 20 μg/ml 45 nm AuNPs and control.

Recovery from AuNP exposure. We had previously seen that it was possible for non-induced ADS cells to recover if the nanoparticles were removed from culture. We therefore also investigated if recovery was possible after differentiation.

This experiment was done in parallel with the differentiation of ADS cells for 4 weeks in the presence of the nanoparticles. Specifically, a separate set of cells were exposed to the AuNPs for 2 weeks following recovery for 2 more weeks. Data from these experiments show that after 2 weeks of AuNP exposure cells exhibit a statistically significant decrease of ~15% and 25% of oil-red absorption indicating lower lipid accumulation for the 45 nm and 13 nm AuNPs, respectively

(Fig. 44). Further, cells exposed to AuNPs for 4 weeks developed a longer delay in accumulation of lipids, with ~45% and 50% for the 45 nm and 13 nm particles, respectively (Fig. 44). One the other hand, samples that were allowed to recover after 2 weeks of differentiation in presence of the AuNPs show a decrease in lipid accumulation that is ~8% and 13% for the 45 nm and 13 nm AuNPs, respectively, indicating recovery (Fig. 44). The fact that the decrease in lipid amount dropped from the 15-25% to the 8-13% after two weeks of recovery shows that recovery is a time dependent process and we might expect complete recovery after longer time. Lastly, to investigate the fate of the internalized AuNPs we repeated this experiment followed by the gold uptake measurements. The data shows that cells that were allowed to recover for 2 weeks have less AuNPs as compared to those that differentiated with AuNPs for 4 weeks. Specifically, cells exposed to 13 nm AuNPs after recovery have ~41% less nanoparticles then the unrecovered ones (Fig. 45). Similarly, the amount of AuNPs is ~35% less in the recovered samples compared to unrecovered in cultures treated with 45 nm gold (Fig. 45).

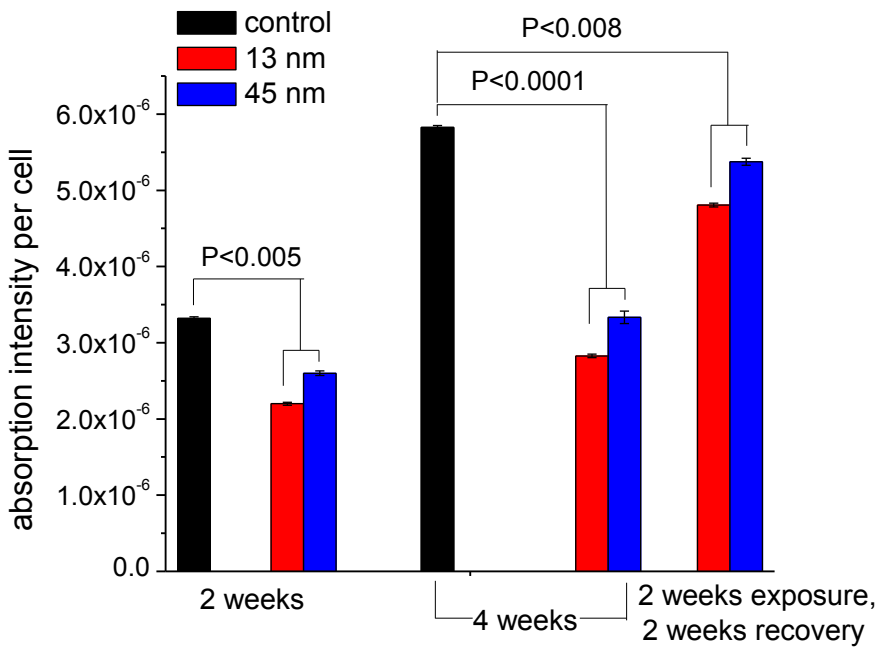

Figure 44. Oil red absorption intensity per cell. ADS cells were cultured for 2 and 4 weeks. Set of samples was exposed to AuNPs for 2 weeks and allowed to recover for following 2 weeks.

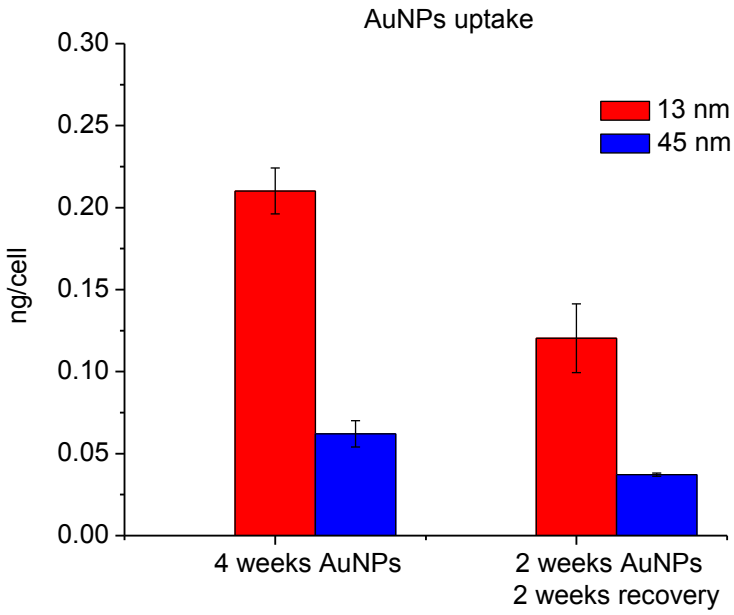

Figure 45. AuNPs uptake per cell. ADS cells were differentiated for 4 weeks, one set of samples was exposed to AuNPs for 4 weeks, another for 2 weeks following 2 weeks of recovery.

Observed 80% recovery within 2 weeks is indicating a temporary effect of the nanoparticles on cell function. We also found that AuNP concentration per cell decreases during recovery indicating the particles are probably eliminated from the cell via exocytosis. That is in agreement with previously published data were the authors quantified the exocytosis of AuNPs as a function of cell type and nanoparticle size [209, 210]. Therefore, the amount of AuNPs inside the cell inversely correlates with an ability of ADS cells to differentiate into adipocytes. This finding can explain the conclusion by Ricles et al [211] that AuNPs have no cytotoxic effects on mesenchymal stem cells and do not inhibit adipogenesis (they exposed cells to nanoparticles for 24 hours prior to 19 days of differentiation).

In summary, our results indicate that AuNPs suppress adipogenesis in ADS cells by down regulation of adipogenic protein adiponectin and lipid accumulation inhibition. In addition, we observed a decrease in cell migration and collagen gel contraction ability with AuNP exposure. Therefore, the discussed in literature noninvasive imaging approach for optical tracking of mesenchymal stem cells by AuNPs during the wound healing process as well as for other therapies [211-213] is still controversial. We also found that differentiation is inversely dependent on AuNPs concentration inside the cell. However, the adverse effect of nanoparticles could be reversed if source of nanoparticles is removed and cells are allowed to recover.

CHAPTER 4

CONCLUSION AND FUTURE WORK

When compared to ADS cells and fibroblasts, epidermal keratinocytes has been affected least by the AuNPs in terms of the detected disruption of the cell functions. These results are in agreement with reports from many research groups and was foreseen as the keratinocytes serves as protective cell layer for the entire body. However, since the experiment was done in vitro where hair follicles as major nanoparticles pathway are not present, the overall affect might be smaller compared to the findings in vivo. On the other hand, topical application is not typical for the AuNPs which are usually injected into the blood stream or directly into the tumor during the chemotherapy.

The effect of AuNPs on the human dermal fibroblasts is more evident and seems to be correlated with the vacuoles formation. Even though the mechanism of sequestration for both particles sizes appears to be similar, the method of penetration into the cytoplasm was determined to be different. In previous studies investigating nanoparticle penetration, gold particles of different shapes or sizes were coated with transferrin [173, 209, 214] for which known membrane recognition pathways exist. In our case, the particles were stabilized with citrate for which no specific recognition site(s) on the plasma membrane is known. Also, to rule out any independent effects of citrate on cells, we exposed cells to citrate and found no differences in cell growth when compared to control cells. Further, most of the previous work was also performed with cancer cells or cell lines whose characteristics are known to differ from primary cells.

It was found that as the human dermal fibroblast cells divide the concentration of particles is decreased, which in turn allows the cells to reduce the number of vacuoles and form normal actin fibers and increase their production of ECM proteins. Hence, after 14 days near full recovery occurs for cells expose to both types of AuNPs. Taken together, these data indicate that AuNPs are toxic for human dermal fibroblasts and the toxicity rate depends on the concentration and size of nanoparticles, as well as the time of exposure. Eventhough, the internalized fate of 13 nm and 45 nm AuNPs is similar the major penetration pathways are different.

Interestingly, western blot analyses reveals that the amount of actin and beta-tubulin formed by the cells is not affected by the presence of the nanoparticles, indicating that it is probably the latter that is responsible for the observed cytoskeletal disruption. We reasoned that the large number of vacuoles as well as “loose" particles found in samples exposed to 45 nm AuNPs interferes with the ability of actin fibers to effectively form linkages with the ECM via integrins. As a result the cell area is decreased and disrupted fibers are observed in the cells. The ECM proteins expression fibronectin and collagen I were found to be significantly reduced in the samples exposed to the AuNPs, more over the fibronectin/collagen ratio was altered leading to harder collagen poor ECM. The two last effects of AuNPs that were found are decrease in the cell velocity in the migration assay and decrease in the collagen gel contraction, these results can be directly linked to the loss of the wound healing ability of the fibroblasts.

ADS cells reaction to nanoparticle exposure was similar to that of dermal fibroblasts. That includes cell proliferation rate dependence on nanoparticle dose and exposure time, loss in the migration and collagen gel contraction ability and recovery after the removal of the AuNPs from the environment. The major

difference was in the morphology of sequestration. In the case of the dermal fibroblasts, the particles were sequestered in vacuoles, and adsorbed to the vacuole membrane. In the case of pre-adipocytes, the particles were uniformly distributed within the vacuole. Yet, despite this difference, the toxicity levels were similar with those observed for both the 13 nm and 45 nm particles in dermal fibroblasts.

Adipocytes that were differentiated in the presence of nanoparticles produced far less lipids. This was further confirmed by confocal microscopy, where the lipid content was imaged using LipidTox. These findings were also consistent with a reduced expression of adiponectin, a known marker of adipogensis which correlates directly with lipid formation. On the other hand, no significant decrease was observed between exposed and non-exposed cells regarding leptin production in day 7.

Finally, we also probed the influence of the AuNPs on ECM proteins production, and found that in contrast to dermal fibroblasts, collagen 1 production was unaffected, while fibronectin production was reduced by 35%. In the case of dermal fibroblasts the fibronectin production was affected to far smaller extend than collagen production. The recovery from nanoparticles exposure was also investigated and we observed increasing lipids formation after the source of the AuNPs was removed from the environment, 80% recovery was observed within 2 weeks indicating permanent effect of the particles exposure.

In summary, our results indicate that overall toxicity of different sizes AuNPs does not depend on total gold concentration in the cell. Rather, sequestration of the particles and the vacuole number and stability play a significant role in the induction of the disruption of the cytoskeleton and extra and

intra cellular proteins expression (fibronectin, collagen I, adiponectin) as well as lipid formation.

These results illustrate the importance of studying the effects of AuNPs on cell function and not simply on proliferation. In vivo the different layers are interdependent. Hence the future direction of this work lies in building an actual constructs of cells exposed to AuNPs both prior and post assembly in order to determine the toxicity effects on the entire tissue.

BIBLIOGRAPHY:

1. Oberdorster, G., *Pulmonary effects of inhaled ultrafine particles.* International Archives of Occupational and Environmental Health, 2001. **74**(1): p. 1-8.

2. Oberdorster, G., *Safety assessment for nanotechnology and nanomedicine: concepts of nanotoxicology.* Journal of Internal Medicine, 2010. **267**(1): p. 89-105.

3. Muhlfeld, C., et al., *Visualization and quantitative analysis of nanoparticles in the respiratory tract by transmission electron microscopy.* Part Fibre Toxicol, 2007. **4**: p. 11.

4. Rothen-Rutishauser, B., et al., *Direct Combination of Nanoparticle Fabrication and Exposure to Lung Cell Cultures in a Closed Setup as a Method To Simulate Accidental Nanoparticle Exposure of Humans.* Environmental Science & Technology, 2009. **43**(7): p. 2634-2640.

5. Buchel, R., S.E. Pratsinis, and A. Baiker, *Influence of controlled spatial deposition of Pt and Pd in NOx storage-reduction catalysts on their efficiency.* Applied Catalysis B-Environmental, 2011. **101**(3-4): p. 682-689.

6. Choi, M., et al., *Electrochemical Characterization of Pt-Ru-Pd Catalysts for Methanol Oxidation Reaction in Direct Methanol Fuel Cells.* Journal of Nanoscience and Nanotechnology, 2011. **11**(1): p. 838-841.

7. Grirrane, A., A. Corma, and H. Garcia, *Stereoselective Single (Copper) or Double (Platinum) Boronation of Alkynes Catalyzed by Magnesia-Supported Copper Oxide or Platinum Nanoparticles.* Chemistry-a European Journal, 2011. **17**(8): p. 2467-2478.

8. Makhubela, B.C.E., A. Jardine, and G.S. Smith, *Pd nanosized particles supported on chitosan and 6-deoxy-6-amino chitosan as recyclable catalysts for Suzuki-Miyaura and Heck cross-coupling reactions.* Applied Catalysis a-General, 2011. **393**(1-2): p. 231-241.

9. Mori, K. and H. Yamashita, *Design of Colloidal and Supported Metal Nanoparticles: Their Synthesis, Characterization, and Catalytic Application.* Journal of the Japan Petroleum Institute, 2011. **54**(1): p. 1-14.

10. Shao, M., *Palladium-based electrocatalysts for hydrogen oxidation and oxygen reduction reactions.* Journal of Power Sources, 2011. **196**(5): p. 2433-2444.

11. Zhang, Z.Y., et al., *Preparation and Characterization of PdFe Nanoleaves as Electrocatalysts for Oxygen Reduction Reaction.* Chemistry of Materials, 2011. **23**(6): p. 1570-1577.

12. Aslan, K., et al., *Saccharide sensing using gold and silver nanoparticles - A review.* Journal of Fluorescence, 2004. **14**(4): p. 391-400.

13. Ding, Y., et al., *Preparation and characterization of NiO-Ag nanofibers, NiO nanofibers, and porous Ag: towards the development of a highly sensitive and selective non-enzymatic glucose sensor.* Journal of Materials Chemistry, 2010. **20**(44): p. 9918-9926.

14. Guascito, M.R., et al., *Ag nanoparticles capped by a nontoxic polymer: Electrochemical and spectroscopic characterization of a novel nanomaterial for glucose detection.* Materials Science & Engineering C-Materials for Biological Applications, 2011. **31**(3): p. 606-611.

15. Li, Y.F., et al., *A nonenzymatic cholesterol sensor constructed by using porous tubular silver nanoparticles.* Biosensors & Bioelectronics, 2010. **25**(10): p. 2356-2360.

16. Park, J.H., et al., *Polymer/Gold nanoparticle nanocomposite light-emitting diodes: Enhancement of electroluminescence stability and quantum efficiency of blue-light-emitting polymers.* Chemistry of Materials, 2004. **16**(4): p. 688-692.

17. Fujiki, A., et al., *Enhanced fluorescence by surface plasmon coupling of Au nanoparticles in an organic electroluminescence diode.* Applied Physics Letters, 2010. **96**(4).

18. Saikia, G., et al., *Tuning the Optical Characteristics of Poly(p-phenylenevinylene) by in Situ Au Nanoparticle Generation.* Journal of Physical Chemistry B, 2010. **114**(46): p. 14821-14826.

19. Son, D.I., et al., *Bistable Organic Memory Device with Gold Nanoparticles Embedded in a Conducting Poly(N-vinylcarbazole) Colloids Hybrid.* Journal of Physical Chemistry C, 2011. **115**(5): p. 2341-2348.

20. Sarkar, D.K., et al., *Single-electron tunneling at room temperature in TixSi1-xO2 nanocomposite thin films.* Applied Physics Letters, 2005. **87**.

21. Shilova, O.A., *Silicate nanosized films prepared by the sol-gel method for use in planar technology for fabricating semiconductor gas sensors.* Glass Physics and Chemistry, 2005. **31**(2): p. 201-218.

22. Alivisatos, A.P., *Semiconductor clusters, nanocrystals, and quantum dots.* Science, 1996. **271**(5251): p. 933-937.

23. McConnell, W.P., et al., *Electronic and optical properties of chemically modified metal nanoparticles and molecularly bridged nanoparticle arrays.* Journal of Physical Chemistry B, 2000. **104**(38): p. 8925-8930.

24. Nath, N. and A. Chilkoti, *Interfacial phase transition of an environmentally responsive elastin biopolymer adsorbed on functionalized gold nanoparticles studied by colloidal surface plasmon resonance.* Journal of the American Chemical Society, 2001. **123**(34): p. 8197-8202.

25. Link, S. and M.A. El-Sayed, *Shape and size dependence of radiative, non-radiative and photothermal properties of gold nanocrystals.* International Reviews in Physical Chemistry, 2000. **19**(3): p. 409-453.

26. Link, S., M.A. El-Sayed, and M.B. Mohamed, *Simulation of the optical absorption spectra of gold nanorods as a function of their aspect ratio and the effect of the medium dielectric constant (vol 103B, pg 3073, 1999).* Journal of Physical Chemistry B, 2005. **109**(20): p. 10531-10532.

27. Link, S., M.B. Mohamed, and M.A. El-Sayed, *Simulation of the optical absorption spectra of gold nanorods as a function of their aspect ratio and the effect of the medium dielectric constant.* Journal of Physical Chemistry B, 1999. **103**(16): p. 3073-3077.

28. Nikoobakht, B., J.P. Wang, and M.A. El-Sayed, *Surface-enhanced Raman scattering of molecules adsorbed on gold nanorods: off-surface plasmon resonance condition.* Chemical Physics Letters, 2002. **366**(1-2): p. 17-23.

29. Bielinska, A., et al., *Imaging {Au-0-PAMAM} gold-dendrimer nanocomposites in cells.* Journal of Nanoparticle Research, 2002. **4**(5): p. 395-403.

30. Niemeyer, C.M., *Nanoparticles, proteins, and nucleic acids: Biotechnology meets materials science.* Angewandte Chemie-International Edition, 2001. **40**(22): p. 4128-4158.

31. Olofsson, L., et al., *Surface-based gold-nanoparticle sensor for specific and quantitative DNA hybridization detection.* Langmuir, 2003. **19**(24): p. 10414-10419.

32. Sanford, J.C., F.D. Smith, and J.A. Russell, *Optimizing the biolistic process for different biological applications*. Methods in Enzymology, 1993. **217**: p. 483-509.

33. Kim, D., et al., *Antibiofouling polymer-coated gold nanoparticles as a contrast agent for in vivo x-ray computed tomography imaging.* Journal of the American Chemical Society, 2007. **129**(24): p. 7661-7665.

34. Kim, H.K., et al., *Gold nanoparticles coated with gadolinium-DTPA-bisamide conjugate of penicillamine (Au@GdL) as a T1-weighted blood pool contrast agent.* Journal of Materials Chemistry, 2010. **20**(26): p. 5411-5417.

35. Ranjbar, H., M. Shamsaei, and M.R. Ghasemi, *Investigation of the dose enhancement factor of high intensity low mono-energetic X-ray radiation with labeled tissues by gold nanoparticles.* Nukleonika, 2010. **55**(3): p. 307-312.

36. Wang, H., et al., *Computed tomography imaging of cancer cells using acetylated dendrimer-entrapped gold nanoparticles.* Biomaterials, 2011. **32**(11): p. 2979-2988.

37. Anderson, S.A., et al., *Magnetic resonance contrast enhancement of neovasculature with alpha(v)beta(3)-targeted nanoparticles.* Magnetic Resonance in Medicine, 2000. **44**(3): p. 433-439.

38. Astruc, D., M.C. Daniel, and J. Ruiz, *Dendrimers and gold nanoparticles as exo-receptors sensing biologically important anions.* Chemical Communications, 2004(23): p. 2637-2649.

39. Csaki, A., R. Moller, and W. Fritzsche, *Gold nanoparticles as novel label for DNA diagnostics.* Expert Rev Mol Diagn, 2002. **2**(2): p. 187-93.

40. Letsinger, R.L., et al., *Chemistry of oligonucleotide-gold nanoparticle conjugates.* Phosphorus Sulfur and Silicon and the Related Elements, 1999. **146**: p. 359-362.

41. Balogh, L.P., et al., *Development of radioactive gold-dendrimer nanocomposite devices to treat tumor microvasculature: Synthesis and biodistribution.* Journal of Nuclear Medicine, 2003. **44**(5): p. 1094.

42. Chen, J., et al., *Gold nanocages: Bioconjugation and their potential use as optical imaging contrast agents.* Nano Letters, 2005. **5**(3): p. 473-477.

43. Copland, J.A., et al., *Bioconjugated gold nanoparticles as a molecular based contrast agent: Implications for imaging of deep tumors using optoacoustic tomography.* Molecular Imaging and Biology, 2004. **6**(5): p. 341-349.

44. Katz, E. and I. Willner, *Integrated nanoparticle-biomolecule hybrid systems: Synthesis, properties, and applications.* Angewandte Chemie-International Edition, 2004. **43**(45): p. 6042-6108.

45. Nam, J.M., S.I. Stoeva, and C.A. Mirkin, *Bio-bar-code-based DNA detection with PCR-like sensitivity.* Journal of the American Chemical Society, 2004. **126**(19): p. 5932-5933.

46. Paciotti, G.F., et al., *Colloidal gold: A novel nanoparticle vector for tumor directed drug delivery.* Drug Delivery, 2004. **11**(3): p. 169-183.

47. Fujimoto, T., et al., *Accumulation of MRI contrast agents in malignant fibrous histiocytoma for gadolinium neutron capture therapy.* Applied Radiation and Isotopes, 2009. **67**(7-8): p. S355-S358.

48. Fukumori, Y. and H. Ichikawa, *Nanoparticles for cancer therapy and diagnosis.* Advanced Powder Technology, 2006. **17**(1): p. 1-28.

49. Maeda, H., G.Y. Bharate, and J. Daruwalla, *Polymeric drugs for efficient tumor-targeted drug delivery based on EPR-effect.* European Journal of Pharmaceutics and Biopharmaceutics, 2009. **71**(3): p. 409-419.

50. Maeda, H., L.W. Seymour, and Y. Miyamoto, *Conjugates of anticancer agents and polymers - advantages of macromolecular therapeutics in vivo.* Bioconjugate Chemistry, 1992. **3**(5): p. 351-362.

51. Yu, D.S., et al., *Antitumor activity of poly(ethylene glycol)-camptothecin conjugate: The inhibition of tumor growth in vivo.* Journal of Controlled Release, 2005. **110**(1): p. 90-102.

52. Hu, K.-W., et al., *Efficient Near-IR Hyperthermia and Intense Nonlinear Optical Imaging Contrast on the Gold Nanorod-in-Shell Nanostructures.* Journal of the American Chemical Society, 2009. **131**(40): p. 14186-14187.

53. Libutti, S.K., et al., *Phase I and Pharmacokinetic Studies of CYT-6091, a Novel PEGylated Colloidal Gold-rhTNF Nanomedicine.* Clinical Cancer Research, 2010. **16**(24): p. 6139-6149.

54. Malugin, A. and H. Ghandehari, *Cellular uptake and toxicity of gold nanoparticles in prostate cancer cells: a comparative study of rods and spheres.* J Appl Toxicol, 2010. **30**(3): p. 212-7.

55. Zhou, Y., et al., *A comparison study of detecting gold nanorods in living cells with confocal reflectance microscopy and two-photon fluorescence microscopy.* Journal of Microscopy-Oxford, 2010. **237**(2): p. 200-207.

56. Geso, M., *Gold nanoparticles: a new X-ray contrast agent.* British Journal of Radiology, 2007. **80**(949): p. 64-65.

57. Kattumuri, V., et al., *Gum arabic as a phytochemical construct for the stabilization of gold nanoparticles: In vivo pharmacokinetics and X-ray-contrast-imaging studies.* Small, 2007. **3**(2): p. 333-341.

58. Park, Y.S., et al., *Concentrated colloids of silica-encapsulated gold nanoparticles: Colloidal stability, cytotoxicity, and X-ray absorption.* Journal of Nanoscience and Nanotechnology, 2007. **7**(8): p. 2690-2695.

59. Tkachenko, A.G., et al., *Cellular trajectories of peptide-modified gold particle complexes: Comparison of nuclear localization signals and peptide transduction domains.* Bioconjugate Chemistry, 2004. **15**(3): p. 482-490.

60. Elghanian, R., et al., *Selective colorimetric detection of polynucleotides based on the distance-dependent optical properties of gold nanoparticles.* Science, 1997. **277**(5329): p. 1078-1081.

61. Sokolov, K., et al., *Optical systems for In vivo molecular imaging of cancer.* Technology in Cancer Research & Treatment, 2003. **2**(6): p. 491-504.

62. Sokolov, K., et al., *Molecular optical imaging of therapeutic targets of cancer.* Advances in Cancer Research, Vol 96, 2007. **96**: p. 299-344.

63. O'Neal, D.P., et al., *Photo-thermal tumor ablation in mice using near infrared-absorbing nanoparticles.* Cancer Letters, 2004. **209**(2): p. 171-176.

64. Tkachenko, A., et al., *Assembly and characterization of biomolecule-gold nanoparticle conjugates and their use in intracellular imaging.* Nanobiotechnology Protocols, 2005. **303**: p. 85-99.

65. Hainfeld, J.F., et al., *Gold nanoparticles: a new X-ray contrast agent.* British Journal of Radiology, 2006. **79**(939): p. 248-253.

66. Hainfeld, J.F., D.N. Slatkin, and H.M. Smilowitz, *The use of gold nanoparticles to enhance radiotherapy in mice.* Physics in Medicine and Biology, 2004. **49**(18): p. N309-N315.

67. Boote, E., et al., *Gold Nanoparticle Contrast in a Phantom and Juvenile Swine: Models for Molecular Imaging of Human Organs using X-ray Computed Tomography.* Academic Radiology, 2010. **17**(4): p. 410-417.

68. Chanda, N., et al., *Radioactive gold nanoparticles in cancer therapy: therapeutic efficacy studies of GA-(AuNP)-Au-198 nanoconstruct in prostate tumor-bearing mice.* Nanomedicine-Nanotechnology Biology and Medicine, 2010. **6**(2): p. 201-209.

69. Kannan, R., et al., *Nanocompatible chemistry toward fabrication of target-specific gold nanoparticles.* Journal of the American Chemical Society, 2006. **128**(35): p. 11342-11343.

70. Baranov, V.I., Y.A. Sopova, and P.V. Zemplyanoy, ccupational hygiene regulations during the manufacture, use, and utilization of nanomaterials. Gigiena i Sanitariya, 2009(6): p. 53-55.

71. Buzea, C., Pacheco, II, and K. Robbie, *Nanomaterials and nanoparticles: Sources and toxicity.* Biointerphases, 2007. **2**(4): p. MR17-MR71.

72. Kwon, J.T., et al., *Body distribution of inhaled fluorescent magnetic nanoparticles in the mice.* Journal of Occupational Health, 2008. **50**(1): p. 1-6.

73. Mo, Y.Q., et al., *Cytokine and NO release from peripheral blood neutrophils after exposure to metal nanoparticles: in vitro and ex vivo studies.* Nanotoxicology, 2008. **2**(2): p. 79-87.

74. Rothen-Rutishauser, B.M., et al., *Interaction of fine particles and nanoparticles with red blood cells visualized with advanced microscopic techniques.* Environmental Science & Technology, 2006. **40**(14): p. 4353-4359.

75. Warheit, D.B., et al., *Testing strategies to establish the safety of nanomaterials: Conclusions of an ECETOC workshop.* Inhalation Toxicology, 2007. **19**(8): p. 631-643.

76. Wu, J.H., et al., *Toxicity and penetration of TiO2 nanoparticles in hairless mice and porcine skin after subchronic dermal exposure.* Toxicology Letters, 2009. **191**(1): p. 1-8.

77. Boverhof, D.R. and R.M. David, *Nanomaterial characterization: considerations and needs for hazard assessment and safety evaluation.* Analytical and Bioanalytical Chemistry, 2010. **396**(3): p. 953-961.

78. Fan, A.M. and G. Alexeeff, *Nanotechnology and Nanomaterials: Toxicology, Risk Assessment, and Regulations.* Journal of Nanoscience and Nanotechnology, 2010. **10**(12): p. 8646-8657.

79. Holgate, S.T., *Exposure, Uptake, Distribution and Toxicity of Nanomaterials in Humans.* Journal of Biomedical Nanotechnology, 2010. **6**(1): p. 1-19.

80. Maynard, A.D., D.B. Warheit, and M.A. Philbert, *The New Toxicology of Sophisticated Materials: Nanotoxicology and Beyond.* Toxicological Sciences, 2011. **120**: p. S109-S129.

81. Savolainen, K., et al., *Risk assessment of engineered nanomaterials and nanotechnologies-A review.* Toxicology, 2010. **269**(2-3): p. 92-104.

82. Savolainen, K., et al., *Nanotechnologies, engineered nanomaterials and occupational health and safety - A review.* Safety Science, 2010. **48**(8): p. 957-963.

83. Borm, P.J.A. and W. Kreyling, *Toxicological hazards of inhaled nanoparticles - Potential implications for drug delivery.* Journal of Nanoscience and Nanotechnology, 2004. **4**(5): p. 521-531.

84. Lam, C.W., et al., *A review of carbon nanotube toxicity and assessment of potential occupational and environmental health risks.* Critical Reviews in Toxicology, 2006. **36**(3): p. 189-217.

85. Pauluhn, J., *Comparative pulmonary response to inhaled nanostructures: considerations on test design and endpoints.* Inhal Toxicol, 2009. **21 Suppl 1**: p. 40-54.

86. Zhang, Q.W., et al., *Comparative toxicity of standard nickel and ultrafine nickel in lung after intratracheal instillation.* Journal of Occupational Health, 2003. **45**(1): p. 23-30.

87. Aschberger, K., et al., *Review of fullerene toxicity and exposure - Appraisal of a human health risk assessment, based on open literature.* Regulatory Toxicology and Pharmacology, 2010. **58**(3): p. 455-473.

88. Donaldson, K., et al., *Carbon nanotubes: A review of their properties in relation to pulmonary toxicology and workplace safety.* Toxicological Sciences, 2006. **92**(1): p. 5-22.

89. Smijs, T.G.M. and J.A. Bouwstra, *Focus on Skin as a Possible Port of Entry for Solid Nanoparticles and the Toxicological Impact.* Journal of Biomedical Nanotechnology, 2010. **6**(5): p. 469-484.

90. Baroli, B., *Penetration of Nanoplarticles and Nanomaterials in the Skin: Fiction or Reality?* Journal of Pharmaceutical Sciences, 2010. **99**(1): p. 21-50.

91. Baroli, B., *Skin Absorption and Potential Toxicity of Nanoparticulate Nanomaterials.* Journal of Biomedical Nanotechnology, 2010. **6**(5): p. 485-496.

92. Wiechers, J.W. and N. Musee, *Engineered Inorganic Nanoparticles and Cosmetics: Facts, Issues, Knowledge Gaps and Challenges.* Journal of Biomedical Nanotechnology, 2010. **6**(5): p. 408-431.

93. Alvarez-Roman, R., et al., *Visualization of skin penetration using confocal laser scanning microscopy.* European Journal of Pharmaceutics and Biopharmaceutics, 2004. **58**(2): p. 301-316.

94. Alvarez-Roman, R., et al., *Enhancement of topical delivery from biodegradable nanoparticles.* Pharmaceutical Research, 2004. **21**(10): p. 1818-1825.

95. Lademann, J., et al., *Nanoparticles - An efficient carrier for drug delivery into the hair follicles.* European Journal of Pharmaceutics and Biopharmaceutics, 2007. **66**(2): p. 159-164.

96. Toll, R., et al., *Penetration profile of microspheres in follicular targeting of terminal hair follicles.* Journal of Investigative Dermatology, 2004. **123**(1): p. 168-176.

97. Souto, E.B., A.J. Almeida, and R.H. Muller, *Lipid nanoparticles (SLN (R), NLC (R)) for cutaneous drug delivery: Structure, protection and skin effects.* Journal of Biomedical Nanotechnology, 2007. **3**(4): p. 317-331.

98. Kuchler, S., et al., *Nanoparticles for skin penetration enhancement - a comparison of dendritic core-multishell nanotransporters and solid lipid nanoparticles.* Naunyn-Schmiedebergs Archives of Pharmacology, 2009. **379**: p. 1.

99. Teeranachaideekul, V., et al., *Influence of oil content on physicochemical properties and skin distribution of Nile red-loaded NLC.* Journal of Controlled Release, 2008. **128**(2): p. 134-141.

100. Rancan, F., et al., *Investigation of Polylactic Acid (PLA) Nanoparticles as Drug Delivery Systems for Local Dermatotherapy.* Pharmaceutical Research, 2009. **26**(8): p. 2027-2036.

101. Baroli, B., et al., *Penetration of metallic nanoparticles in human full-thickness skin.* Journal of Investigative Dermatology, 2007. **127**(7): p. 1701-1712.

102. Mortensen, L.J., et al., *Progress and Challenges in Quantifying Skin Permeability to Nanoparticles Using a Quantum Dot Model.* Journal of Biomedical Nanotechnology, 2010. **6**(5): p. 596-604.

103. Ryman-Rasmussen, J.P., J.E. Riviere, and N.A. Monteiro-Riviere, *Penetration of intact skin by quantum dots with diverse physicochemical properties.* Toxicological Sciences, 2006. **91**(1): p. 159-165.

104. Zhang, L.W. and N.A. Monteiro-Riviere, *Assessment of quantum dot penetration into intact, tape-stripped, abraded and flexed rat skin.* Skin Pharmacology and Physiology, 2008. **21**(3): p. 166-180.

105. Zhang, L.W., et al., *Biological interactions of quantum dot nanoparticles in skin and in human epidermal keratinocytes.* Toxicology and Applied Pharmacology, 2008. **228**(2): p. 200-211.

106. Kohli, A.K. and H.O. Alpar, *Potential use of nanoparticles for transcutaneous vaccine delivery: effect of particle size and charge.* International Journal of Pharmaceutics, 2004. **275**(1-2): p. 13-17.

107. Lademann, J., et al., *Hair follicles - A long-term reservoir for drug delivery.* Skin Pharmacology and Physiology, 2006. **19**(4): p. 232-236.

108. Vogt, A., et al., *40 nm, but not 750 or 1,500 nm, nanoparticles enter epidermal CD1a+ cells after transcutaneous application on human skin.* Journal of Investigative Dermatology, 2006. **126**: p. 1316-1322.

109. Cattani, V.B., et al., *Lipid-core nanocapsules restrained the indomethacin ethyl ester hydrolysis in the gastrointestinal lumen and wall acting as mucoadhesive reservoirs.* European Journal of Pharmaceutical Sciences, 2010. **39**(1-3): p. 116-124.

110. Chen, M.C., et al., *The characteristics, biodistribution and bioavailability of a chitosan-based nanoparticulate system for the oral delivery of heparin.* Biomaterials, 2009. **30**(34): p. 6629-6637.

111. Gao, F., et al., *Nanoemulsion improves the oral absorption of candesartan cilexetil in rats: Performance and mechanism.* Journal of Controlled Release, 2011. **149**(2): p. 168-174.

112. Takeuchi, H. and H. Sugihara, *Absorption of Calcitonin in Oral and Pulmonary Administration with Polymer-coated Liposomes.* Yakugaku Zasshi-Journal of the Pharmaceutical Society of Japan, 2010. **130**(9): p. 1135-1142.

113. Wong, T.W., *Design of oral insulin delivery systems.* Journal of Drug Targeting, 2010. **18**(2): p. 79-92.

114. Florence, A.T., *Issues in oral nanoparticle drug carrier uptake and targeting.* Journal of Drug Targeting, 2004. **12**(2): p. 65-70.

115. Hillyer, J.F. and R.M. Albrecht, *Gastrointestinal persorption and tissue distribution of differently sized colloidal gold nanoparticles.* Journal of Pharmaceutical Sciences, 2001. **90**(12): p. 1927-1936.

116. Lambkin, I. and C. Pinilla, *Targeting approaches to oral drug delivery.* Expert Opinion on Biological Therapy, 2002. **2**(1): p. 67-73.

117. Mahato, R.I., et al., *Emerging trends in oral delivery of peptide and protein drugs.* Critical Reviews in Therapeutic Drug Carrier Systems, 2003. **20**(2-3): p. 153-214.

118. Beier, R. and A. Gebert, *Kinetics of particle uptake in the domes of Peyer's patches.* American Journal of Physiology-Gastrointestinal and Liver Physiology, 1998. **275**(1): p. G130-G137.

119. Eldridge, J.H., et al., *Vaccine containing biodegradable microspheres specifically enter the gut assosiated lymphoid tissue following oral administration and induce a disseminated mucosal immune responce*. Immunobiology of Proteins and Peptides V : Vaccines, 1989. **251**: p. 191-202.

120. Di Stefano, A., et al., *Drug delivery strategies for Alzheimer's disease treatment.* Expert Opinion on Drug Delivery, 2011. **8**(5): p. 581-603.

121. Jain, S., et al., *Nanocarriers for Transmucosal Vaccine Delivery.* Current Nanoscience, 2011. **7**(2): p. 160-177.

122. Mittal, G., et al., *Development and evaluation of polymer nanoparticles for oral delivery of estradiol to rat brain in a model of Alzheimer's pathology.* Journal of Controlled Release, 2011. **150**(2): p. 220-228.

123. Wang, J.J., et al., *Recent advances of chitosan nanoparticles as drug carriers.* International Journal of Nanomedicine, 2011. **6**: p. 765-774.

124. Goodman, C.M., et al., *Toxicity of gold nanoparticles functionalized with cationic and anionic side chains.* Bioconjugate Chemistry, 2004. **15**(4): p. 897-900.

125. Takahashi, H., et al., *Modification of gold nanorods using phospatidylcholine to reduce cytotoxicity.* Langmuir, 2006. **22**(1): p. 2-5.

126. Tsoli, M., et al., *Cellular uptake and toxicity of AU(55) clusters.* Small, 2005. **1**(8-9): p. 841-844.

127. Pernodet, N., et al., *Adverse effects of citrate/gold nanoparticles on human dermal fibroblasts.* Small, 2006. **2**(6): p. 766-773.

128. Qu, Y.H. and X.Y. Lu, *Aqueous synthesis of gold nanoparticles and their cytotoxicity in human dermal fibroblasts-fetal.* Biomedical Materials, 2009. **4**(2).

129. Jan, E., et al., *High-content screening as a universal tool for fingerprinting of cytotoxicity of nanoparticles.* Acs Nano, 2008. **2**(5): p. 928-938.

130. Shukla, R., et al., *Biocompatibility of gold nanoparticles and their endocytotic fate inside the cellular compartment: A microscopic overview.* Langmuir, 2005. **21**(23): p. 10644-10654.

131. Patra, H.K., et al., *Cell selective response to gold nanoparticles.* Nanomedicine-Nanotechnology Biology and Medicine, 2007. **3**(2): p. 111-119.

132. Ryan, J.A., et al., *Cellular uptake of gold nanoparticles passivated with BSA-SV40 large T antigen conjugates.* Analytical Chemistry, 2007. **79**(23): p. 9150-9159.

133. Sonavane, G., et al., *In vitro permeation of gold nanoparticles through rat skin and rat intestine: Effect of particle size.* Colloids and Surfaces B-Biointerfaces, 2008. **65**(1): p. 1-10.

134. Khlebtsov, N. and L. Dykman, *Biodistribution and toxicity of engineered gold nanoparticles: a review of in vitro and in vivo studies.* Chemical Society Reviews, 2011. **40**(3): p. 1647-1671.

135. Murphy, C.J., et al., *Gold Nanoparticles in Biology: Beyond Toxicity to Cellular Imaging.* Accounts of Chemical Research, 2008. **41**(12): p. 1721-1730.

136. Hauck, T.S., A.A. Ghazani, and W.C.W. Chan, *Assessing the effect of surface chemistry on gold nanorod uptake, toxicity, and gene expression in mammalian cells.* Small, 2008. **4**(1): p. 153-159.

137. Khan, J.A., et al., *Molecular effects of uptake of gold nanoparticles in HeLa cells.* Chembiochem, 2007. **8**(11): p. 1237-1240.

138. Ponti, J., et al., *A quantitative in vitro approach to study the intracellular fate of gold nanoparticles: from synthesis to cytotoxicity.* Nanotoxicology, 2009. **3**(4): p. 296-306.

139. Connor, E.E., et al., *Gold nanoparticles are taken up by human cells but do not cause acute cytotoxicity.* Small, 2005. **1**(3): p. 325-327.

140. Huang, Y.C., et al., *Epidermal morphogenesis in an in-vitro model using a fibroblasts-embedded collagen scaffold.* Journal of Biomedical Science, 2005. **12**(6): p. 855-867.

141. Ikuta, S., et al., *Mouse epidermal keratinocytes in three-dimensional organotypic coculture with dermal fibroblasts form a stratified sheet resembling skin.* Bioscience Biotechnology and Biochemistry, 2006. **70**(11): p. 2669-2675.

142. Sawyer, R.H., et al., *Evolutionary origin of the feather epidermis.* Developmental Dynamics, 2005. **232**(2): p. 256-267.

143. Wang, T.W., et al., *Biomimetic bilayered gelatin-chondroitin 6 sulfate-hyaluronic acid biopolymer as a scaffold for skin equivalent tissue engineering.* Artificial Organs, 2006. **30**(3): p. 141-149.

144. Yamaguchi, Y., et al., *Mesenchymal-epithelial interactions in the skin: Aiming for site-specific tissue regeneration.* Journal of Dermatological Science, 2005. **40**(1): p. 1-9.

145. Burgeson, R.E. and A.M. Christiano, *The dermal-epidermal junction.* Current Opinion in Cell Biology, 1997. **9**(5): p. 651-658.

146. Marinkovich, M.P., et al., *Cellular origin of the dermal-epidermal basement membrane.* Developmental Dynamics, 1993. **197**(4): p. 255-267.

147. Amano, S., et al., *Importance of balance between extracellular matrix synthesis and degradation in basement membrane formation.* Experimental Cell Research, 2001. **271**(2): p. 249-262.

148. Nishiyama, T., et al., *The importance of laminin 5 in the dermal-epidermal basement membrane.* Journal of Dermatological Science, 2000. **24**: p. S51-S59.

149. Kahari, V.M., et al., *Differential modulation of basement membrane gene expression in human fibrosarcoma HT-1080 cells by transforming growth*

factor-beta-1-enchanced type-IV collagen and fibronectin gene expression correlates with altered culture phenotype of the cells. Laboratory Investigation, 1991. **64**(6): p. 807-818.

150. Konig, A. and L. Brucknertuderman, *Transforming growth-factor-beta stimulates collagen-VII expression by cutaneous cells - in vitro.* Journal of Cell Biology, 1992. **117**(3): p. 679-685.

151. El-Ghalbzouri, A., et al., *Effect of fibroblasts on epidermal regeneration.* British Journal of Dermatology, 2002. **147**(2): p. 230-243.

152. Ezure, T. and S. Amano, *Influence of subcutaneous adipose tissue mass on dermal elasticity and sagging severity in lower cheek.* Skin Research and Technology, 2010. **16**(3): p. 332-338.

153. Srisuma, S., et al., *Fibroblast Growth Factor Receptors Control Epithelial-Mesenchymal Interactions Necessary for Alveolar Elastogenesis.* American Journal of Respiratory and Critical Care Medicine, 2010. **181**(8): p. 838-850.

154. Turkevich, J., *Colloidal gold. Part I.* Gold Bulletin, 1985. **18**(3): p. 86-92.

155. Turkevich, J., *Colloidal gold. Part II.* Gold Bulletin, 1985. **18**(4): p. 125-131.

156. Haiss, W., et al., *Determination of size and concentration of gold nanoparticles from UV-Vis spectra.* Analytical Chemistry, 2007. **79**(11): p. 4215-4221.

157. Kolwas, K., A. Derkachova, and M. Shopa, *Size characteristics of surface plasmons and their manifestation in scattering properties of metal particles.* Journal of Quantitative Spectroscopy & Radiative Transfer, 2009. **110**(14-16): p. 1490-1501.

158. Njoki, P.N., et al., *Size correlation of optical and spectroscopic properties for gold nanoparticles.* Journal of Physical Chemistry C, 2007. **111**: p. 14664-14669.

159. Kelly, K.L., et al., *The optical properties of metal nanoparticles: The influence of size, shape, and dielectric environment.* Journal of Physical Chemistry B, 2003. **107**(3): p. 668-677.

160. Daniel, M.C. and D. Astruc, *Gold nanoparticles: Assembly, supramolecular chemistry, quantum-size-related properties, and applications toward*

biology, catalysis, and nanotechnology. Chemical Reviews, 2004. **104**(1): p. 293-346.

161. Henzie, J., et al., *Manipulating the optical properties of pyramidal nanoparticle arrays*. Journal of Physical Chemistry B, 2006. **110**(29): p. 14028-14031.

162. Mie, G., *Articles on the optical characteristics of turbid tubes, especially colloidal metal solutions.* Annalen Der Physik, 1908. **25**(3): p. 377-445.

163. Stratton, J.A. and L.J. Chu, *Steady-state solutions of electromagnetic field problems II. Forced oscillations of a conducting sphere.* Journal of Applied Physics, 1941. **12**(3): p. 236-240.

164. Bohren, C.F. and T.J. Nevitt, *Absorption by a sphere - a simple approximation.* Applied Optics, 1983. **22**(6): p. 774-775.

165. Kittler, S., et al., *Toxicity of Silver Nanoparticles Increases during Storage Because of Slow Dissolution under Release of Silver Ions.* Chemistry of Materials, 2010. **22**(16): p. 4548-4554.

166. Auffan, M., et al., *Chemical stability of metallic nanoparticles: A parameter controlling their potential cellular toxicity in vitro.* Environmental Pollution, 2009. **157**(4): p. 1127-1133.

167. Pourbaix, M., *Applications of electrochemistry in corrosion science and in practice.* Corrosion Science, 1974. **14**(1): p. 25-82.

168. Eckert, R.L. and E.A. Rorke, *Molecular-biology of keratinocyte defferentiation.* Environmental Health Perspectives, 1989. **80**: p. 109-116.

169. Geiser, M., et al., *Ultrafine particles cross cellular membranes by nonphagocytic mechanisms in lungs and in cultured cells.* Environmental Health Perspectives, 2005. **113**(11): p. 1555-1560.

170. Gibson, A.E., et al., *Phenylarsine oxide inhibition of endocytosis - effects on asialofetuin internalization.* American Journal of Physiology, 1989. **257**(2): p. C182-C184.

171. Sudhakaran, P.R., R. Prinz, and K. Vonfigura, *Effect of temperature on endocytosis and degradation of sulfated proteoglycans by cultured skin fibroblasts.* Journal of Biosciences, 1982. **4**(4): p. 413-418.

172. Mamdouh, Z., et al., *Temperature dependence of endocytosis in renal epithelial cells in culture.* Biochimica Et Biophysica Acta-Biomembranes, 1996. **1282**(2): p. 171-173.

173. Cornell, E., *Cytotoxicity of Gold Nanoparticles in Mast Cells.* Biological Applications, 2006. **2**(3).

174. Pan, Y., et al., *Size-dependent cytotoxicity of gold nanoparticles.* Small, 2007. **3**: p. 1941-1949.

175. Chithrani, B.D., A.A. Ghazani, and W.C.W. Chan, *Determining the size and shape dependence of gold nanoparticle uptake into mammalian cells.* Nano Letters, 2006. **6**(4): p. 662-668.

176. Krpetic, Z., F. Porta, and G. Scari, *Selective entrance of gold nanoparticles into cancer cells.* Gold Bulletin, 2006. **39**(2): p. 66-68.

177. Sundelacruz, S., M. Levin, and D.L. Kaplan, *Membrane Potential Controls Adipogenic and Osteogenic Differentiation of Mesenchymal Stem Cells.* Plos One, 2008. **3**(11).

178. Yu, H., et al., *Mechanical behavior of human mesenchymal stem cells during adipogenic and osteogenic differentiation.* Biochemical and Biophysical Research Communications, 2010. **393**(1): p. 150-155.

179. Yi, C.Q., et al., *Gold Nanoparticles Promote Osteogenic Differentiation of Mesenchymal Stem Cells through p38 MAPK Pathway.* Acs Nano, 2010. **4**(11): p. 6439-6448.

180. Ibrahimi, A., et al., *Essential role of collagens for terminal differentiation of preadipocytes.* Biochemical and Biophysical Research Communications, 1992. **187**(3): p. 1314-1322.

181. Gregoire, F.M., *Adipocyte differentiation: From fibroblast to endocrine cell.* Experimental Biology and Medicine, 2001. **226**(11): p. 997-1002.

182. Gregoire, F.M., C.M. Smas, and H.S. Sul, *Understanding adipocyte differentiation.* Physiological Reviews, 1998. **78**(3): p. 783-809.

183. Nakajima, I., et al., *Extracellular matrix development during differentiation into adipocytes with a unique increase in type V and VI collagen.* Biology of the Cell, 2002. **94**(3): p. 197-203.

184. Le Pillouer-Prost, A., *Fibroblasts: what's new in cellular biology?* J Cosmet Laser Ther, 2003. **5**(3-4): p. 232-8.

185. Gosain, A., M.D. Luisa, and A. DiPietro, *Aging and wound healing.* World Journal of Surgery, 2004. **28**(3): p. 321-326.

186. Kim, W.S., et al., *Wound heating effect of adipose-derived stem cells: A critical role of secretory factors on human dermal fibroblasts.* Journal of Dermatological Science, 2007. **48**(1): p. 15-24.

187. Heo, S.C., et al., *Tumor Necrosis Factor-alpha-Activated Human Adipose Tissue-Derived Mesenchymal Stem Cells Accelerate Cutaneous Wound Healing through Paracrine Mechanisms.* Journal of Investigative Dermatology, 2011. **131**(7): p. 1559-1567.

188. Lee, S.H., J.H. Lee, and K.H. Cho, *Effects of Human Adipose-derived Stem Cells on Cutaneous Wound Healing in Nude Mice.* Annals of Dermatology, 2011. **23**(2): p. 150-155.

189. Iyengar, P. and P.E. Scherer, *Adiponectin/Acrp30, an adipocyte-specific secretory factor: physiological relevance during development.* Pediatr Diabetes, 2003. **4**(1): p. 32-7.

190. Pajvani, U.B., et al., *Structure-function studies of the adipocyte-secreted hormone Acrp30/adiponectin - Implications for metabolic regulation and bioactivity.* Journal of Biological Chemistry, 2003. **278**(11): p. 9073-9085.

191. Rajala, M.W. and P.E. Scherer, *Minireview: The adipocyte - At the crossroads of energy homeostasis, inflammation, and atherosclerosis.* Endocrinology, 2003. **144**(9): p. 3765-3773.

192. Pajvani, U.B., et al., *Complex distribution, not absolute amount of adiponectin, correlates with thiazolidinedione-mediated improvement in insulin sensitivity.* Journal of Biological Chemistry, 2004. **279**(13): p. 12152-12162.

193. Hotta, K., et al., *Circulating concentrations of the adipocyte protein adiponectin are decreased in parallel with reduced insulin sensitivity during the progression to type 2 diabetes in rhesus monkeys.* Diabetes, 2001. **50**(5): p. 1126-1133.

194. Yamauchi, T., et al., *Adiponectin stimulates glucose utilization and fatty-acid oxidation by activating AMP-activated protein kinase.* Nature Medicine, 2002. **8**(11): p. 1288-1295.

195. Yamauchi, T., et al., *Cloning of receptors for adiponectin that mediates anti-diabetic and anti-atherogenic effeccts.* Circulation, 2003. **108**(17): p. 533.

196. Yamauchi, T., et al., *The fat-derived hormone adiponectin reverses insulin resistance associated with both lipoatrophy and obesity.* Nature Medicine, 2001. **7**(8): p. 941-946.

197. Maeda, N., et al., *Diet-induced insulin resistance in mice lacking adiponectin/ACRP30.* Nature Medicine, 2002. **8**(7): p. 731-737.

198. Fruebis, J., et al., *Proteolytic cleavage product of 30-kDa adipocyte complement-related protein increases fatty acid oxidation in muscle and causes weight loss in mice.* Proceedings of the National Academy of Sciences of the United States of America, 2001. **98**(4): p. 2005-2010.

199. Tomas, E., et al., *Enhanced muscle fat oxidation and glucose transport by ACRP30 globular domain: Acetyl-CoA carboxylase inhibition and AMP-activated protein kinase activation.* Proceedings of the National Academy of Sciences of the United States of America, 2002. **99**(25): p. 16309-16313.

200. Rodriguez, A.M., et al., *Adipocyte differentiation of multipotent cells established from human adipose tissue.* Biochemical and Biophysical Research Communications, 2004. **315**(2): p. 255-263.

201. Han, J.F., et al., *Cathepsin K Regulates Adipocyte Differentiation: Possible Involvement of Type I Collagen Degradation.* Endocrine Journal, 2009. **56**(1): p. 55-63.

202. Weiner, F.R., et al., *Regulation of collagen gene expression in 3T3-L1 cells effects of adipocyte differentiation and tumor necrosis factor alpha*. Biochemistry, 1989. **28**(9): p. 4094-4099.

203. Sampaolesi, M., et al., *Cell therapy of alpha-sarcoglycan null dystrophic mice through intra-arterial delivery of mesoangioblasts.* Science, 2003. **301**(5632): p. 487-492.

204. Jiang, Y.H., et al., *Multipotent progenitor cells can be isolated from postnatal murine bone marrow, muscle, and brain.* Experimental Hematology, 2002. **30**(8): p. 896-904.

205. Aratani, Y. and Y. Kitagawa, *Enhanced synthesis and secretion of type-IV collagen and entactin during adipose conversion of 3T3-L1 cells and production of unorthodox laminin complex*. Journal of Biological Chemistry, 1988. **263**(31): p. 16163-16169.

206. Antras, J., et al., *Decreased biosynthesis of actin and cellular fibronectin during adipose conversion ofcells - reorganization of the cytoarchitecture and extracellular matrix fibronectin.* Biology of the Cell, 1989. **66**(3): p. 247-254.

207. Mironava, T., et al., *Gold nanoparticles cellular toxicity and recovery: Effect of size, concentration and exposure time.* Nanotoxicology, 2010. **4**(1): p. 120-137.

208. Lilla, J., D. Stickens, and Z. Werb, *Metalloproteases and adipogenesis: A weighty subject.* American Journal of Pathology, 2002. **160**(5): p. 1551-1554.

209. Chithrani, B.D. and W.C.W. Chan, *Elucidating the mechanism of cellular uptake and removal of protein-coated gold nanoparticles of different sizes and shapes.* Nano Letters, 2007. **7**(6): p. 1542-1550.

210. Chen, R., G. Huang, and P.C. Ke, *Calcium-enhanced exocytosis of gold nanoparticles.* Applied Physics Letters, 2010. **97**(9).

211. Ricles, L.M., et al., *Function of mesenchymal stem cells following loading of gold nanotracers.* International Journal of Nanomedicine, 2011. **6**: p. 407-416.

212. Lammers, G., et al., *An Overview of Methods for the In Vivo Evaluation of Tissue-Engineered Skin Constructs.* Tissue Engineering Part B-Reviews, 2011. **17**(1): p. 33-55.

213. Levi, B., et al., *Studies in Adipose-Derived Stromal Cells: Migration and Participation in Repair of Cranial Injury after Systemic Injection.* Plastic and Reconstructive Surgery, 2011. **127**(3): p. 1130-1140.

214. Yang, P.H., et al., *Transferrin-mediated gold nanoparticle cellular uptake.* Bioconjugate Chemistry, 2005. **16**(3): p. 494-496.